

Validation of the GeoClaw Model

NTHMP MMS Tsunami Inundation Model Validation Workshop

GeoClaw Tsunami Modeling Group, University of Washington.

Frank I. González, Randall J. LeVeque, Paul Chamberlain, Bryant Hirai, Jonathan Varkovitzky
and David L. George (USGS)

1 Introduction

1.1 Geographic area

The west coast, with a focus on Washington State, including Puget Sound, the San Juan Island group, and other islands in the Strait of Juan de Fuca.

1.2 NTHMP support

This group has no current or past support from NTHMP.

NTHMP approval of this model will allow us to seek funding in the future to perform tsunami hazard and risk assessment modeling, such as from NTHMP partner FEMA's Risk Mapping, Assessment, and Planning (Risk MAP) Program.

Funding will also be sought to provide Washington State with tsunami modeling and mapping in support of tsunami hazard assessment and emergency management planning and education.

Tsunami sources in these geographic areas include earthquakes and landslides, and we will therefore address benchmark problems that deal with these sources.

2 Model description

2.1 Model equations

For all benchmark problems we used the two-dimensional nonlinear shallow water equations

$$\begin{aligned} h_t + (hu)_x + (hv)_y &= 0, \\ (hu)_t + (hu^2 + \frac{1}{2}gh^2)_x + (huv)_y &= -ghB_x - Du, \\ (hv)_t + (huv)_x + (hv^2 + \frac{1}{2}gh^2)_y &= -ghB_y - Dv, \end{aligned} \tag{2.1.1}$$

where $u(x, y, t)$ and $v(x, y, t)$ are the depth-averaged velocities in the two horizontal directions, $B(x, y, t)$ is the topography or bathymetry, and $D = D(h, u, v)$ is the drag coefficient.

Most of the benchmark problems use no bottom friction, so $D = 0$. When used, it has the form

$$D = \frac{gM^2 \sqrt{(u^2 + v^2)}}{h^{5/3}} \tag{2.1.2}$$

where M is the Manning coefficient, generally taken to be 0.025. Comparisons with and without friction have been performed in Section 3.9 for Benchmark Problem #9 and Section 3.6 for Benchmark Problem #6.

Coriolis terms can be turned on in GeoClaw, but have not been used for any of the benchmark problems.

2.2 Methods implemented in GeoClaw

GeoClaw is a variant of the Clawpack open source software [32] that LeVeque and collaborators have been developing since 1994. The “wave-propagation algorithms” used in this software are described in great detail in the textbook [29] and in several journal publications [27, 28, 26].

Adaptive mesh refinement (AMR) has been incorporated since the inception of this software, in joint work with Marsha Berger at the Courant Institute of Mathematical Sciences, one of the foremost authorities on block structured AMR technology, often referred to as Berger-Colella-Oliger style AMR [5, 8]. The AMR algorithms in Clawpack are described in detail in [7]. Berger has also played a significant role in adapting the AMR routines to work well in GeoClaw [6, 34] in connection with well-balancing and inundation modeling.

The GeoClaw software is described in some detail in [6], an invited contribution to a special issue of *Advances in Water Resources* on “New Computational Methods and Software Tools”, and in [34], an invited paper in *Acta Numerica*, which serves as an “annual review of numerical analysis”. There is also on-line documentation [18] that is part of the extensive documentation of Clawpack. The Riemann solvers and inundation model are described in more detail in [20, 21]

The open source Clawpack software (including GeoClaw) can be freely downloaded from the website <http://www.clawpack.org>. Recent developments have taken place using a Subversion repository that is openly accessible (linked from the Clawpack webpage), using issue tracking and a wiki, as well as the `claw-dev` google group to discuss development issues. Clawpack is currently transitioning to use of the Git, a more modern distributed version control system, and the future home of Clawpack is on Github (<https://github.com/organizations/clawpack>).

GeoClaw was initiated in the PhD work of David George [20, 33, 23, 21] and was originally called TsunamiClaw. It has more recently been extended to handle other geophysical flows such as storm surge [37] dam break problems [19], and debris flows [22].

The GeoClaw model solves the two-dimensional nonlinear shallow water equations using high-resolution finite volume methods. Values of h , hu , and hv in each grid cell represent cell averages of the depth and momentum components. With flat bathymetry, the methods are exactly conservative for both mass and momentum, and conserve mass for arbitrary bathymetry when used on a fixed grid. They do not exactly conserve mass during regridding when AMR is used because, for example, a grid cell that is dry on a coarse grid may contain part of the shoreline on a finer grid. This is not an issue as long as the region of interest is refined before the main wave arrives.

These methods are based on Godunov’s method, which means that at each cell interface a one-dimensional Riemann problem is solved normal to the edge, which reduces to a one-dimensional shallow water model with piecewise constant initial data, with left and right values given by the cell averages on each side. The jump in bathymetry between the cells is incorporated into the Riemann solution in a manner that makes the method “well balanced”: the steady state of the ocean at rest is exactly maintained. This is done using the “f-wave formulation” of the wave propagation method, as discussed in [1, 21, 29, 31].

Godunov’s method consists of solving the Riemann problem and using the resulting wave structure to update cell averages in the adjacent finite volume cells. In practice an approximate

Riemann solution is used, which reduces to the standard Roe solver [29, 39] in f-wave form in general, but is modified to also handle dry states in order to model inundation [21].

Accuracy is improved by adding in high-resolution correction terms. These terms are based on Taylor series approximation of the exact solution at time t_{n+1} about time t_n , using the same approach as used to derive the classical second-order accurate Lax-Wendroff method [30]. However, the terms are only added where the solution is smooth. Near steep gradients, these terms lead to severe numerical dispersion and potentially undershoots or overshoots that can lead to instability or unphysical states (e.g. negative fluid depth). A limiter is applied to the correction term using the standard approach described in detail in [29] and references found there, based on the theory of total variation diminishing (TVD) methods that has been well developed since the early 1980s. The resulting “high-resolution” shock-capturing methods exhibit minimal numerical dispersion or dissipation and have been shown to be very robust for both linear and nonlinear hyperbolic problems, even when the solution contains strong shock waves.

2.3 Boundary conditions

Boundary conditions at edges of the computational domain are handled as described in Chapter 7 of [29]. At the start of each time step, solution values are assigned in two rows of ghost cells surrounding the computational domain. This allows the high-resolution finite volume methods to be applied on all cells that lie inside the computational domain. One row of ghost cells is required in order to solve Riemann problems at edges of the physical cells adjacent to the boundary. The second row is required in order to apply limiters. Here we summarize the boundary conditions used in the benchmark problems.

2.3.1 Non-reflecting boundaries

Zero-order extrapolation from the grid cells along the boundary to ghost cells in every time step is used to implement non-reflecting boundary conditions, for example when truncating the ocean or wave tank. The Godunov-type methods implemented in GeoClaw solve Riemann problems at each grid interface and having equal values in the grid cell at the boundary and the adjacent ghost cell results in no incoming wave. These boundary conditions are described in more detail in Section 7.3.1 of [29]. Although not perfectly absorbing for waves hitting the boundary at a non-normal angle, they perform very well in practice and have been extensively used for similar problems.

2.3.2 Solid wall boundaries

Several benchmark problems are posed in wave tanks with solid (reflecting) walls. Solid wall boundary conditions are implemented as described in Section 7.3.3 of [29]. The values in each grid cell adjacent to the boundary are extrapolated into ghost cells and then the normal velocity is negated. When solving the Riemann problem, this anti-symmetric setup results in a Riemann solution with zero normal velocity at the interface, modeling the correct boundary condition at this boundary.

2.3.3 Inflow boundaries

Some benchmark problems specify an incoming wave, typically by tabulated values of the depth at a gage near the inflow boundary. This can be implemented by filling ghost cells at each time step with the desired values of the fluid depth and momentum values that are determined using the Riemann invariants for the shallow water equations, by assuming the depth and momentum are related in such a way that the solution is a simple wave in the incoming wave family.

For example, at the left edge of the computational domain, an incoming wave would be a right-going wave with constant values of the Riemann invariant $u - 2\sqrt{gh}$ throughout the wave. This value must be $-2\sqrt{gh_0}$ where h_0 is the depth of the undisturbed water before the wave arrives. From this the velocity $u = 2(\sqrt{gh} - \sqrt{gh_0})$ can be determined for any depth h . Hence the given depth as a function of time at a wave gauge can be used to determine the depth and momentum at this point as a function of time, which in turn is used to fill ghost cells.

2.3.4 Initial conditions

In other problems, an initial wave form $h(x, t = 0)$ is specified as a function of x at time $t = 0$, representing a propagating wave form. Again the Riemann invariants can be used to determine the momentum at each point in order to specify initial conditions.

For Benchmark Problem #9 (Section 3.9) the seafloor displacement is specified. This is what is generally done in real applications. GeoClaw allows specifying a time-varying seafloor displacement as well, to model the dynamic rupture of faults. This capability has been used in the landslide problems (Section 3.3 and Section 3.8) as well to model the changing bathymetry.

2.4 Other validation studies

Several of the benchmark problems were solved using TsunamiClaw, an early version of GeoClaw, in preparation for the Catalina benchmarking workshop in 2004. These results are available in the proceedings paper [33].

Validation studies of the more recent GeoClaw software have been presented in several peer-reviewed papers:

- In [6] a test problem is used that consists of a radially symmetric ocean with a continental shelf, and a radially symmetric initial hump of water at the center. At one position along the coast a island is placed on the shelf. Several gauges are located near the island. If the island is rotated to a different position on the coast the results at the gauges should be identical. Numerically they will not be identical due to differences in how the coast intersects the Cartesian grid. Very similar results are obtained for locations near an axis and near the diagonal, both in gauge results and in plots of the surface and inundation. This is true even when AMR is used to concentrate fine grids only in the direction towards the island. In this paper the Chile 2010 tsunami is also used as a test problem and good agreement with measured results at DART Buoy 32412 are obtained, on two different grid resolutions to test convergence. See also <http://www.clawpack.org/links/awr11/> for codes and animations.

- Further tests of this same problems are presented in [34]. See also <http://www.clawpack.org/links/an11/> for codes and animations.
- Grid refinement studies and comparison with field data for the widely studied Malpasset dam failure are presented in [19].
- In [4] tests are performed for a tsunami-like wave propagating on the full sphere, using a novel mapped grid that covers the sphere with a logically rectangular finite volume grid. Tests are presented in which the bathymetry and the initial conditions are axisymmetric so that the solution should remain so and can be compared to fine grid one-dimensional simulations. See also <http://www.amath.washington.edu/~rjl/pubs/amrsphere09/index.html> for codes used in this paper.

Independent validation of GeoClaw has also been performed by Spatial Vision Group (<http://www.spatialvisiongroup.com/>), a private consulting company in Vancouver, BC. David Alexander and Bill Johnstone from this group used the TsunamiClaw software to perform hazard studies of the communities of Ucluelet and Tofino on Vancouver Island. As part of their validation, they compared TsunamiClaw results to those obtained using MOST for a standard model of a Magnitude 9.0 Cascadia Subduction Zone event. Comparisons were performed for several tide gauges on the coast of Washington and Oregon.

Our group is currently using GeoClaw to model the Great Tohoku Tsunami of 11 March 2011 and preliminary comparisons with DART buoy data looks very good. Some results were posted online as computed in the days after the event and can be viewed at <http://www.clawpack.org/links/honshu2011/>. Some comparisons were also presented in a recent article in SIAM News on tsunami modeling [2]. Preliminary results have also been obtained by other groups, e.g. [45].

3 Benchmark results

The sections below contain the GeoClaw results for each benchmark problem. Benchmark problem descriptions can be found in the Github repository <https://github.com/rjleveque/nthmp-benchmark-problems> [3] along with data that was provided as part of the problem specification.

3.1 BP 1: Single wave on a simple beach (Analytic)

Documentation:

- A description of this benchmark problem is provided by [3] and [40].
- Problem description provided by Dmitry Nicolsky, at [3]:
 BP01-DmitryN-Single_wave_on_simple_beach/description.pdf

3.1.1 Problem Description

The focus is on comparing computed and analytic solutions for a wave incident on a simple beach, in which:

- The bathymetry consists of a deep region of constant depth d connected to a sloping beach of angle $\beta = \text{arccot}(19.85)$. Note that the toe of the beach is located at $x = X_0 = d \cot \beta$
- The initial waveform of the wave is given by

$$\eta(x, 0) = H \text{sech}^2(\gamma(x - X_1)/d) \quad (3.1.1)$$

where $L = \text{arccosh}(\sqrt{(20)})/\gamma$, $X_1 = X_0 + L$, and $\gamma = \sqrt{(3H/4d)}$. The speed of the wave is given by the following:

$$u(x, 0) = -\sqrt{g/d} \eta(x, 0) \quad (3.1.2)$$

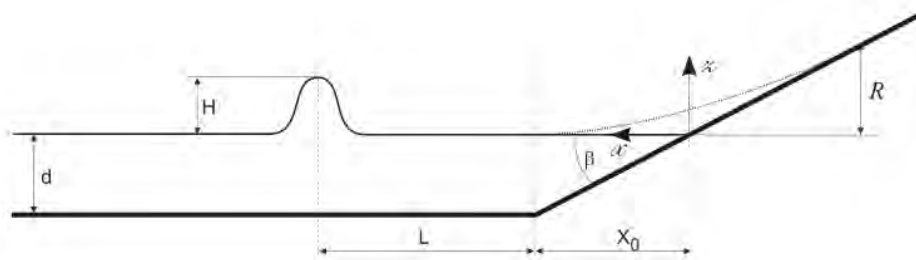


Figure 3.1.1: Sketch of canonical beach and approaching wave.

3.1.2 Problems encountered

- The analytic solution of the wave equation was hard to determine and compute. The analytic solution was obtained from the benchmark problem champion; it would be very helpful if it were provided in an Excel file as part of the benchmark problem description.
- No analytical solution was provided for time $t = 25s$
- The Clawpack code does not currently include maximum runup calculations. An additional module had to be written.

3.1.3 What we did

- Used $g = 1$ and no friction.
- The problem was solved on an 800×2 grid, where the x domain spanned $x = -10$ to 60 .
- Variable time stepping was allowed, based on a CFL number of 0.9

3.1.4 Results

- Task 1. Good agreement between computed and analytic water level profiles at $t = 35(d/g)^{1/2}$, $t = 45(d/g)^{1/2}$, $t = 55(d/g)^{1/2}$, $t = 65(d/g)^{1/2}$ are presented in Figure 3.1.2. Data were missing from file `canonical_profiles.txt` for $t = 25(d/g)^{1/2}$, so this time was omitted.
- Task 2. Good agreement between computed and analytic water levels at locations $x/d = 0.25$ and $x/d = 9.95$ during the propagation and reflection of the wave is presented in Figure 3.1.3.
- Task 3. Maximum runup on the beach was 0.085 , as presented in the time series of runup values in Figure 3.1.4.
- Task 4. The optional demonstration of convergence was not performed.

3.1.5 Lessons learned

- This benchmark problem is a good test of the shallow water wave computation against an analytic solution in one dimension.
- Because of its complexity, the analytical solution should be provided in a data file on the benchmark problem website to ensure all participants are solving the same problem.

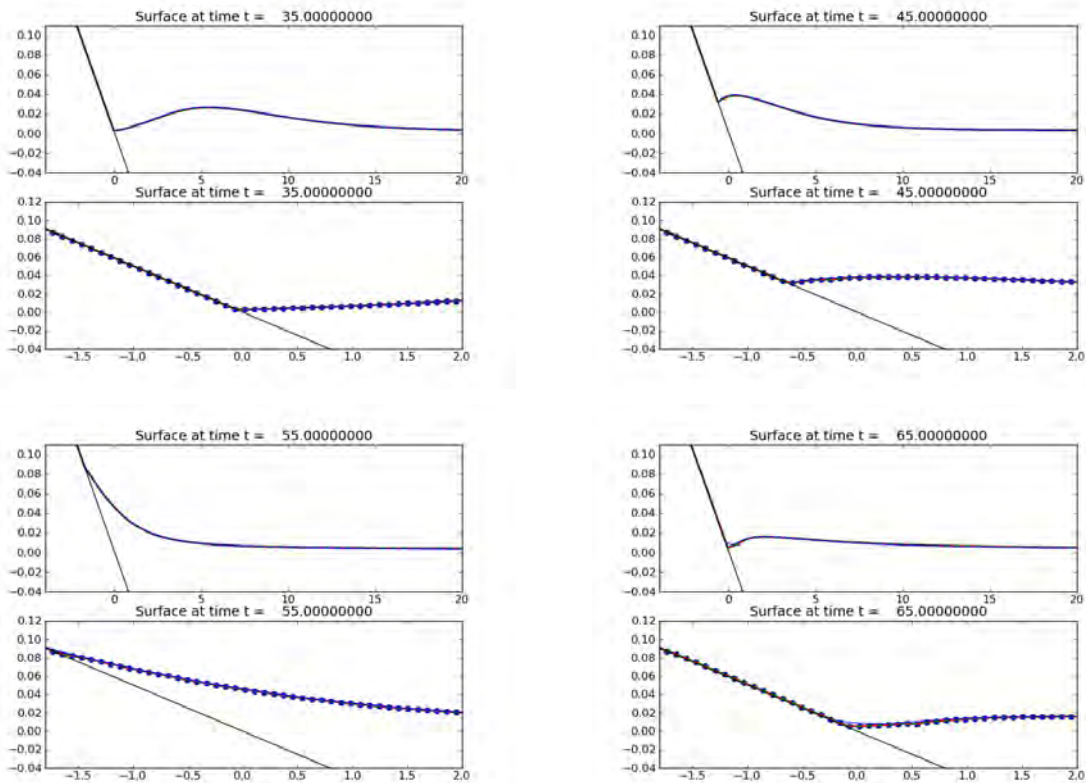


Figure 3.1.2: Profile plots for the times specified in Task 2. For each pair of plots at a particular time, the top frame provides a full view of the incoming wave and the bottom frame provides an expanded view of the inundation area. In some regions the analytic and GeoClaw solutions lie atop one another.

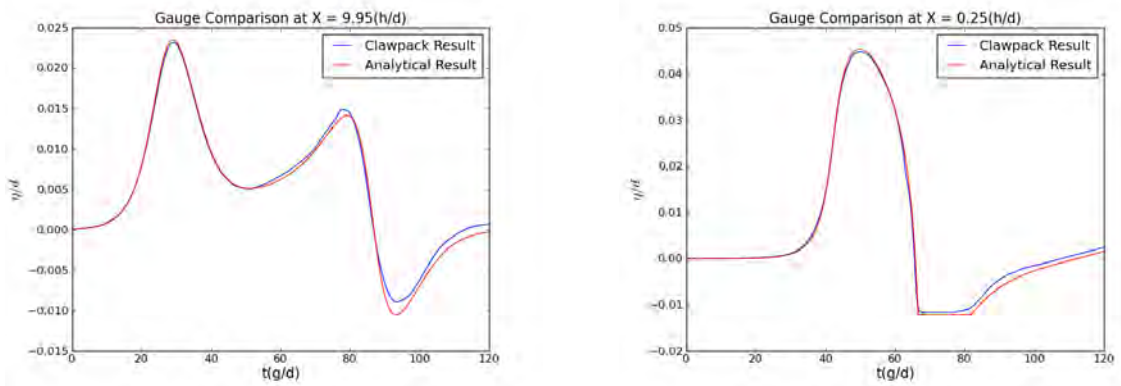


Figure 3.1.3: Left column: Water level time series at location $x/d = 9.95$. Right column: Water level time series at location $x/d = 0.25$.

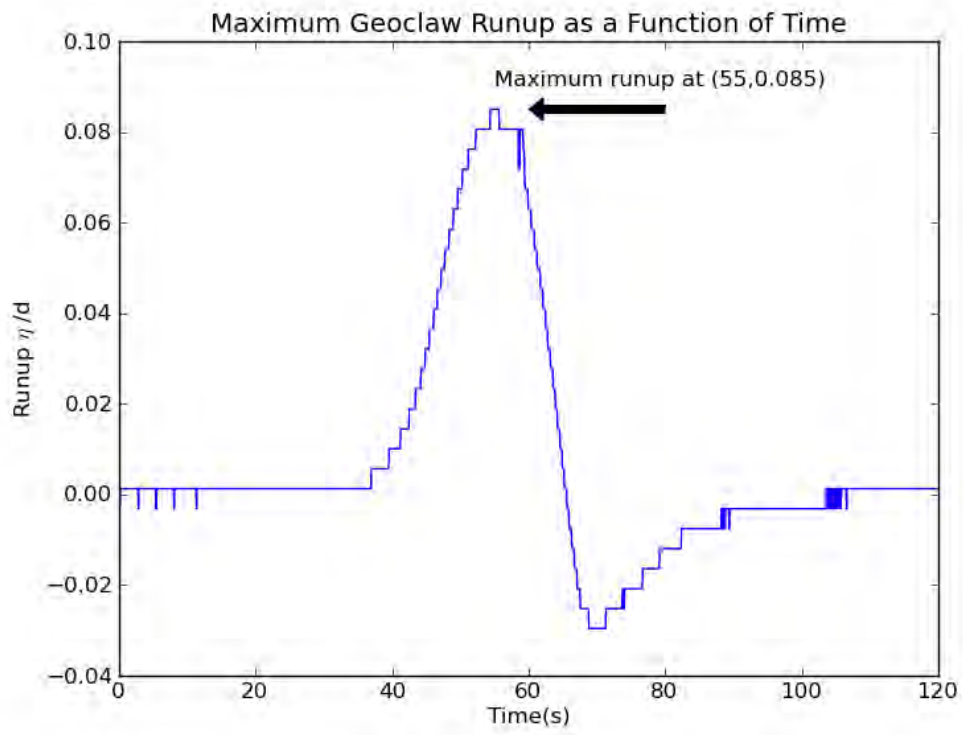


Figure 3.1.4: Runup on canonical beach as a function of time

3.2 BP 2: Solitary wave on composite beach (Analytic)

Documentation:

- PMEL-135, pp 5 & 30-33 [40].
- Problem description provided by Dmitry Nicolsky, at [3]:
BP02-DmitryN-Solitary_wave_on_composite_beach_analytic/description.pdf
- Coastal Hydraulics Laboratory Problem Description [9].

3.2.1 What we did

- We solved the shallow water wave equation in Cartesian coordinates with $g = 9.81$ and no friction.
- To specify the incoming wave from the left boundary of our computational domain we used the first ten seconds of measurements taken at Gage 4. After ten seconds the left boundary switched to be a non-reflecting boundary. This boundary is selected since the end of our computational domain is not the end of the physical wave tank. The implementation of these boundary conditions is described in Section 2.3.
- Since the problem is one-dimensional, we solved on a 600×2 grid with no adaptive mesh refinement.
- To impose linearization we scaled the incoming wave by 10^{-4} to remove any nonlinear behavior, then scaled up the gage readings by 10^4 to compare with the analytical solution.

3.2.2 Gage comparisons

For these Gage comparisons we ran our code linearly with friction set to zero.

The results for cases A, B, and C are shown in figures Figure 3.2.1, Figure 3.2.2, Figure 3.2.3 respectively where Gage 11 is placed at the vertical wall.

3.2.3 Convergence Study

We performed a test to see how well Clawpack converged to the analytic solution as we increased the number of grid cells in our computational domain (using 200, 400, and 600 cells). We found that as the number of grid cells was increased, the computed solution approached the analytic solution. The convergence plot is shown in Figure 3.2.4.

3.2.4 Lessons learned

In this benchmark problem we found that using the analytic solution at Gage 4 as boundary conditions on a shorter domain, starting at gage 4, provided more accurate results than using the wave maker position and a longer domain to model the entire tank. It appears that a similar assumption is made in the provided analytic solutions, as they match up nearly perfectly with the lab data for the first ten seconds.

Overall this benchmark problem is a good test for one dimensional codes. The benchmark problem specifications could be improved by specifying the computational domain and the specific data source that should be used to model the incoming wave.

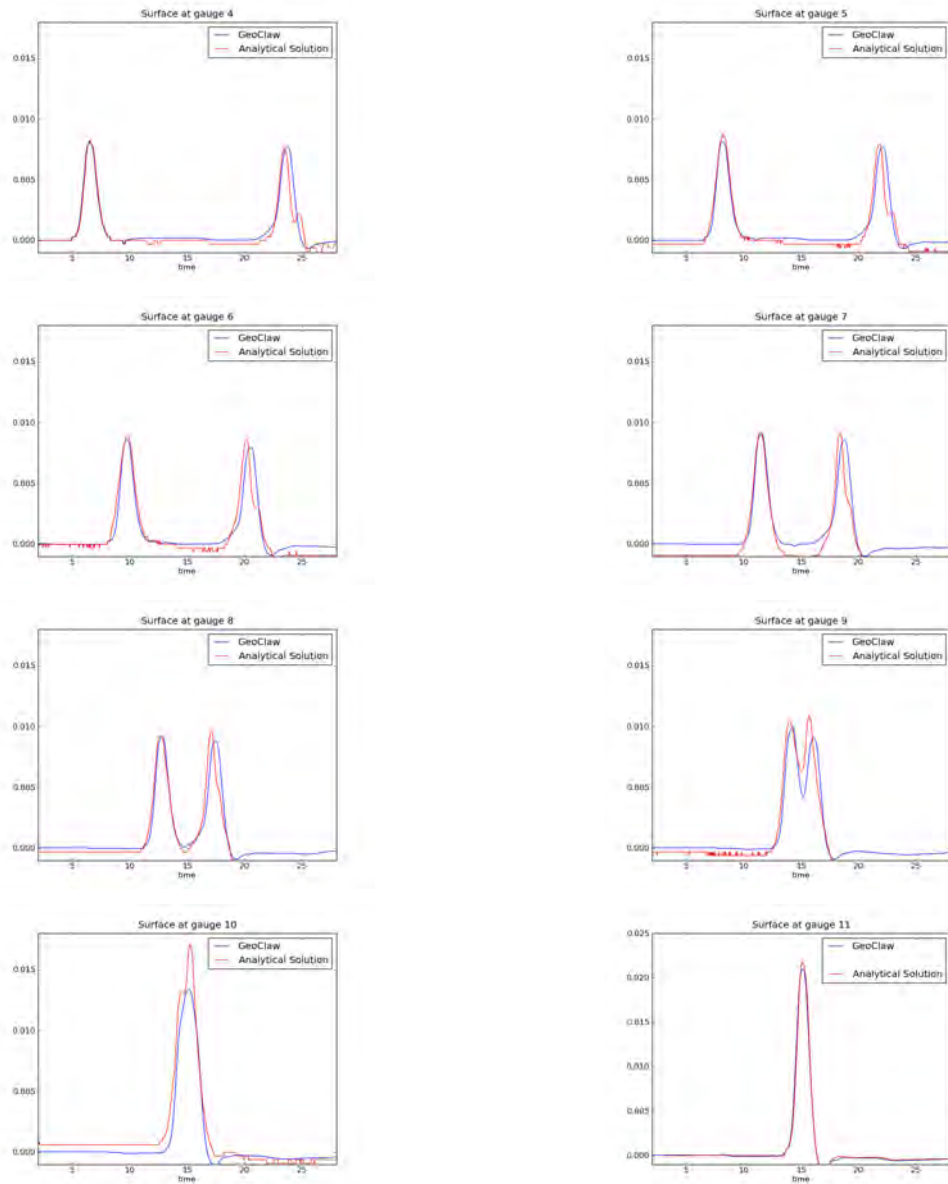


Figure 3.2.1: Case A

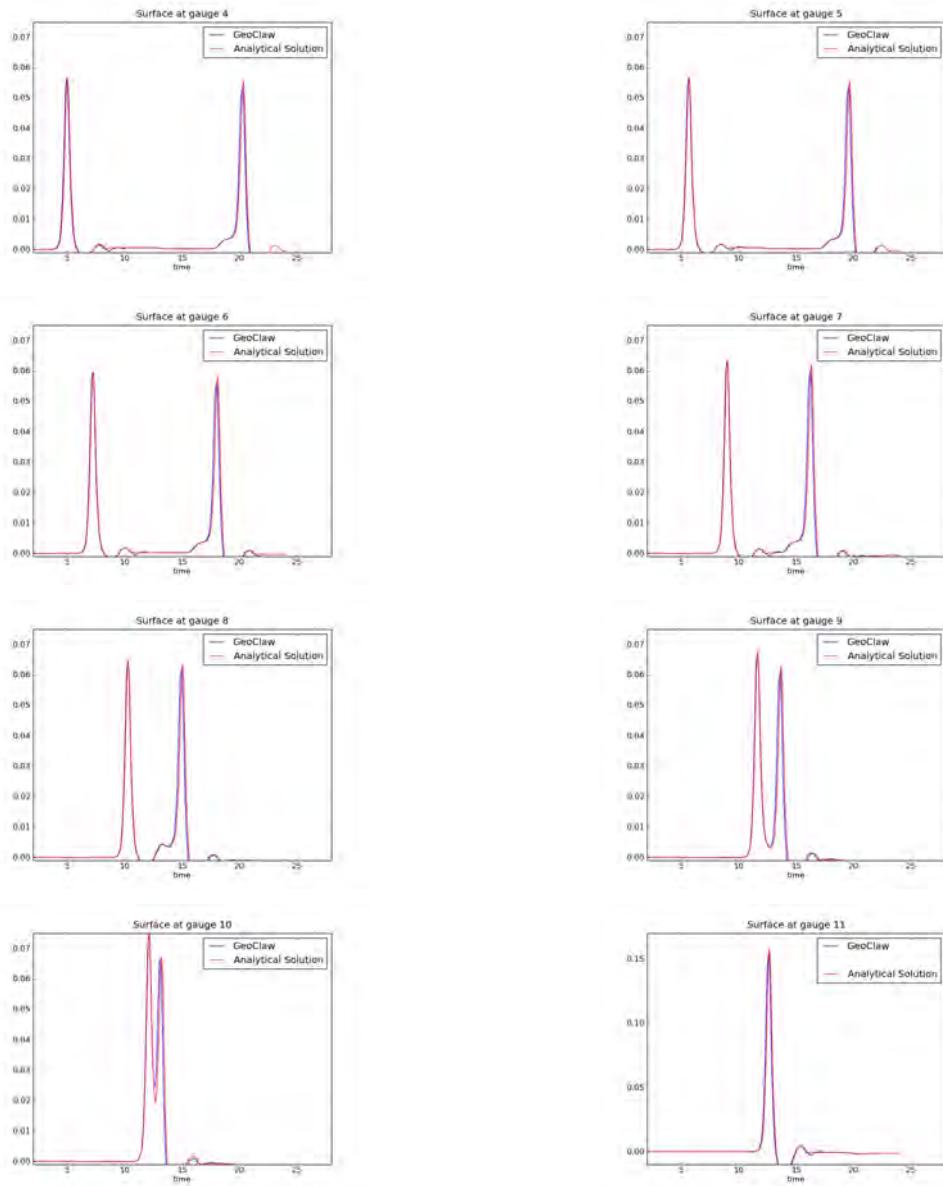


Figure 3.2.2: Case B

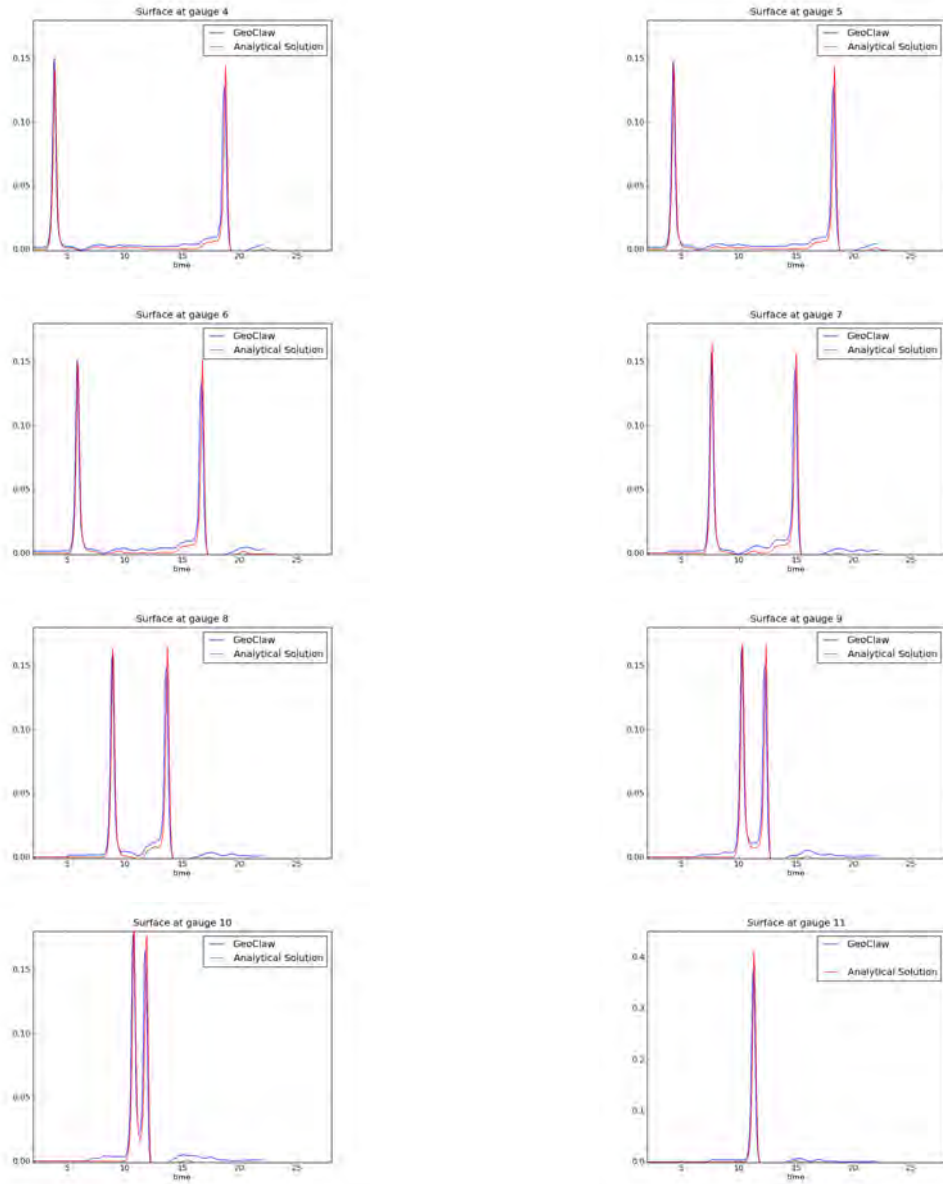


Figure 3.2.3: Case C

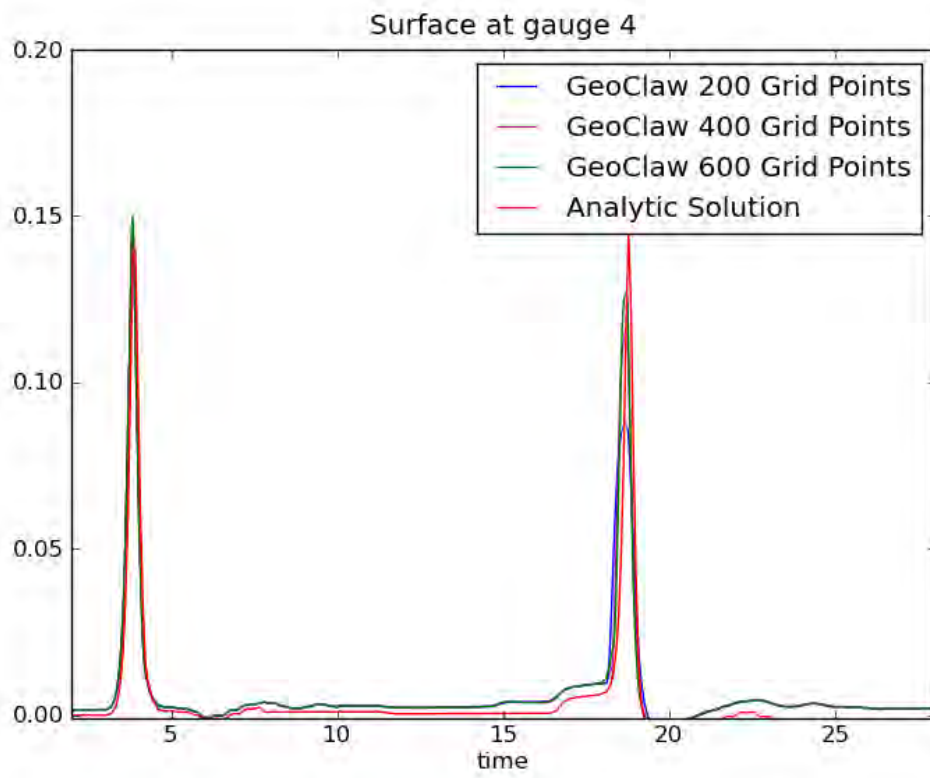


Figure 3.2.4: Convergence Plot for Gage 4 in Case C

3.3 BP 3: Saucer landslide (Laboratory)

3.3.1 Problem specification

- Problem description provided by Stephan Grilli:
 BP03-StephanG-Saucer_landslide/EG07_slide_benchmark.pdf at [3].
- Original paper of Enet and Grilli [14] describing laboratory experiments.

3.3.2 Problems encountered

The moving bathymetry is specified in terms of $\zeta(\xi, \eta)$, the thickness of the sliding mass in the direction orthogonal to the sloping beach. In each time step this must be converted into values $B(x, y, t)$ in the vertical z -direction, at horizontal distance x from the initial shore. Note that

$$x = \xi \cos(\theta), \quad y = \eta.$$

The bathymetry of the wave tank and beach without the sliding mass is given by

$$B_0(x, y) = \begin{cases} -\tan(\theta)x & \text{if } x < 5.598, \\ -1.5 & \text{if } x \geq 5.598 \end{cases}$$

The value $5.598 \approx 1.5/\tan(\theta)$ is determined by the fact that the water has a depth of 1.5 m on the flat portion and the beach slope is 15° so $\theta = 15\pi/180 \approx 0.2618$.

At time $t = 0$ the sliding mass is located at $x = x_0$, determined by the initial depth d according to

$$x_0 = \frac{d}{\tan(\theta)} + \frac{T'}{\sin(\theta)}.$$

At time t the sliding mass is centered at $x_c = x_0 + s(t) \cos(\theta)$ where $s(t)$ is the function discretized in the data file `kinematics.txt`. However, this is only true for small t . After some time the mass hits the horizontal bottom of the tank. According the paper [14] and communication with Stephan Grilli, the mass stops at this point. This is not made clear in the problem specification [3].

To determine $B(x, y, t)$, for each finite volume grid cell with center (x_i, y_j) the value ξ must be found so that

$$\xi \cos(\theta) + \zeta(\xi - \xi_c, y_j) \sin(\theta) = x_i$$

where $\xi_c = x_0/\cos(\theta) + s(t)$ is the ξ location of the center of mass at this time. Determining ξ requires solving the nonlinear equation

$$\cos(\theta)\xi + \zeta(\xi - \xi_c, y_j) \sin(\theta) - x_i = 0.$$

In our Fortran code this equation is solved using the library routine `zeroin` available from Netlib (<http://www.netlib.org/go/zeroin.f>).

Once ξ has been found, the bathymetry is

$$B(x_i, y_j, t) = -\tan(\theta)\xi + \cos(\theta)\zeta(\xi - \xi_c, y_j).$$

3.3.3 What we did

- The moving bathymetry is handled by recomputing $B_{ij}^n = B(x_i, y_j, t_n)$ in each time step, at the center of each finite volume grid cell, by solving a nonlinear equation as described above. This is the standard approach for handling moving bathymetry in GeoClaw: the value B_{ij}^n is adjusted but the fluid depth h_{ij}^n remains the same, so that the water column is simply displaced vertically in any cell where the bathymetry changes. For bathymetry that is smoothly varying in space and time, as in this problem, this is considered a reasonable approach. Note, however, that no momentum is directly imparted to the water by the moving bathymetry.
- The problem was solved using a fixed grid with $72n \times 18n$ grid cells on the domain $-1 \leq x \leq 6.2$ and $0 \leq y \leq 1.8$ meters. Three resolutions corresponding to $n = 1, 2, 4$ were used to test convergence.

A second level of refined grid was used in the region $-0.1 \leq x \leq 0.1$ and $0 \leq y \leq 0.1$ surrounding the point $x \approx 0, y = 0$ on the shoreline where the runup R_u must be calculated. In each case this grid was 10 times finer in each direction than the base grid.

Adaptive mesh refinement (with moving grids) was not used.

- The problem was solved on $0 \leq y \leq 1.8$ with solid wall boundary conditions at $y = 0$. This gives the correct solution in this domain and the solution in the other half of the wave tank $-1.8 \leq y \leq 0$ is easily constructed by symmetry if desired.

Solid wall boundary conditions were also used at $y = 1.8$. At $x = -1$ the boundary condition doesn't matter since this region is always dry, and at $x = 6.2$ outflow boundary conditions were used. Zero-order extrapolation, which generally gives a very good approximation to non-reflecting boundary conditions as described in Section 7.3.1 of [29]. Solid wall boundary conditions are implemented as described in Section 7.3.3 of [29]. See Section 2.3 for more information about these boundary conditions.

3.3.4 Numerical simulations

Figure 3.3.1 shows two frames from a sample computation for the case $d = 0.061$. Colors indicate the surface elevation $\eta(x, y, t)$ and contours show the bathymetry with the upper half of the sliding mass.

3.3.5 Gauge comparisons

Simulated gauges were placed at the 4 locations that match the wave tank measurements, as indicated in Figure 3.3.1. The surface elevation $\eta(t)$ at each gauge was recorded every time step. These results are shown in Figures 3.3.2 through 3.3.8 for the 7 test cases.

Reasonable agreement is generally seen for the initial peak and trough at Gauges 1, 2, and 4. On the other hand Gauge 3, located along the centerline, shows quite different results than the measurements and generally exhibits a steeper dip in η as the mass passes this point. The

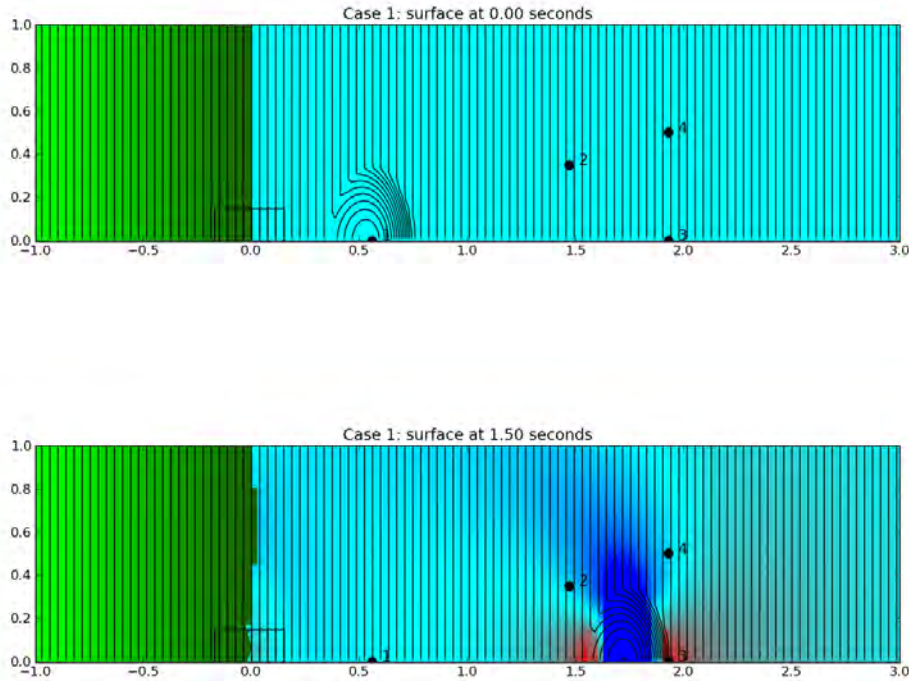


Figure 3.3.1: Sample results for $d = 0.061$. The water surface $\eta(x, y, t)$ (colors with dark red $+0.02$ m and dark blue -0.02 m) and bathymetry (0.01 m contour levels). Only a portion of the computational domain is shown. Grid resolution: $\Delta x = \Delta y = 0.025$ m on the full domain, with refinement to $\Delta x = \Delta y = 0.0025$ m in the nearshore region in the the rectangular box. The full domain goes to $x = 6.2$ and to $y = 1.8$.

measurements also show an oscillatory wave train behind the initial peak and trough that is not captured in the simulations obtained with the shallow water equations. This is consistent with claims in [3] and [14] that dispersive effects are important for these short wavelength waves that cannot be captured by the non-dispersive shallow water equations. By contrast, the Boussinesq model used in [15] does display these dispersive ripples.

3.3.6 Runup measurements

The runup is measured near $y = 0$ by keeping track of the approximate shoreline position in the first row of grid cells $j = 1$, whose centers lie at $y = \Delta y/2$. In each time step, we loop over all cells $i = 1, 2, \dots$ and look for the first cell for which $h_{ij} > \epsilon$, where $\epsilon = 0.001$ (1 mm) was chosen as a depth below which the cell is considered dry. The value $x_s = i\Delta x$, the right edge of this finite volume cell, was then used as the shoreline location at this time. The runup at each time is then computed as $x_s \tan(\theta)$, and this value was output for later plotting, and for computing the maximum runup R_u required for the benchmark.

Figures 3.3.2 through 3.3.8 show the runup as functions of time for each test case. Some of

these plots exhibit strange behavior for later times. This was due to the fact that we used a limited domain and also that we used a refined grid only over a fairly small region near the origin.

Approximate maximum runup values are tabulated in Table 3.3.1. These values are based on the minimum values seen in the figures for early times. It is not clear if these are correct in all cases. Also these grids are fairly coarse. But since the gauge data does not match particularly well and we do not believe shallow water is a suitable model for this problem, we did not pursue this further.

d	Lab	my = 36	my = 72
0.061	6.2	8.0	8.7
0.080	5.7	5.4	6.0
0.100	4.4	2.7	4.3
0.120	3.4	2.7	3.4
0.140	2.3	2.7	2.7
0.149	2.7	2.7	2.7
0.189	2.0	1.4	2.0

Table 3.3.1: Runup values in mm. Lab results taken from Table 1 of [3]. Two different resolutions with 36 and 72 points in the y direction were compared, with $m_x = 4m_y$ points in the x direction.

3.3.7 Lessons learned and suggestions for improvement

- It might be useful to other groups doing this problem in the future if the bathymetry $z = B_0(x, y)$ were tabulated, corresponding to the mass centered at $x_0 = 0$ on the slope with $\theta = 15^\circ$. From this, the bathymetry at later times could be interpolated by shifting by x_c . Computing $B_0(x, y)$ from the given $\zeta(\xi, \eta)$ would require solving a nonlinear equation at each (x, y) as outlined in Section 3.3.3.
- It is stated in [3] that $\zeta(\xi, \eta)$ represents a “Gaussian mass” but this is not a Gaussian function.
- The non-dispersive shallow water equations do not appear adequate to model the oscillatory wave train observed in the laboratory. The shallow water equations may still be useful for modeling landslides of this nature since the initial peak amplitude and run up values are in the right ballpark, but comparison with laboratory measurements is not a suitable means of judging convergence or accuracy of the numerical method. For this reason it would be valuable if the community could agree on what the “correct” converged solution to the shallow water equations is for this problem, and if this solution (or at least the values at the gauges) were tabulated for comparison in future benchmark studies.
- The runup results in the laboratory might be affected by the rail along which the mass slides, which is visible in Figure 1 of [3] and is along $y = 0$, the point where it is stated that the runup should be measured. In fact the runup must have been measure slightly above this point, as indicated in Figure 9 of [14]. The rail appears to be several mm high and

should affect the fluid dynamics. This rail could easily be added to the bathymetry if its dimensions were known.

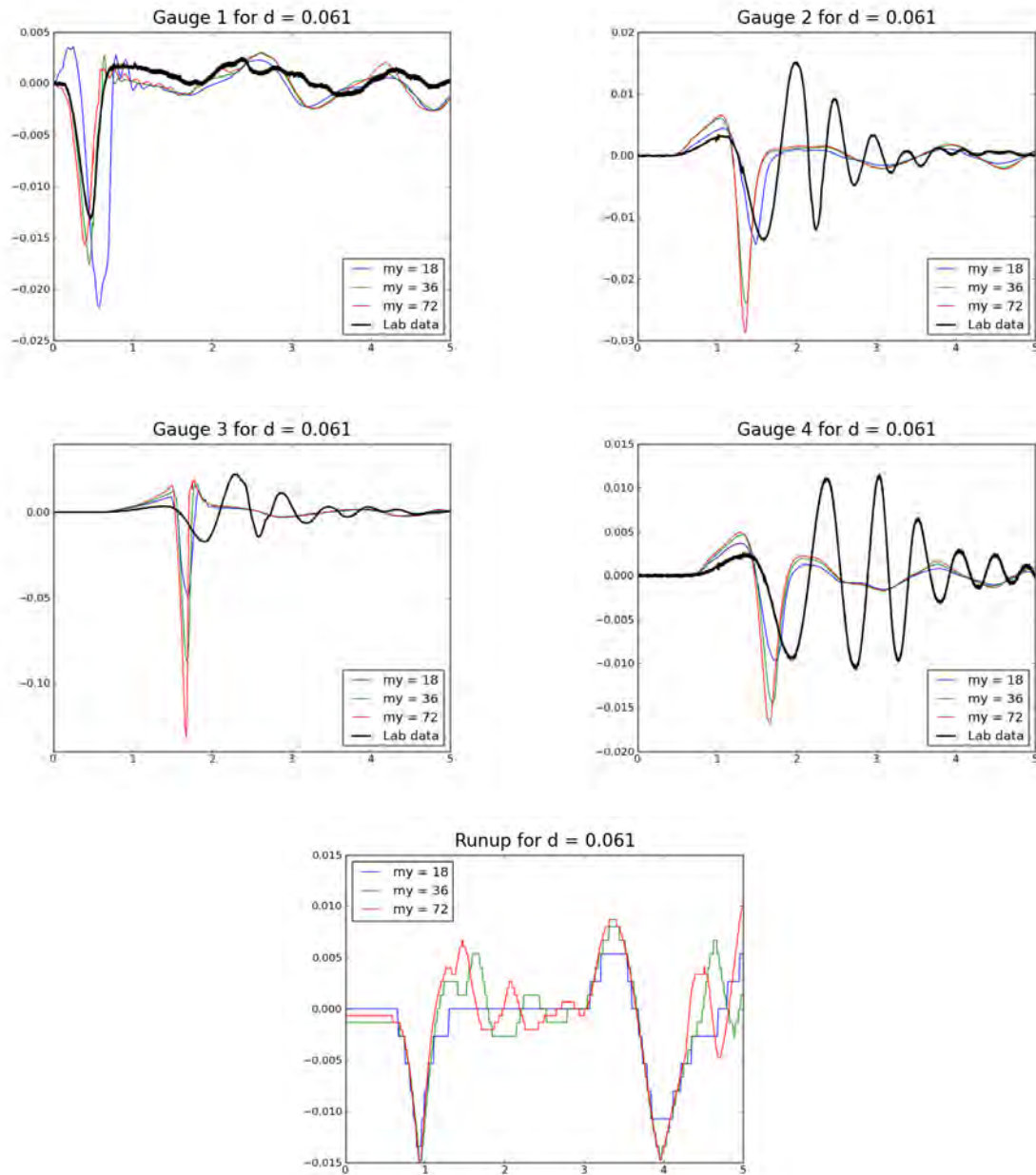


Figure 3.3.2: Gauge and runup results for $d = 0.061$. Three different resolutions with $my = 18, 36,$ and 72 points in the y direction were compared, with $mx = 4my$ points in the x direction.

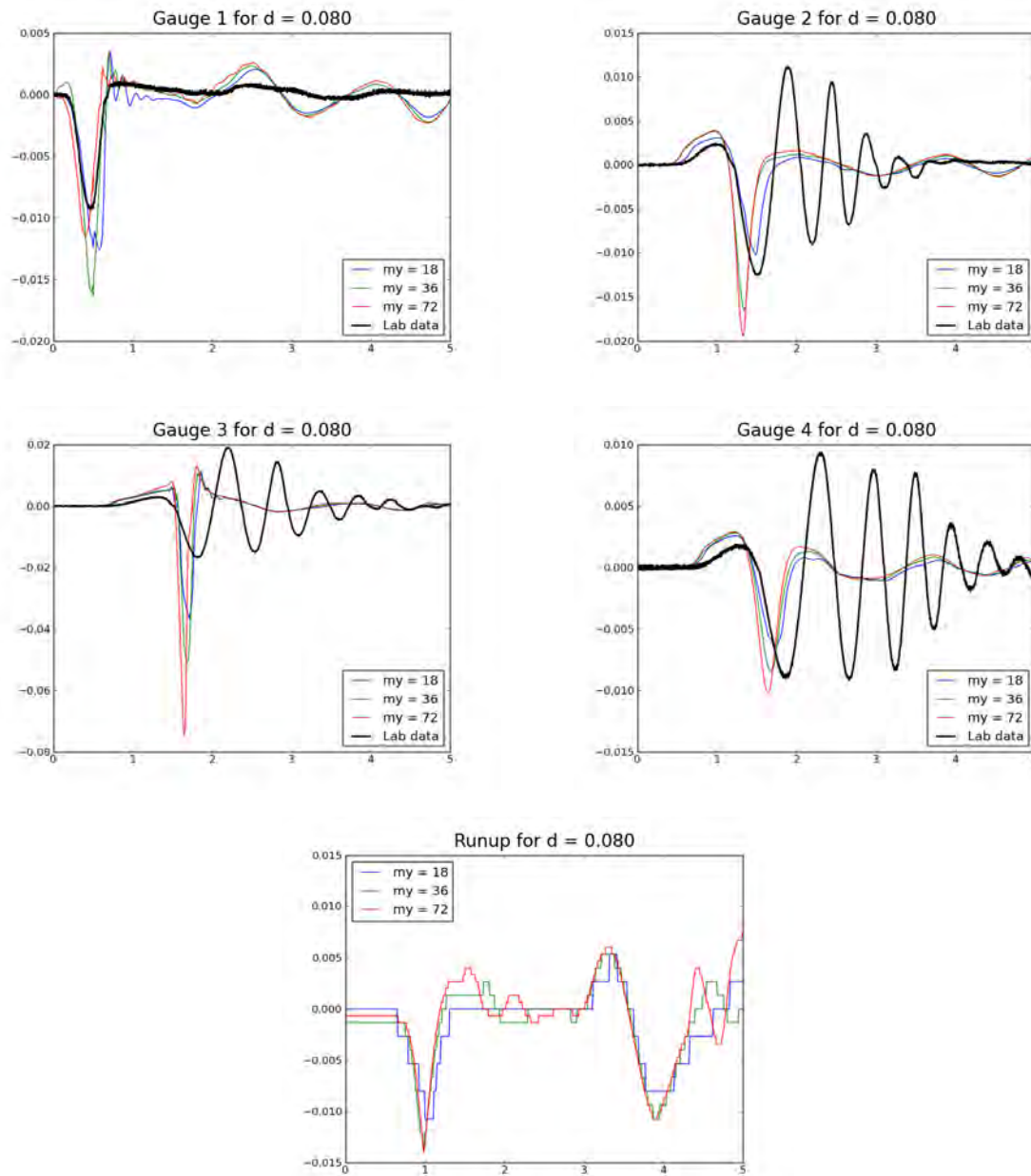


Figure 3.3.3: Gauge and runup results for $d = 0.08$.

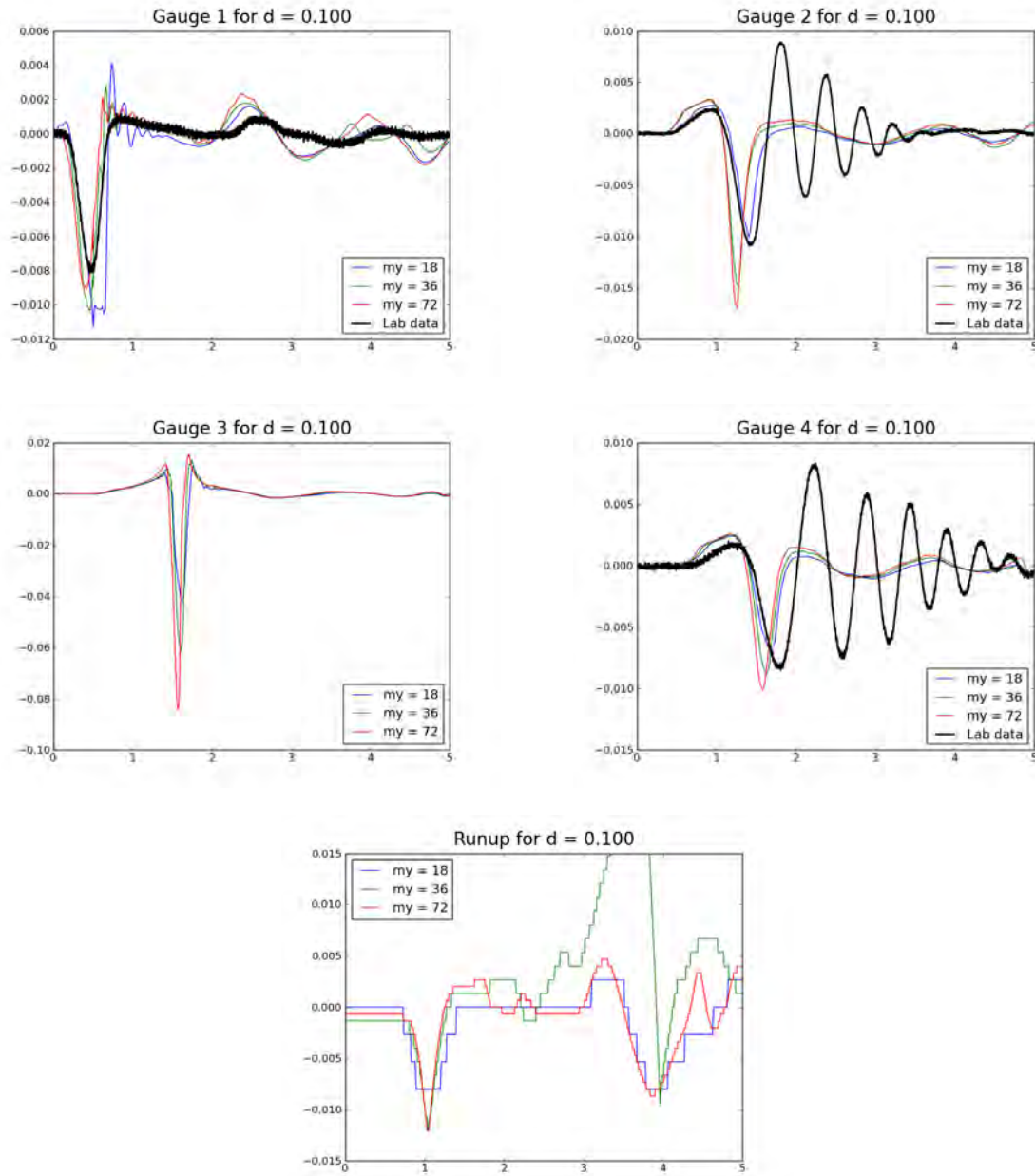


Figure 3.3.4: Gauge and runup results for $d = 0.1$.

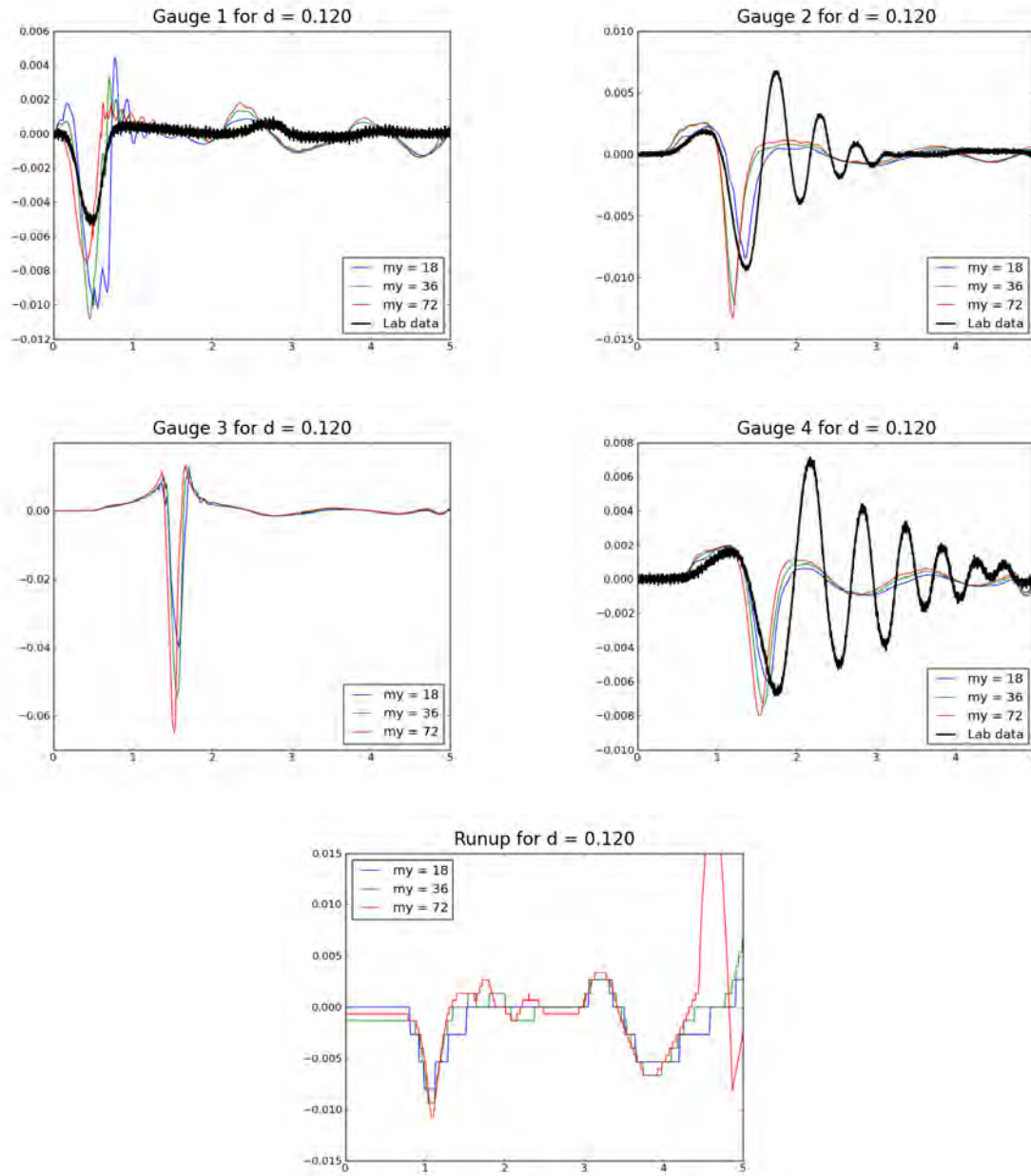


Figure 3.3.5: Gauge and runup results for $d = 0.12$.

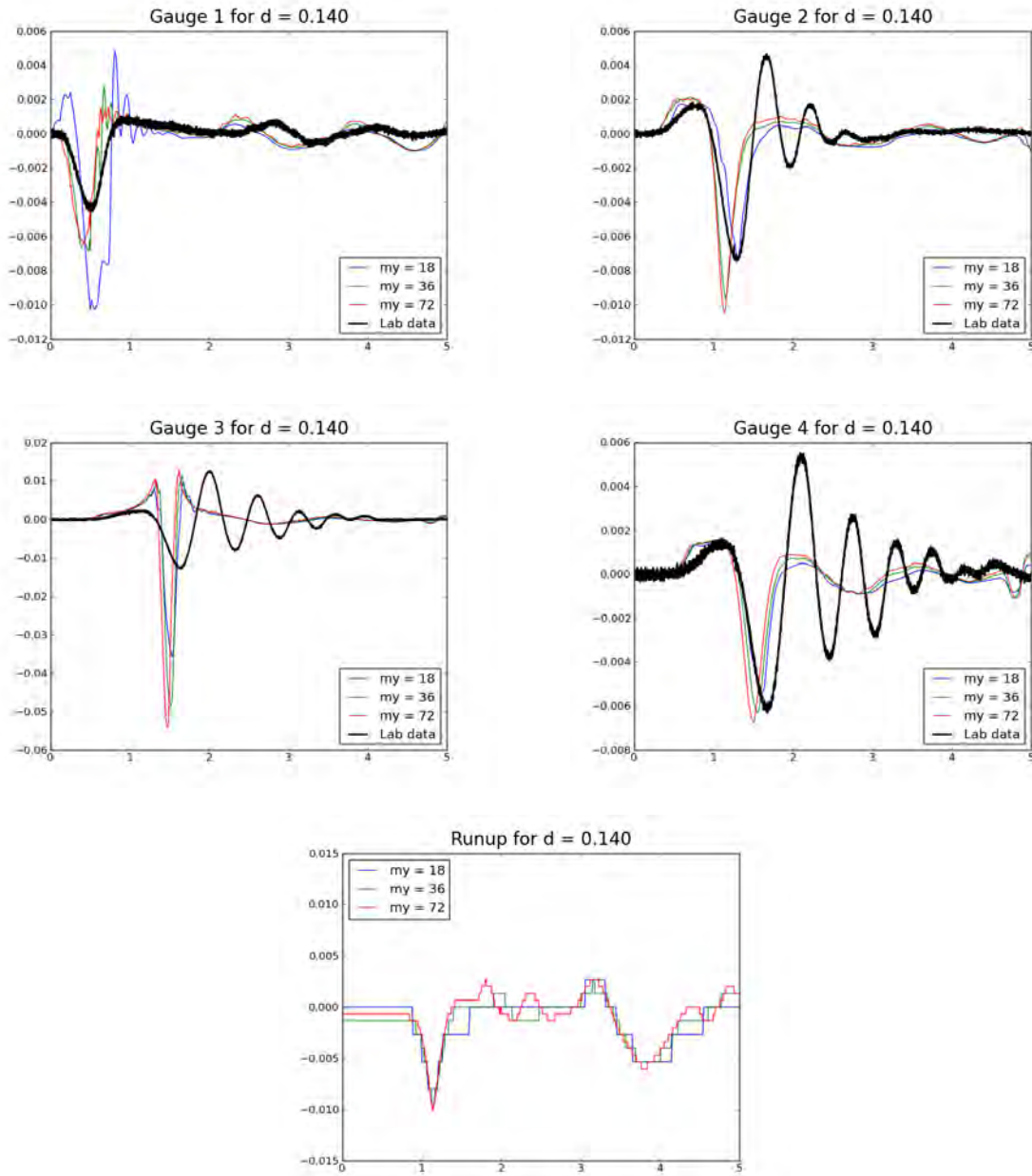


Figure 3.3.6: Gauge and runup results for $d = 0.14$.

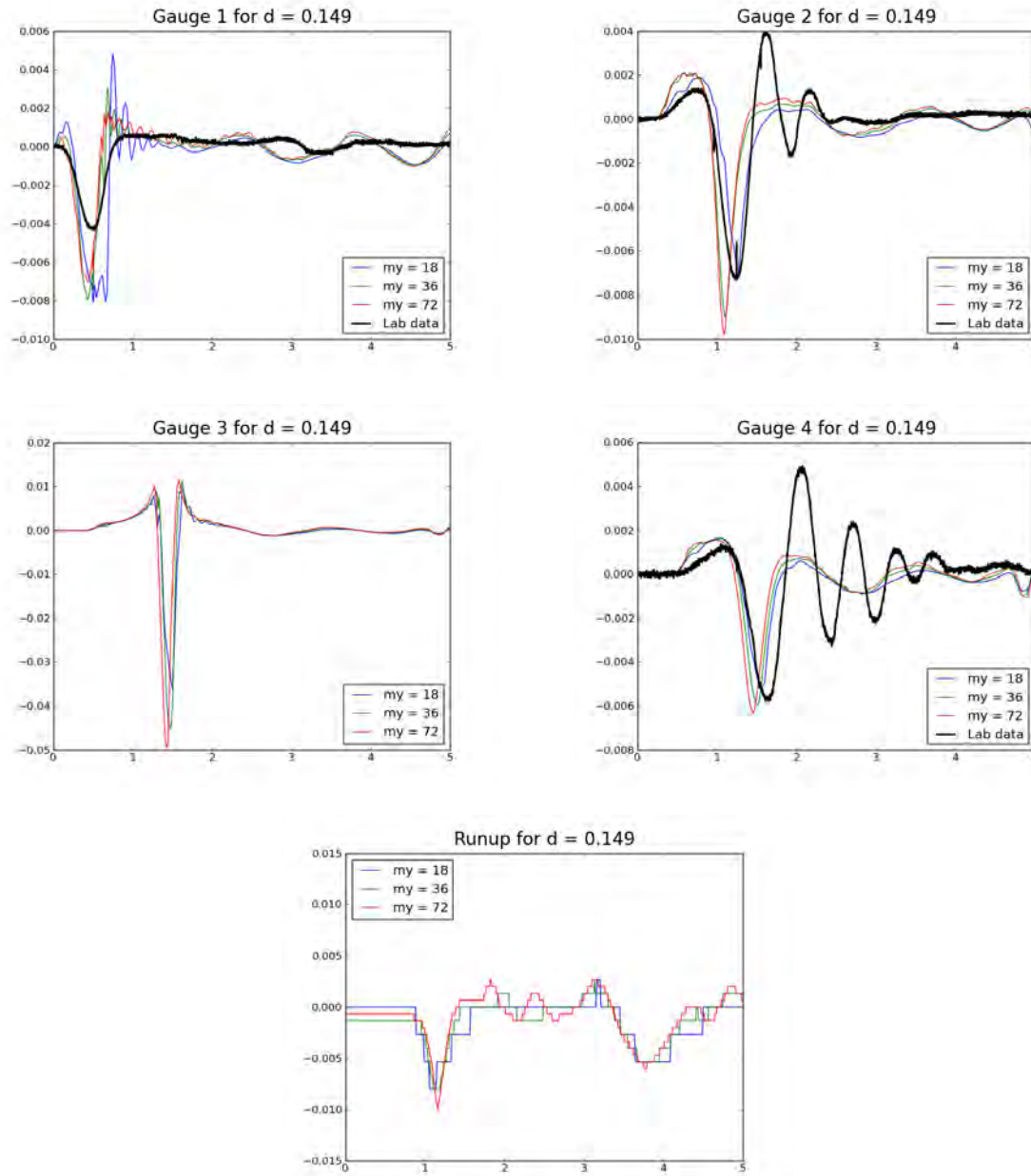


Figure 3.3.7: Gauge and runup results for $d = 0.149$.

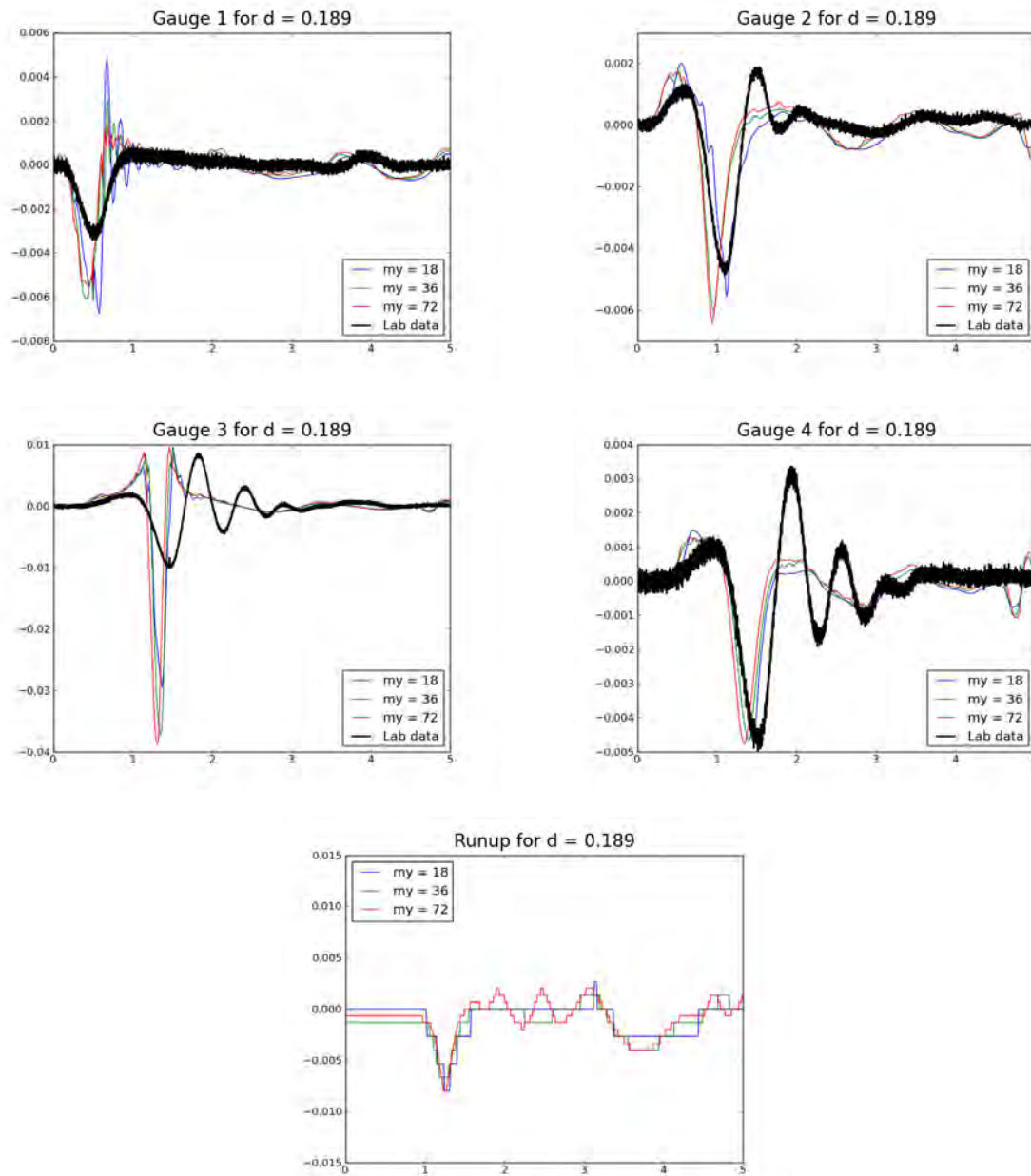


Figure 3.3.8: Gauge and runup results for $d = 0.189$.

3.4 BP 4: Single wave on simple beach (Laboratory)

Documentation:

- PMEL-135, pp 5 & 30-33
- Problem description provided by Y. Joseph Zhan, at [3].

3.4.1 Description

This benchmark is the laboratory counterpart to BP1 (Single wave on a simple beach: Analytic). A wave tank at the California Institute of Technology in Pasadena was used. The tank was 31.73 m long, 60.96 cm deep, and 39.97 cm wide; the bottom of the tank consisted of painted stainless steel plates. An instrument carriage was mounted on rails that ran along the entire length of the tank, permitting the arbitrary positioning of measurement sites. A ramp was installed at one end of the tank to model the bathymetry of the canonical beach configuration – i.e., a constant-depth region adjoining a sloping beach. The beach ramp was sealed to the tank side walls and the beach slope corresponded to angle $\beta = \text{arccot}(19.85)$ Figure 3.4.1 presents the computational domain used in this test.

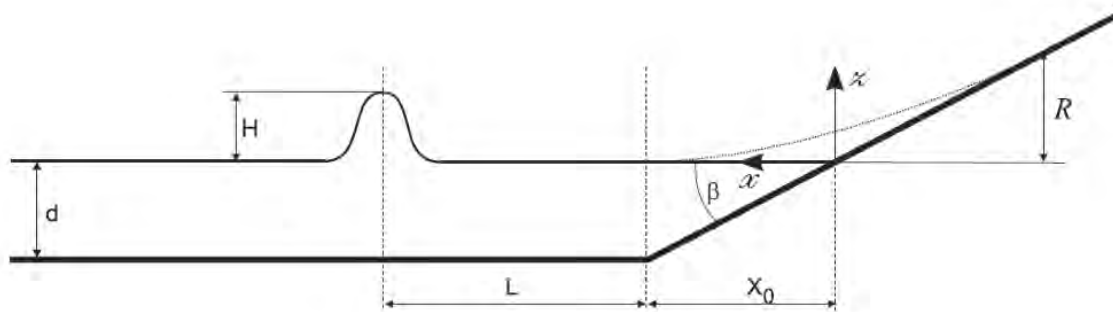


Figure 3.4.1: Schematic of computational domain.

3.4.2 Tasks

- a. Compare numerically calculated surface profiles at $t/T=30:10:70$ for the non-breaking case $H/d=0.0185$ with the lab data.
- b. Compare numerically calculated surface profiles at $t/T=15:5:30$ for the breaking case $H/d=0.3$ with the lab data
- c. (Optional) Demonstrate the scalability of the code by using different d
- d. Compute maximum runups for at least one non-breaking and one breaking wave case.

3.4.3 Problems encountered

- Problems that prevented completion of the benchmark were not encountered.

3.4.4 What we did

- Used $g = 1$ and no friction.
- The bathymetry consisted of a deep plateau of constant depth d connected to a sloping beach of angle $\beta = \text{arccot}(19.85)$. Note that the toe of the beach was located at $x = X_0 = d \cot \beta$
- The initial waveform of the wave was given by

$$\eta(x, 0) = H \text{sech}^2(\gamma(x - X_1)/d) \quad (3.4.1)$$

where $L = \text{arccosh}(\sqrt{(20)})/\gamma$, $X_1 = X_0 + L$, and $\gamma = \sqrt{(3H/4d)}$. The speed of the wave is given by:

$$u(x, 0) = -\sqrt{g/d}\eta(x, 0) \quad (3.4.2)$$

- For the low amplitude case, we set $d = 1$ cm, $H = 0.0185$ cm, and ran the computations on an 800×2 grid, where the x domain spanned from $x = -10$ to $x = 60$.
- For the high amplitude case, we set $d = 1$ cm, $H = 0.3$ cm, and ran the computations on a 1200×2 grid, where the x domain spanned from $x = -10$ to $x = 60$.
- We allowed variable time stepping based on a CFL number of 0.9

3.4.5 Results

- Tasks a and b: Figures 3.4.2 and 3.4.3 present the computed and measured surface profiles for the low and high amplitude cases, respectively. Correspondence is excellent in the low amplitude case. In the high amplitude case the computed amplitude is smaller and the steepness greater than that of the measured wave – a consequence of the fact that the experimental parameters violate the shallow water wave assumptions.
- Task c: This optional task was not addressed.
- Task d: Figures 3.4.4 and 3.4.5 present the results for maximum runup computations for the low amplitude and high amplitude wave cases. The results can be expressed as the non-dimensional data pairs $(H/d, R/d) = (0.0185, 0.085)$ and $(0.3, 0.42)$ for the high and low amplitude cases, respectively. The low amplitude result falls well within the scatter plot results of Zhan [3] presented in Figure 3.4.6, while the high amplitude result falls somewhat below, as might be expected in light of the comments made in the Task a and b discussion, above.

3.4.6 Lessons learned

For test cases in which amplitudes are so large that the shallow water wave assumptions are violated, it can be expected that computed and observed wave height and runup will not agree as well as in cases characterized by amplitudes for which the shallow water wave assumptions are valid.

For the high-amplitude $H/d = 0.3$ case, our observed runup of 0.42 agrees well with the experimental results shown in Figure 3.4.6.

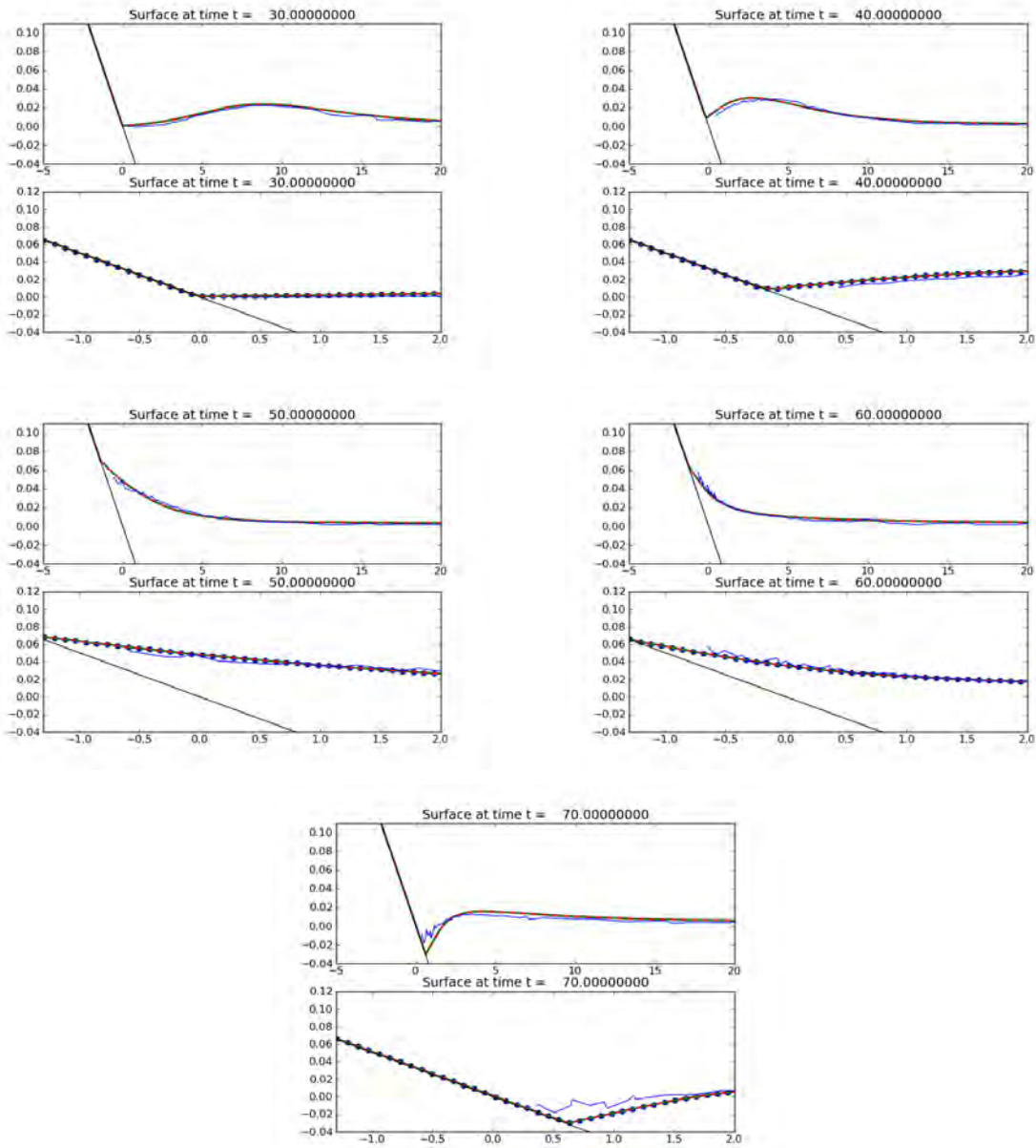


Figure 3.4.2: Runup computations for the low amplitude case. In the paired plots for each time value, the bottom frame provides a zoomed view of the inundation area for the incident wave presented in the top frame.

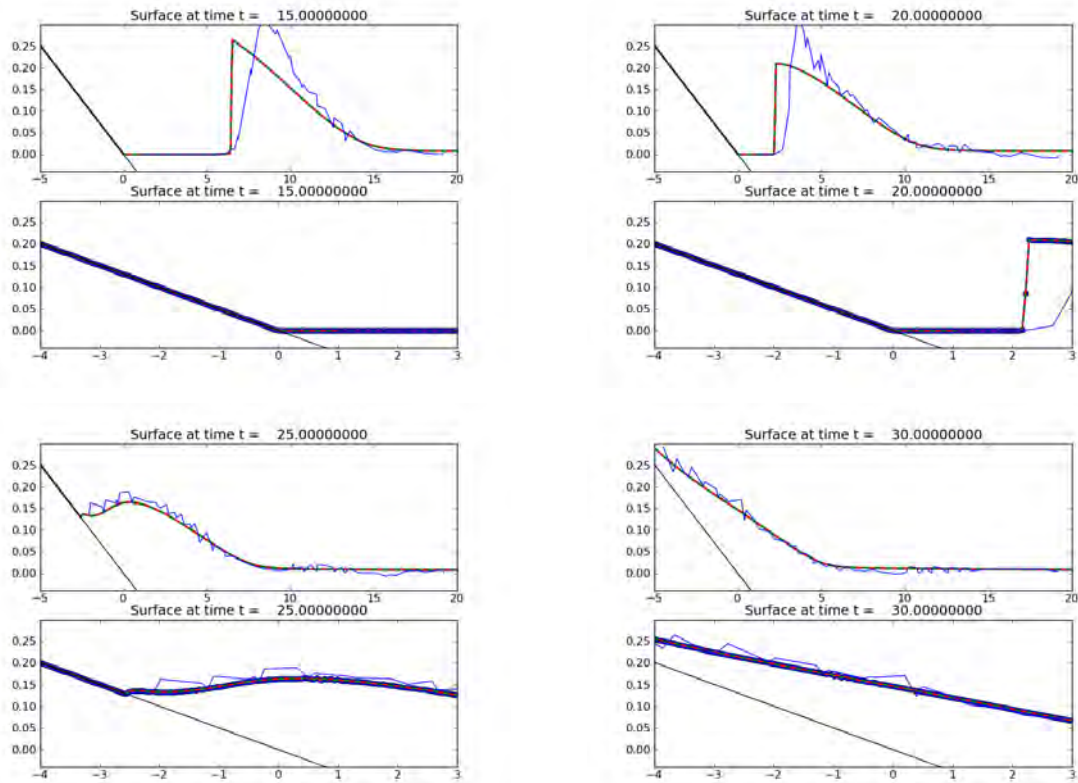


Figure 3.4.3: Runup computations for the high amplitude case. In the paired plots for each time value, the bottom frame provides a zoomed view of the inundation area for the incident wave presented in the top frame.

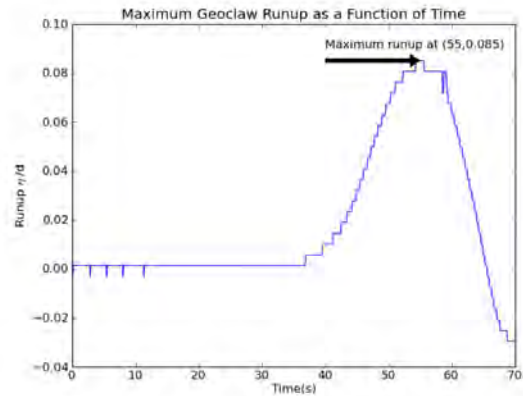


Figure 3.4.4: Maximum runup estimate of 0.085 cm for the low amplitude case, occurring at 55 seconds of the computation.

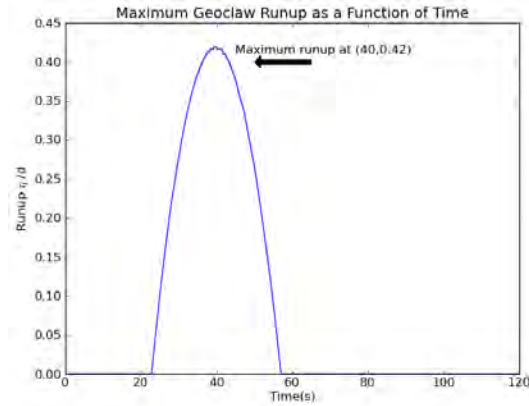


Figure 3.4.5: Maximum runup estimate of 0.42 cm for the high amplitude case, occurring at 40 seconds of the computation.

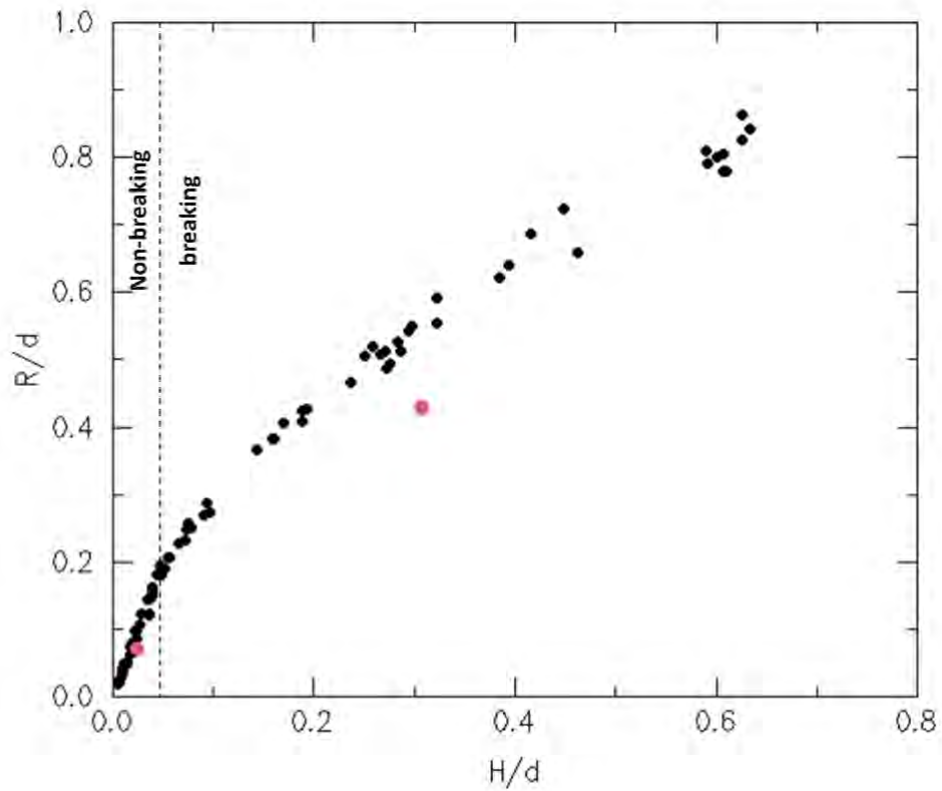


Figure 3.4.6: Scatter plot of nondimensional maximum runup, R/d , versus nondimensional incident wave height, H/d , resulting from a total of more than 40 experiments conducted by Y. Joseph Zhan and described at [3].

3.5 BP 5: Solitary wave on composite beach (Laboratory)

3.5.1 Problem specification

- PMEL-135, pp 6 & 37-39.
- Problem description provided by Elena Tolkova at [3]:
BP05-ElenaT-Solitary_wave_on_composite_beach_laboratory/BP5_description.pdf
- Coastal Hydraulics Laboratory Problem Description[9]

This is the same problem as in BP 2, but using the nonlinear shallow water equations and comparing to laboratory data rather than to the analytic solution of the linear equations.

3.5.2 What we did

- We solved the shallow water wave equation in Cartesian coordinates with $g = 9.81$ and no friction.
- To specify the incoming wave from the left boundary of our computational domain we used the first ten seconds of measurements taken at Gage 4. After ten seconds the left boundary switched to be a non-reflecting boundary. This boundary is selected since the end of our computational domain is not the end of the physical wave tank. The implementation of these boundary conditions is described in Section 2.3.
- We solved on a 600×2 grid with no adaptive mesh refinement.

3.5.3 Gage comparisons

The results for cases A, B, and C are shown in figures Figure 3.5.1, Figure 3.5.2, Figure 3.5.3 respectively where Gage 11 is placed at the vertical wall.

3.5.4 Convergence Study

We performed a test to see how well Clawpack converged to the gage measurements as we increased the number of grid cells in our computational domain. We found that as the number of grid cells was increased that the computed solution converged and had a shock in approximately the same location as in the gage data. The results shown in figure Figure 3.5.4.

3.5.5 Lessons learned

In this benchmark problem we found that using the measured data from Gage 4 as boundary conditions on a shorter domain, starting at this Gage, provided more accurate results than using the wave maker position and a longer domain to model the entire tank. It appears that a similar assumption is made in the provided analytic solutions, as they match up nearly perfectly with the lab data for the first ten seconds.

Overall this benchmark problem is a good test for one dimensional codes. Case C exhibits dispersion in the laboratory results not seen with the nonlinear shallow water equations.

The benchmark problem specifications could be improved by specifying the computational domain and the specific data source that should be used to model the incoming wave.

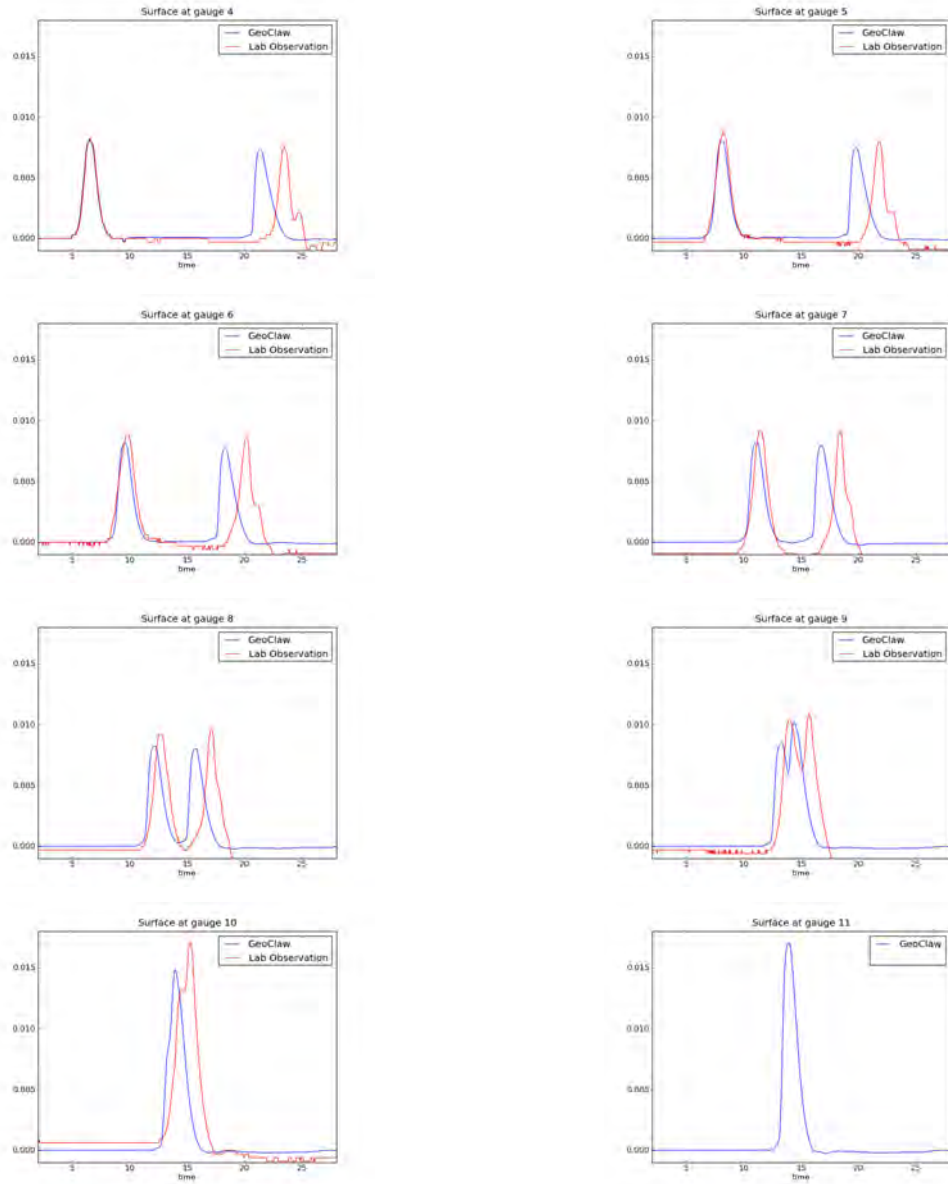


Figure 3.5.1: Case A

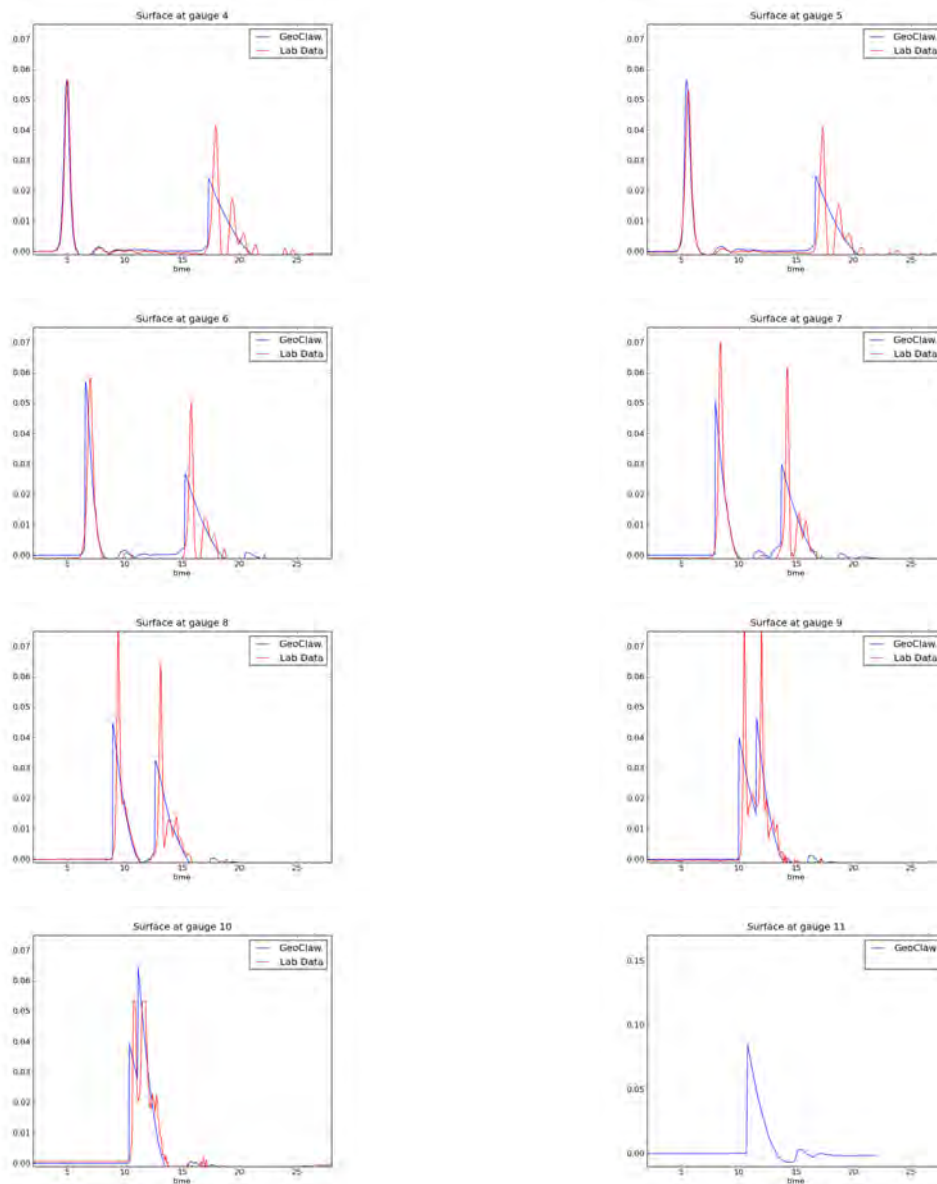


Figure 3.5.2: Case B

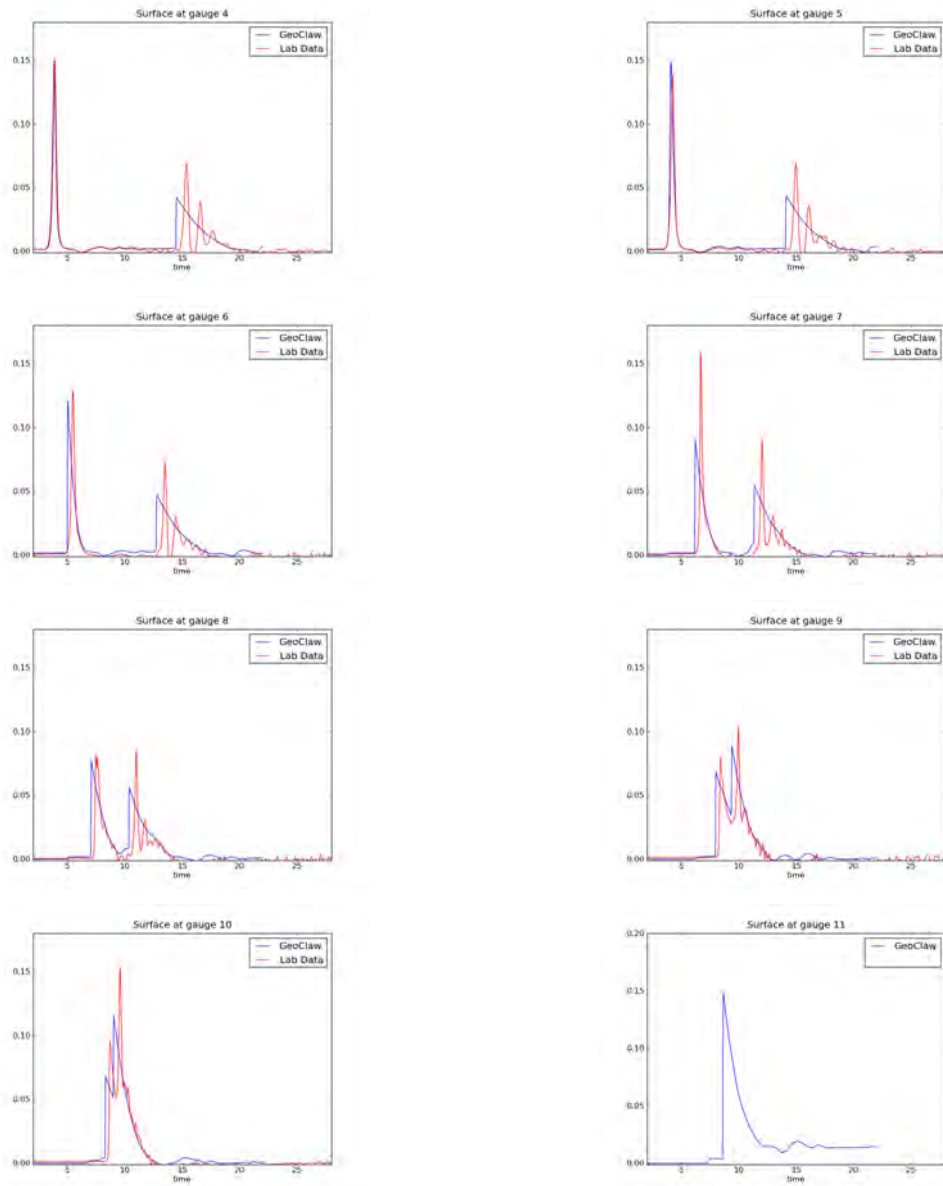


Figure 3.5.3: Case C

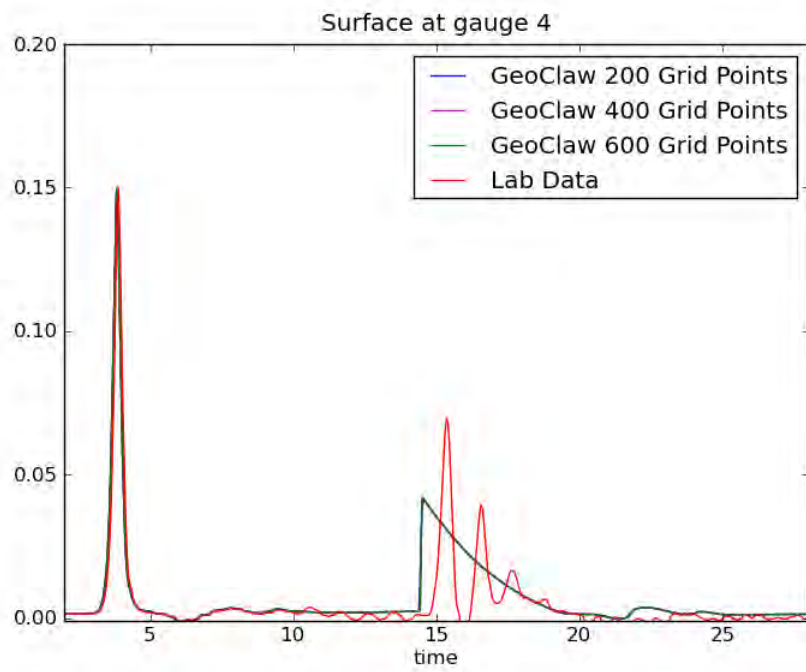


Figure 3.5.4: Convergence Plot for Gage 4 in Case C

3.6 BP 6: Solitary wave on a conical island (Laboratory)

Documentation:

- The Corps of Engineers website is the primary documentation for this benchmark problem: <http://chl.erd.c.usace.army.mil/chl.aspx?p=s&a=Projects;35>
- A problem description is also provided by Frank González at [3]: BP06-FrankG-Solitary_wave_on_a_conical_island/Description.pdf
- Numerous other publications also describe this experiment, in varying detail: [40, 10, 36, 11, 35, 12, 16]

3.6.1 Description

The goal of this Benchmark Problem (BP) is to compare computed model results with laboratory measurements obtained during a physical modeling experiment conducted at the Coastal and Hydraulic Laboratory, Engineering Research and Development Center of the U.S. Army Corps of Engineers. The laboratory physical model was constructed as an idealized representation of Babi Island in the Flores Sea, Indonesia, to compare with Babi Island runup measured shortly after the 12 December 1992 Flores Island tsunami [43].

3.6.2 Problems encountered

- Details of the laboratory setup and, therefore, the computational domain could not be determined by the available documentation (above). The version of the domain used in this report is presented in Figure 3.6.1; this specification of the domain was developed after personal communication with Michael Briggs, U.S. Army Corps of Engineers, who provided additional information on physical details of the laboratory experiment. Unfortunately, it is not certain that accurate specification of details of the laboratory setup have been resolved. In particular, the following items were not well documented and remain open to question: (a) the distance from the wavemaker face to the island center and (b) open gaps at each end of the wavemaker.
- Erroneous entries were found in data files ts2a.txt, ts2b.txt and ts2cnew1.txt. Several entries of the letter 'M' triggered read-in error messages; they were replaced by linear interpolation or extrapolation of neighboring values.
- Initial values for some laboratory data were non-zero, rather than the zero values expected for initial wave basin conditions corresponding to still water.

3.6.3 What we did

- Used $g = 9.81$ and no friction.
- Used the computational domain presented in Figure 3.6.1.

- Used open boundary conditions for the top, bottom and right walls, and for the gaps between the ends of the wavemaker and the top and bottom walls.
- Used inflow boundary conditions for the face of the wavemaker, as described in the Model Description section of this report.
- Simulated Cases A and C, each with three different grid sizes and resolution, to demonstrate convergence: 28 X 24 (100 cm), 56 X 47 (50 cm) and 223 X 185 (12.5 cm)
- Simulated optional Case B; the results are not presented here, but they were submitted for analysis and inclusion in the workshop summary report.
- An additional computational experiment was conducted to document the effect of varying two model parameters on the results – the Manning coefficient of friction (M) and the 'Dry Cell Depth' (DCD) threshold. Several values of each parameter were used in this experiment.

3.6.4 Results

Requirements of this benchmark test were to:

- Demonstrate that two wave fronts split in front of the island and collide behind it
- Demonstrate convergence of the solution as the computational grid is refined
- Compare computed water level with laboratory data for Cases A and C at gauges 1, 2, 3, 4, 6, 9, 16, and 22 (files ts2a.txt, ts2cnew1.txt).
- Compare computed island runup with laboratory gage data (files run2a.txt, run2c.txt)

The first benchmark requirement was satisfied, as seen in Figures 3.6.3 and 3.6.4. Thus, for Cases A & C we see in frames $t=30$ to $t=36$ seconds that the initial wave splits into two wave fronts in front of the island, which then collide behind the island.

The second benchmark requirement was satisfied, as seen in Figures 3.6.5, 3.6.6 and 3.6.7. The agreement between Lab and GeoClaw time series is seen to improve as the computational grid resolution is decreased from 100 to 12.5 cm. The most obvious manifestation of this convergence is the improved value of the first wave amplitude.

The third benchmark requirement is satisfied by the comparisons presented in Figures 3.6.8 and 3.6.7. Good agreement is seen overall and, in particular, between computed and measured time series for the first wave. The agreement for later wave details becomes progressively worse, as multiple reflections and refraction occur at the basin boundaries, the wavemaker face, and the island. Note that in some cases, the laboratory gage data are characterized by non-zero initial values, which would be expected in the case of an initial condition corresponding to still water in the wave basin (see, e.g., gauge 2 for Cases A and C).

The final benchmark requirement is satisfied by the runup values presented in Figures 3.6.9 and 3.6.10, in which good agreement is seen between the computed and measured runup on the conical island.

3.6.5 Sensitivity of runup to friction and 'Dry Cell Depth' parameters

Nine additional simulations of Case C were run on the 12.5 cm grid to test the sensitivity of computed runup values to variations in Manning's friction coefficient and the threshold depth for which a "Dry Cell" is identified by GeoClaw. The results are presented in Figure 3.6.11. We see that runup estimates can be significantly affected by changes in the value of each parameter. Because the friction term is a function of water depth, we also see that these effects vary spatially over the computational domain; for example, the frame (DCD,M)=(0.01, 0.0) provides the best fit for inundation values on the lower side of the conical island, but increasing the friction degrades this fit and improves the fit to runup measurements directly behind the conical island – see frames (DCD,M)=(0.01, 0.012) and (0.01, 0.025). Similar frictional effects are seen in the Okushiri Island Field Benchmark Problem, in which runup computations with $M=0.0$ and $M=0.25$ are compared with field observations (see Figure 3.9.7).

3.6.6 Lessons learned

- Accurate specification of the computational domain is essential, and every effort should be made to acquire this information.
- Results demonstrate that the long wave equations are adequate to describe the major features of propagation, refraction and runup observed in the laboratory experiment.
- Even with the unresolved details of the computational domain and lab data (i.e., non-zero initial values) the available data still provide a good benchmark test.
- Both the friction and the dry cell depth parameters have a significant, spatially variable, effect on runup computations.

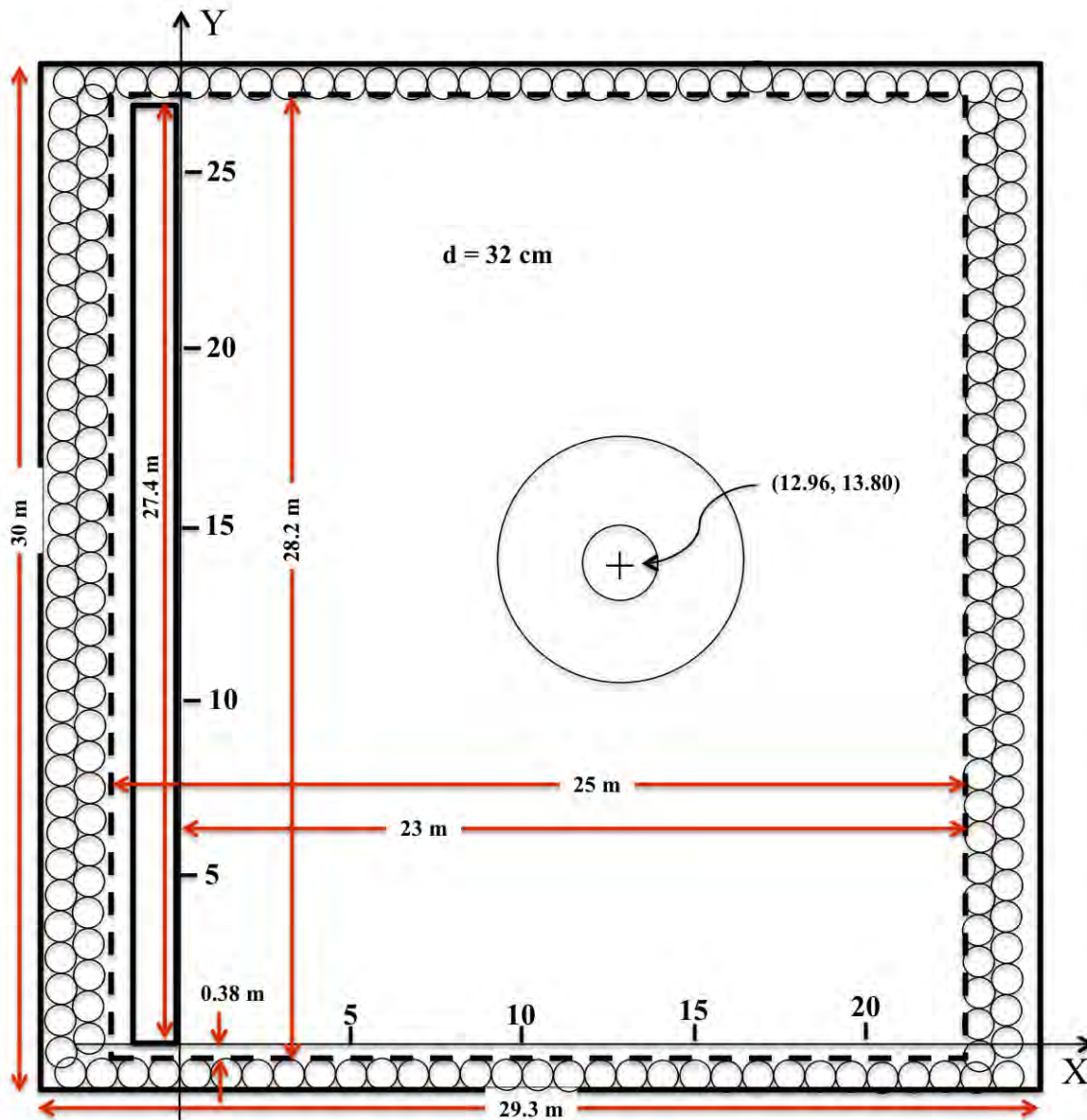


Figure 3.6.1: Basin geometry and coordinate system. Solid lines represent approximate basin and wavemaker vertical surfaces. Circles along walls and dashed lines represent rolls of wave absorbing material. Note the gaps of approximately 0.38 m between each end of the wavemaker and the adjacent wall. Gage positions are given in Figure 3.6.2.

Gage ID	X, m	Y, m	Z, cm	Comment
1	A: 5.76 B: 6.82 C: 7.56	16.05	32.0	Incident gage
2		14.55	32.0	
3		13.05	32.0	
4		11.55	32.0	
6	9.36	13.80	31.7	270 deg transect
9	10.36	13.80	8.2	
16	12.96	11.22	7.9	0 deg transect
22	15.56	13.80	8.3	90 deg transect

Figure 3.6.2: Coordinates of laboratory gauges 1, 2, 3, 4, 6, 9, 16, and 22.

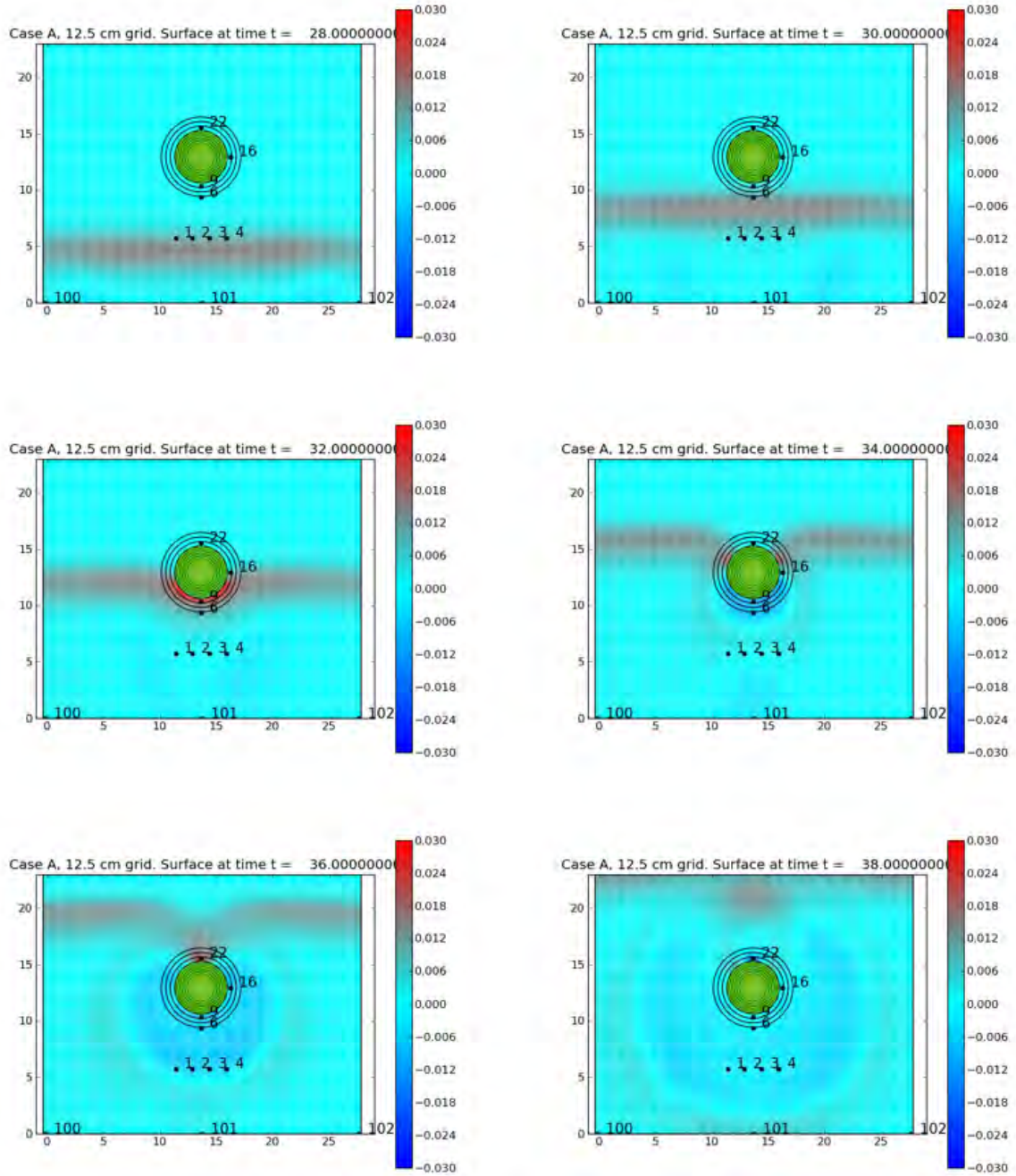


Figure 3.6.3: Animation snapshots of Case A for 12.5 cm resolution computational grid.

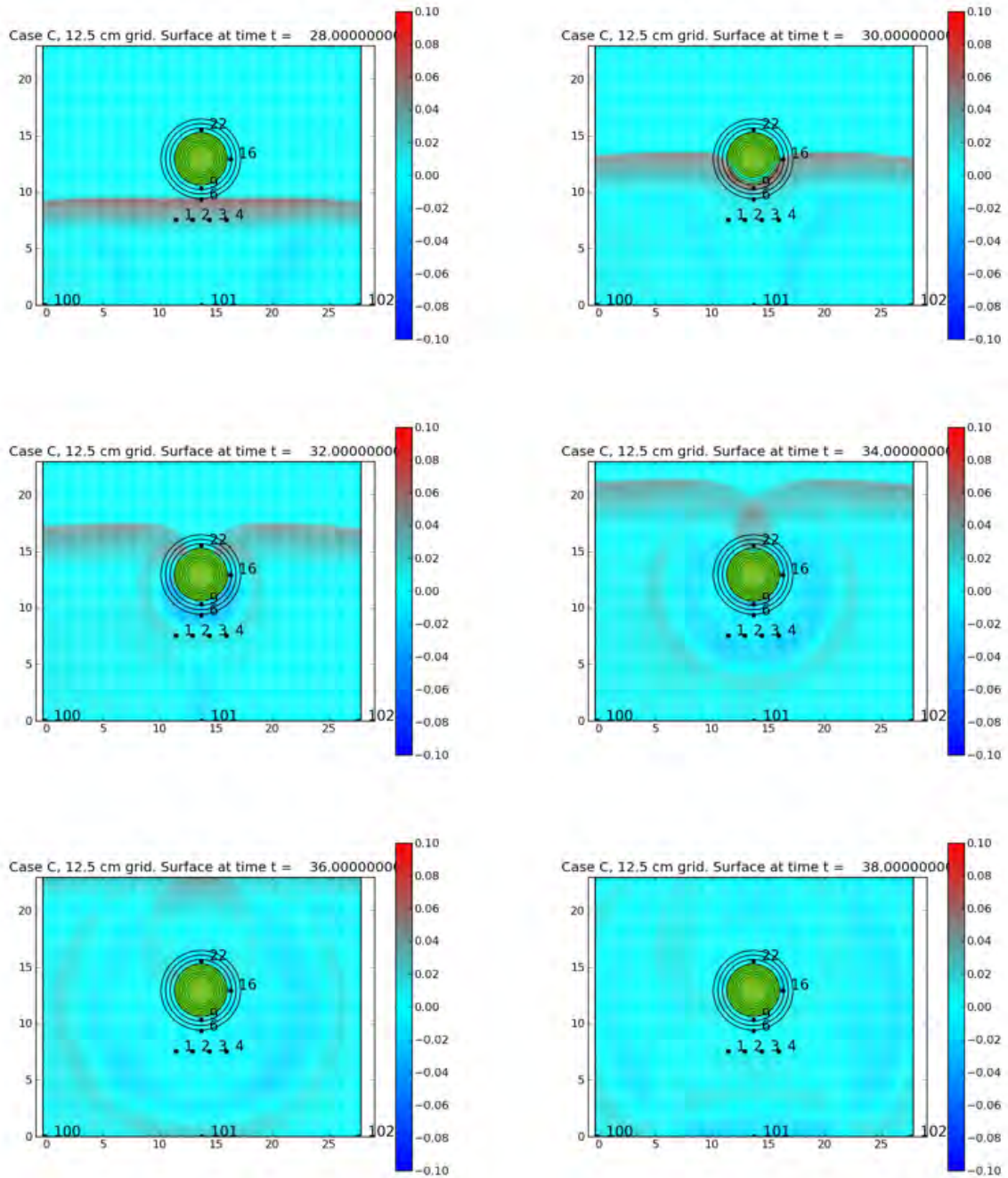


Figure 3.6.4: Animation snapshots of Case C for 12.5 cm resolution computational grid.

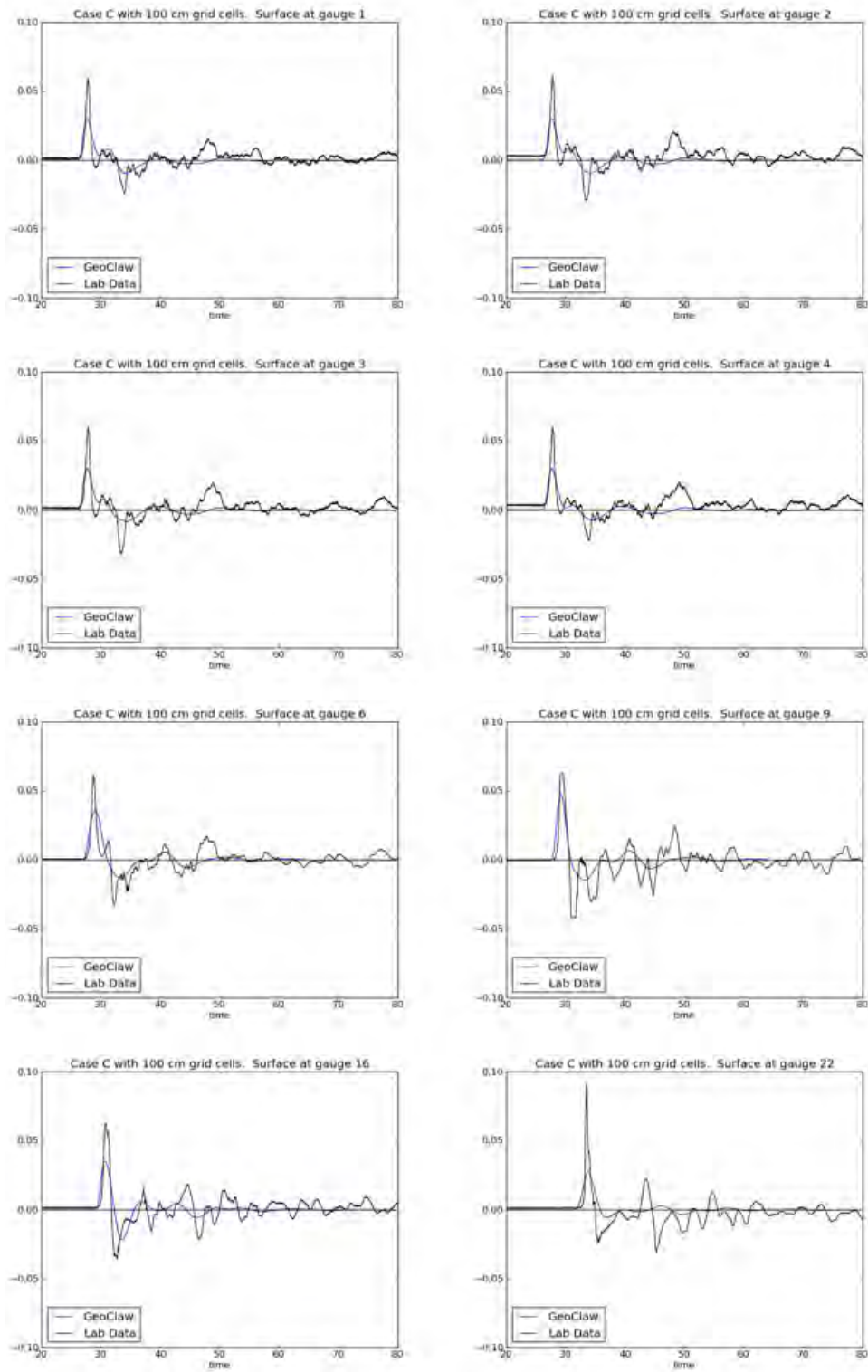


Figure 3.6.5: Comparison of laboratory gauge and GeoClaw time series for Case C, 100 cm resolution computational grid.

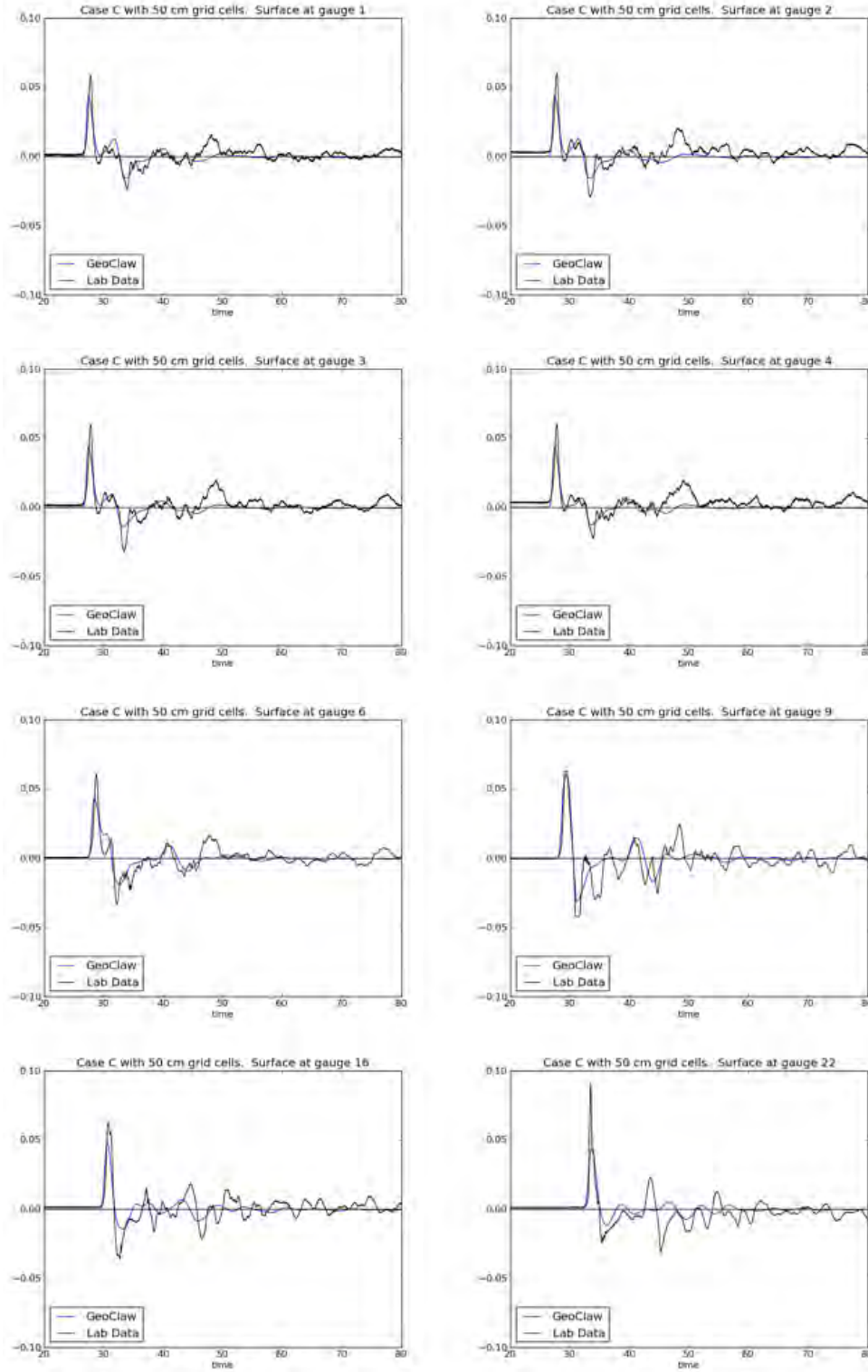


Figure 3.6.6: Comparison of laboratory gauge and GeoClaw time series for Case C, 50 cm resolution computational grid.

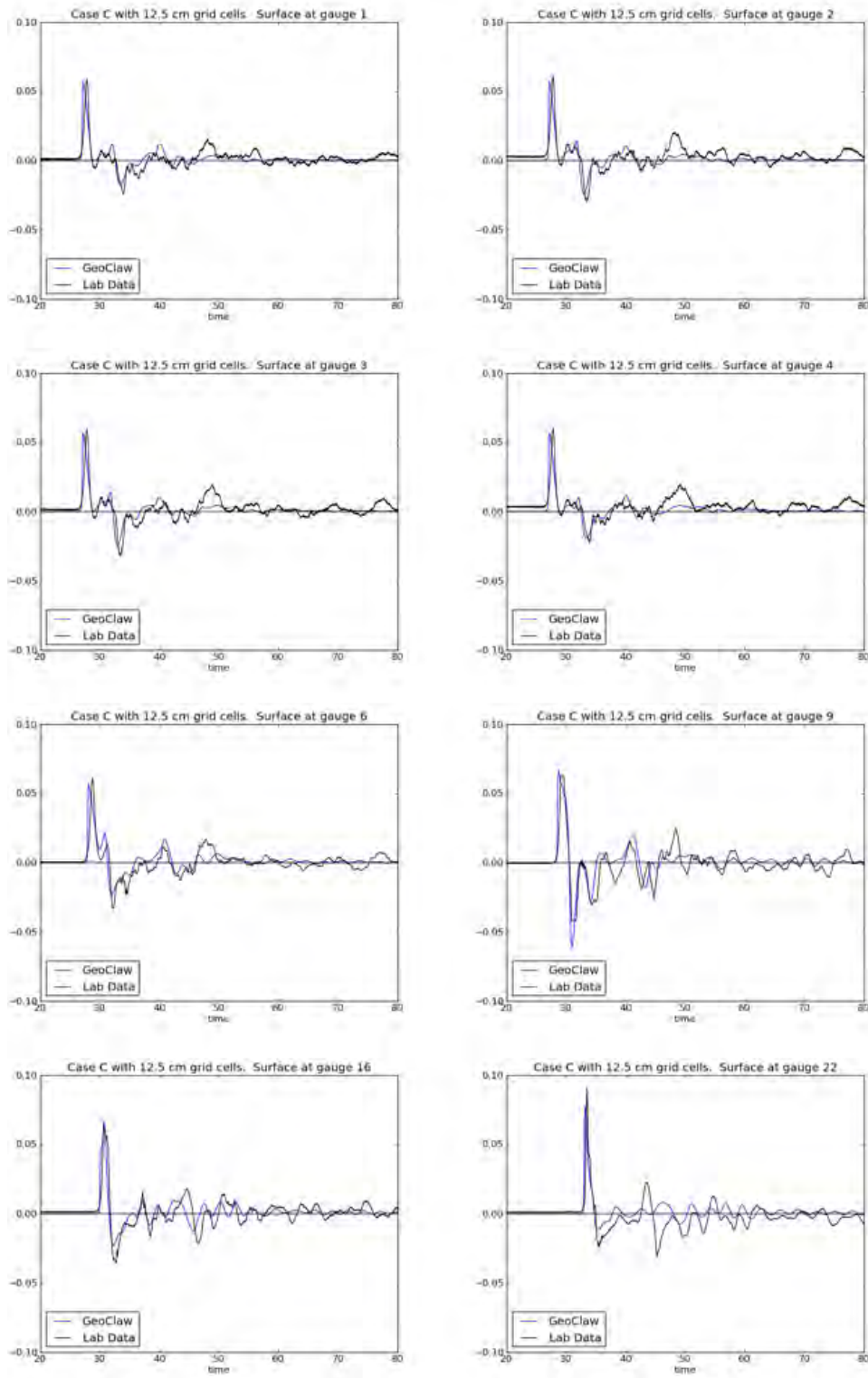


Figure 3.6.7: Comparison of laboratory gauge and GeoClaw time series for Case C, 12.5 cm resolution computational grid.

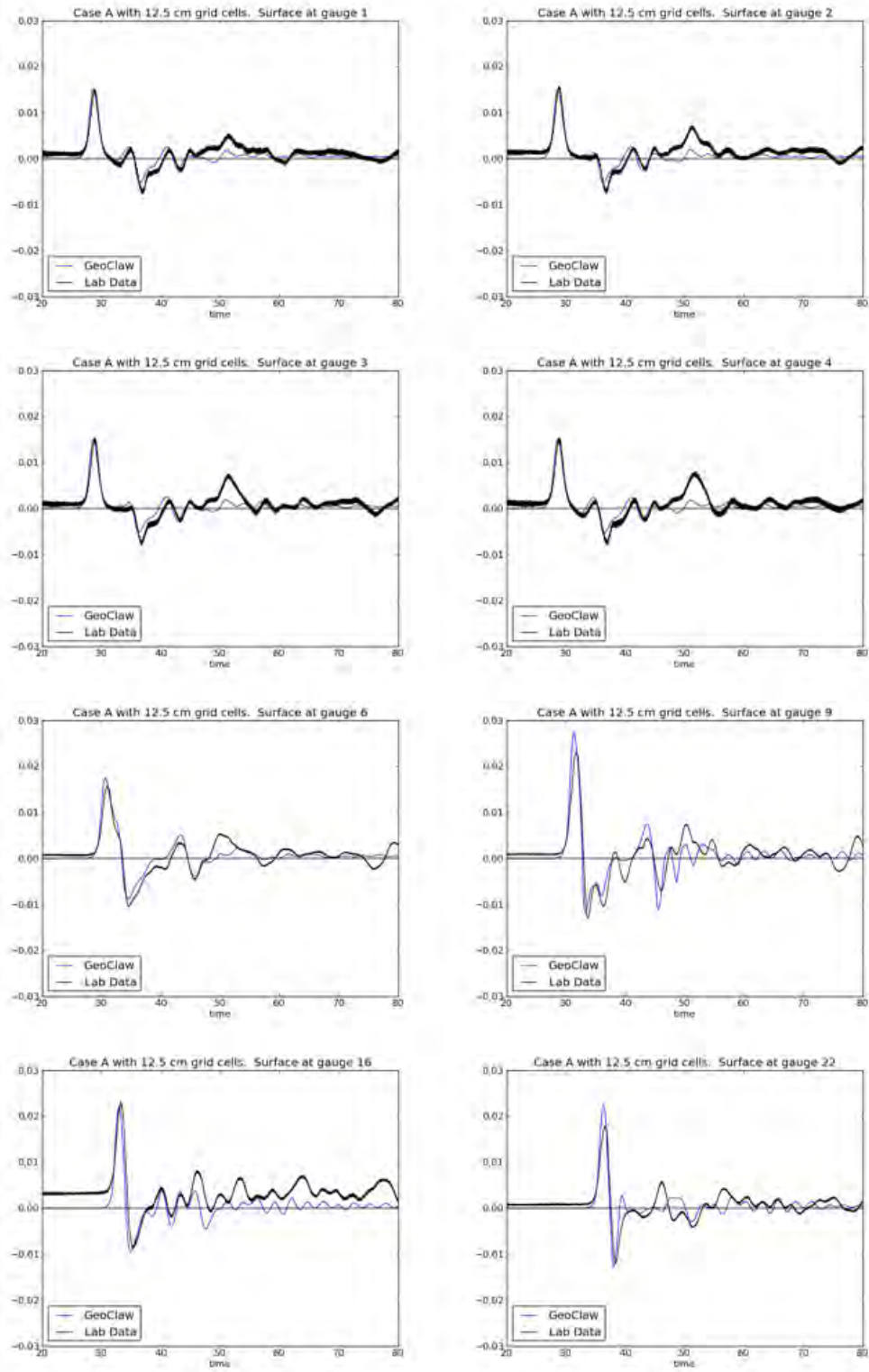


Figure 3.6.8: Comparison of laboratory gauge and GeoClaw time series for Case A, 12.5 cm resolution computational grid.

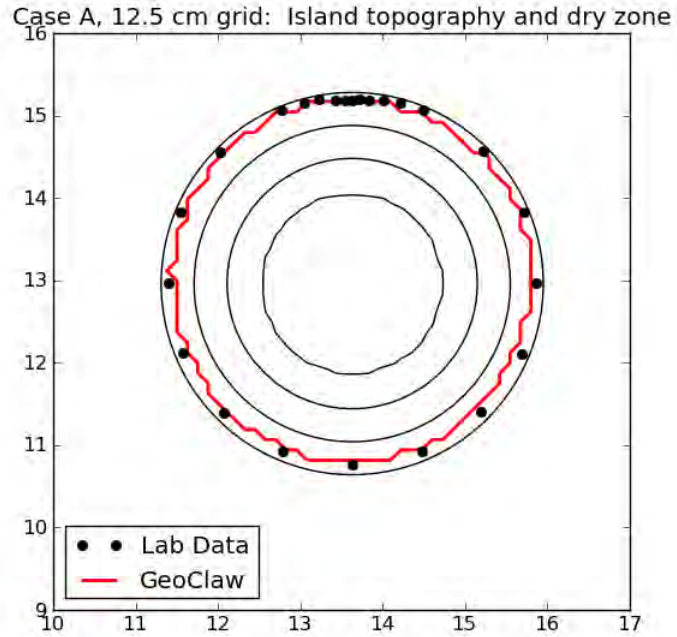


Figure 3.6.9: Island runoff for Case A, using a 12.5 cm resolution computational grid.

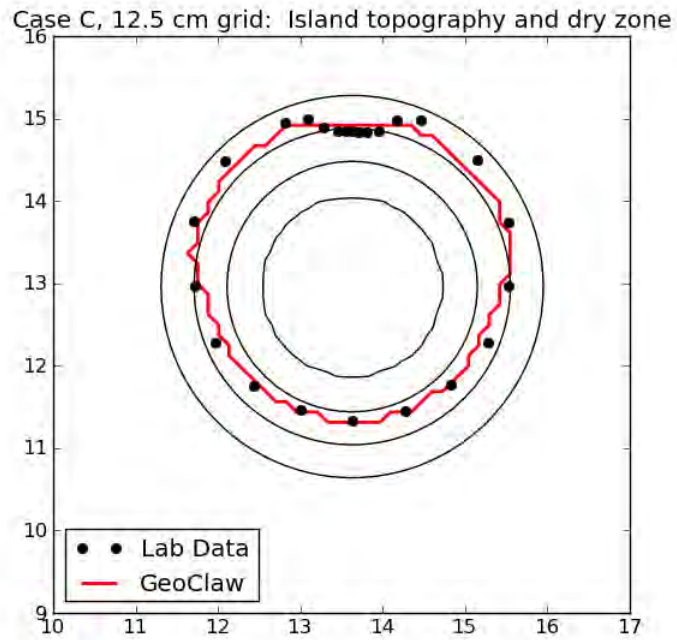


Figure 3.6.10: Island runoff for Case C, using a 12.5 cm resolution computational grid.

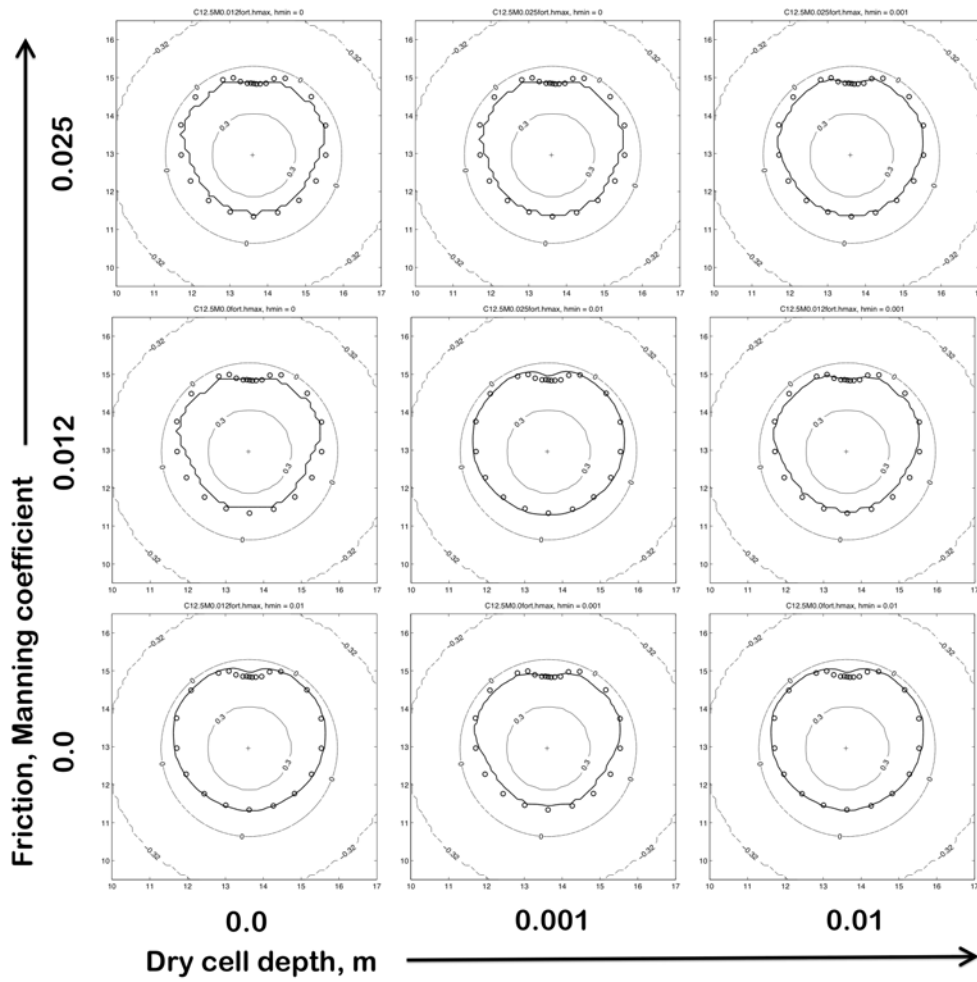


Figure 3.6.11: Island runup for Case C on a 12.5 cm grid, for differing values of Manning's friction coefficient, M , and the 'Dry Cell Depth', DCD, threshold.

3.7 BP 7: Monai valley beach (Laboratory)

3.7.1 Problem specification

- PMEL-135, pp 6 & 45-46.
- Problem description provided by Dmitry Nicolsky, at [3]:
BP07-DmitryN-Monai_valley_beach/description.pdf
- The original experiment is fully described by Matsuyama and Tanaka [38].

3.7.2 What we did

- We solved the nonlinear shallow water equations in Cartesian coordinates with $g = 9.81$ and no friction.
- We used the given initial wave to specify a boundary condition at the left boundary up to time 20. This was done by filling ghost cells each time step at the left edge of the computational domain with depth values interpolated from the given time trace at $x = 0$. Momentum values were determined as described in Section 2.3.3.
- After time 20, the boundary condition procedure switched to non-reflecting boundary conditions (see Section 2.3.1) at the left boundary, so reflected waves exit. (Note that the wave tank was much longer than computational domain specified.)
- We solved on 423×243 grid (same as bathymetry), with no adaptive mesh refinement. Solid wall boundary conditions were used at the top and bottom.
- We also solved on 211×121 grid, coarser by roughly a factor of 2, for comparison as a test of convergence.

3.7.3 Gauge comparisons

Figure 3.7.1 shows a comparison of the GeoClaw results with the laboratory values at the three gauges requested, with both grid resolutions. The two resolutions give very comparable results, indicating that the solution presented is close to a converged solution of the shallow water equations. The results are in general a good match to the laboratory measurements.

3.7.4 Frame comparisons

See Figure 3.7.2 and Figure 3.7.3 for comparisons of the Frames 10, 25, 40, 55, and 70 from the overhead movie with GeoClaw results at roughly corresponding times. These results are from the 423×243 grid (same as given bathymetry).

The movie had a rate of 30 fps, so the frames are 0.5 seconds apart. However, it is not clear what the starting time was for Frame 1 relative to the simulation time. In the Benchmark Description [3], it is stated that “frame 10 approximately occurs at 15.3 seconds”, but then later

“it is recommend that each modeler find times of the snapshots that best fit the data”. We found reasonably good agreement starting at 15.0 seconds for Frame 1 and then taking 0.5 second increments, as shown in Figure 3.7.2 and Figure 3.7.3.

The yellow dashed lines on the frames from the movie show the approximate shoreline (and were provided as part of the benchmark specification [3]). The actual shoreline location is of course somewhat ambiguous in the movie, and also in the computation. The figures of the GeoClaw computation show the shoreline two different ways:

- The cells colored blue are finite volume cells where the fluid depth is greater than 0.0001 m. Those colored green have less fluid or are dry.
- The black dashed line is a contour line where depth = 0.002 m, which agrees better with the movie frames and might be a depth that can actually be detected in the movie frames.

3.7.5 Runup in the valley

The file `OBS_RUNUP.txt` from the benchmark specification contains the runup at 3 locations as observed in 6 runs of the same wavetank experiment. The relevant location for runup in the valley is the first point at $x = 5.1575, y = 1.88$ m. The six values given are 0.0875, 0.09, 0.08, 0.09, 0.1, 0.09, with an average value of approximately 0.09.

In the computation, the maximum runup was observed at time $t \approx 16.5$. This frame is shown in Figure 3.7.4 with a white dot at the location $x = 5.1575, y = 1.88$ and several contour levels marked. The contour lines are at levels 0.01 m apart. The maximum runup appears to be around 0.08 to 0.10 meters depending on what water depth is used to judge.

3.7.6 Lessons learned

- This problem has data that is fairly well specified, and has wave tank geometry that scales up to a reasonable physical tsunami problem (since it was designed by scaling down a physical problem).
- Solutions to the shallow water equations fit the data quite well, as found both in our experiments and by other modellers. This gives a reassuring test of the validity of shallow water equations for real tsunamis.

This benchmark problem appears to be a good test for tsunami models. It has been widely used and many models have been shown to give results that agree quite well with the laboratory measurements.

- The laboratory test also appears to agree very well with the actual tsunami it was designed to model. Compare Figure 3.7.4 to Figure 3.9.9.
- The benchmark problem specification could be improved by specifying the computational grid(s) that are to be used. We show results for a grid that matches the resolution of the bathymetry provided and a second computation at half the resolution, but this should be specified as part of the problem.

- The input data only goes out to 20 seconds. The first waves are modeled well, but later waves in the laboratory data (not shown here) are not seen in the computation. If a longer time history was provided for the input data, it may be possible to match later waves better. Note that the computational domain is only part of the wave tank, which was 205 m long [38]. Presumably it is impossible to obtain more data at this point.

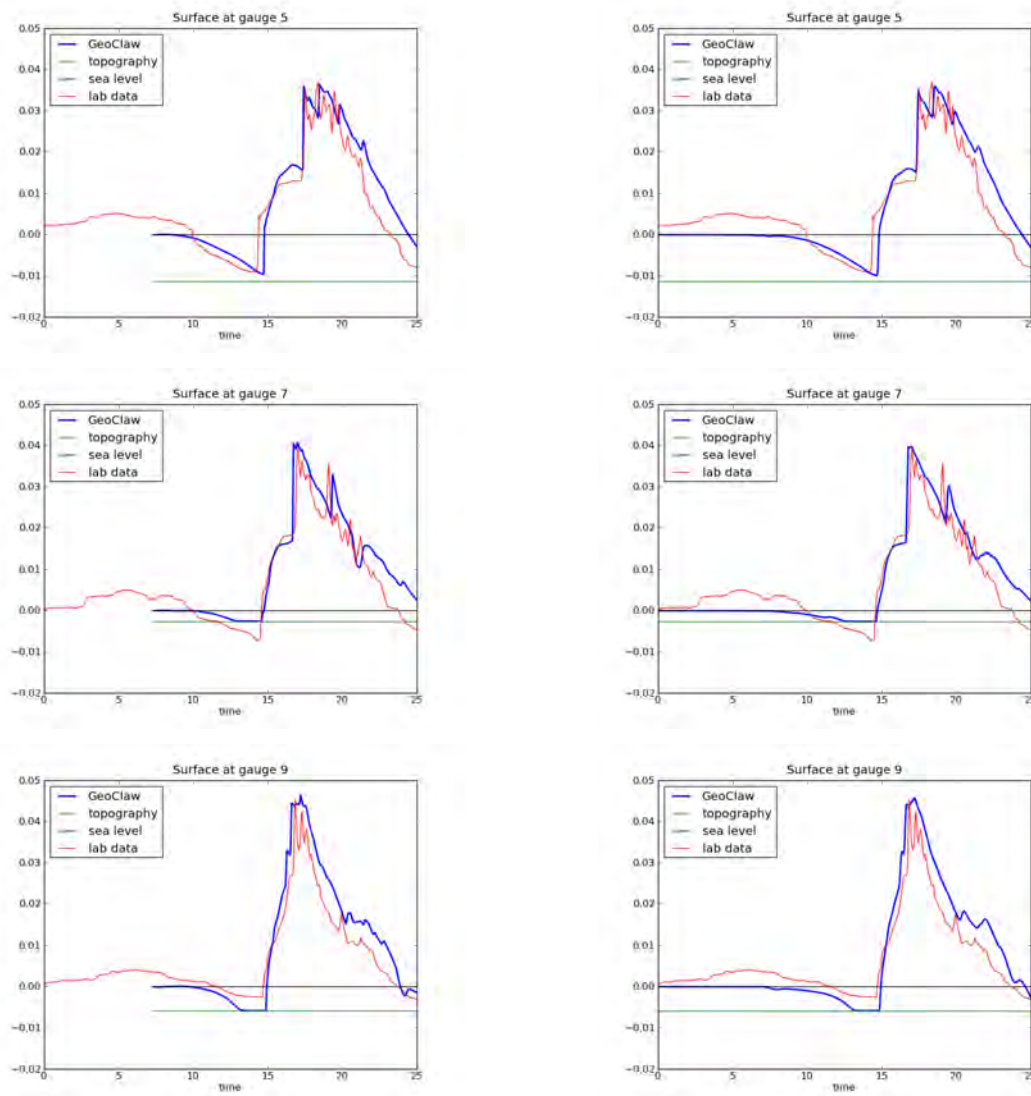


Figure 3.7.1: Left column: on 423×243 grid (same as given bathymetry). Right column: 211×121 grid.

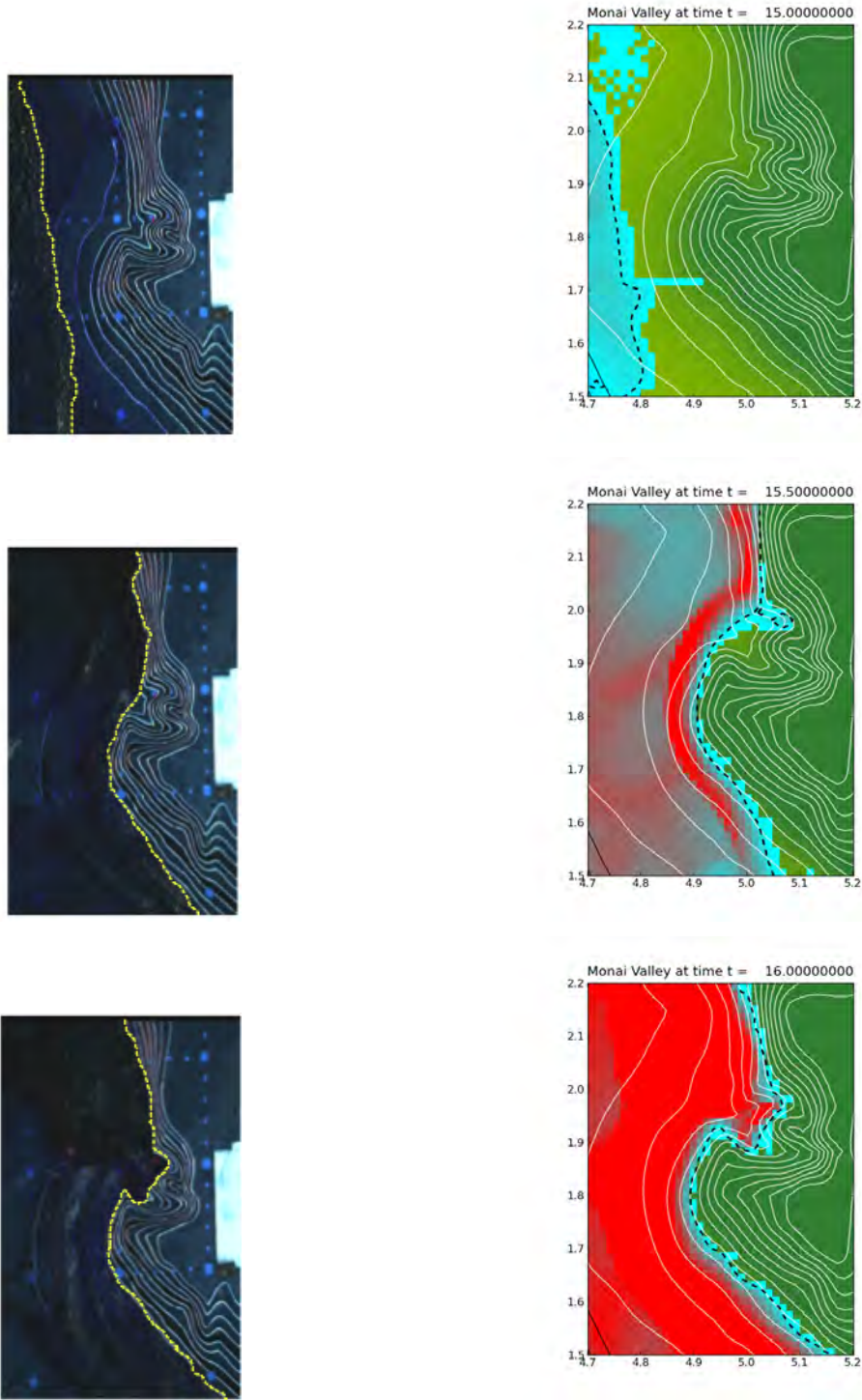


Figure 3.7.2: Left column: Frames 10, 25, and 40 from the movie. Right column: Zoomed view of computation.

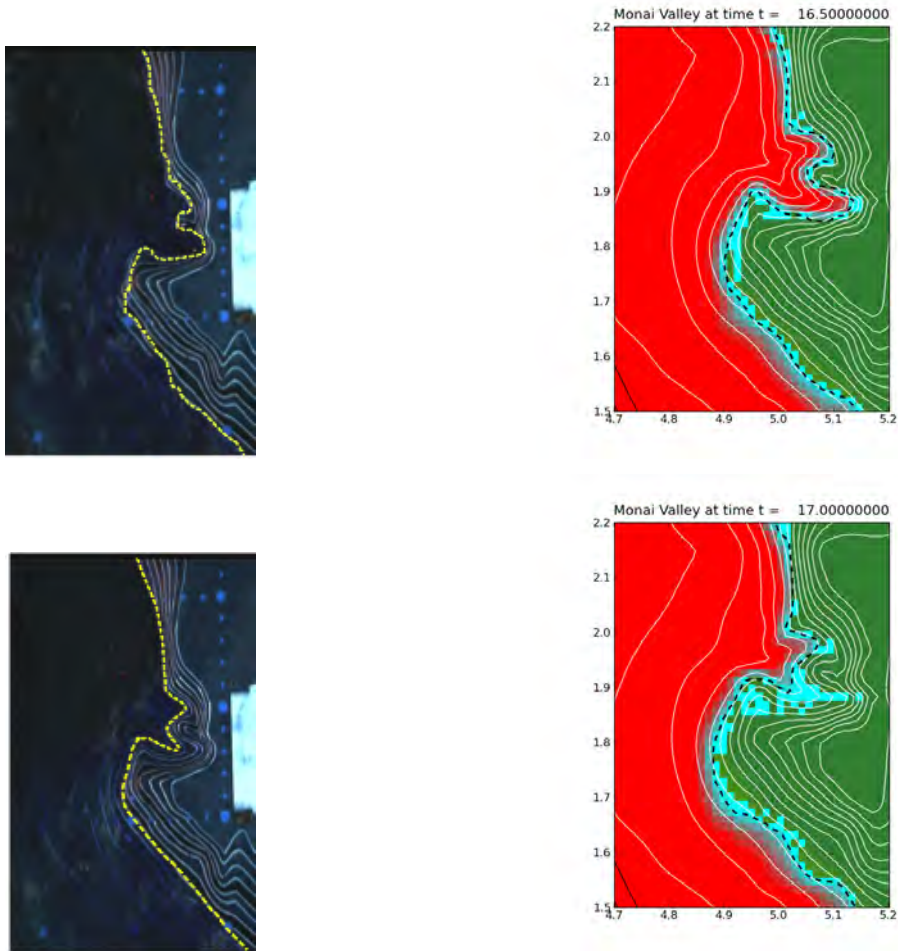


Figure 3.7.3: Left column: Frames 55 and 70 from the movie. Right column: Zoomed view of computation.

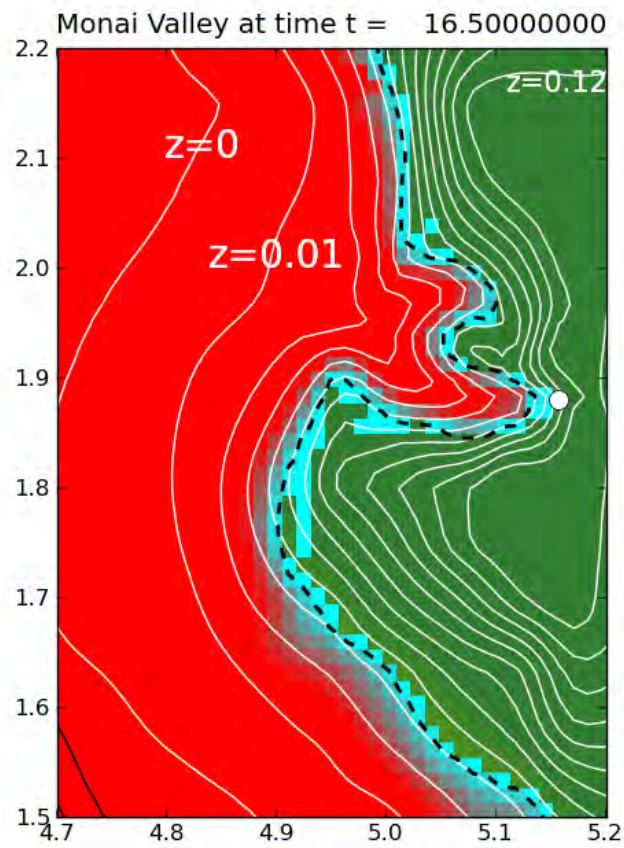


Figure 3.7.4: Maximum runup relative to observed location (white dot).

3.8 BP 8a: Old 3D landslide (Laboratory)

There are plans to replace this benchmark problem with a new one. This has not yet happened. This old benchmark problem consists of a wedge sliding on a plane beach. See Figure 3.8.1.

3.8.1 Problem specification

- PMEL-135, pp 7 & 47-48 [40].
- The original experiment is fully described on NOAA's benchmarking website which can be found at
<http://nctr.pmel.noaa.gov/benchmark/Laboratory/>

3.8.2 What we did

- We solved the nonlinear shallow water equations in Cartesian coordinates with $g = 9.81$ and no friction.
- We used the given laboratory data and problem set up to create our initial topography and bathymetry. While there was data provided up to time 20 s, we only conducted simulations up to time 10 s, as was done on NOAA's benchmarking website. We specified the movement of the wedge by using the time histories of the block motion provided for the problem. In order to implement this, we adjusted the bathymetry every time step to capture the wedge sliding down the linear beach. The slope of this linear beach was $\frac{1}{2}$. Due to the symmetry of the problem, we simplified the problem to half of the domain of the tank, specifying an outflow or non-reflecting boundary condition at the right boundary so reflected waves exit. We also specified a solid wall boundary condition at all other boundaries. (Note that the wave tank was much longer than computational domain specified.) Zero-order extrapolation, which generally gives a very good approximation to non-reflecting boundary conditions as described in Section 7.3.1 of [29]. Solid wall boundary conditions are implemented as described in Section 7.3.3 of [29]. See Section 2.3 for more information on how these boundary conditions were specified.
- The moving bathymetry is handled by recomputing $B_{ij}^n = B(x_i, y_j, t_n)$ in each time step, at the center of each finite volume grid cell, based on the specified bathymetry. This is the standard approach for handling moving bathymetry in GeoClaw: the value B_{ij}^n is adjusted but the fluid depth h_{ij}^n remains the same, so that the water column is simply displaced vertically in any cell where the bathymetry changes. For bathymetry that is smoothly varying in space and time this is considered a reasonable approach (see Section 3.3, for example). Note, however, that no momentum is directly imparted to the water by the moving bathymetry.

For this problem, the vertical face of the wedge makes this approach inadequate. The discontinuity in the moving bathymetry means that in each time step the bathymetry near

the face will gain an increment of 0.455 m, lifting the water in this cell by this amount. This is not at all physical. Instead, the moving face should impart horizontal momentum to the water.

Given this inaccuracy and the full three-dimensional nature of the physical flow, we do not expect to obtain very good comparisons computationally.

- We solved on 35×10 grid with 3 levels of adaptive mesh refinement. We refined in the x - and y - directions by a factor of 6 from levels 1 to 2 and levels 2 to 3. We refined in time by a factor of 3. We specified level 3 refinement on a rectangle with x values of $[-0.4, 2]$ and y values of $[0, 1]$.
- We compared the simulated gauge data with the laboratory gauge data to determine GeoClaw's accuracy on this problem.

3.8.3 Gauge comparisons

Figure 3.8.2 shows a comparison of the GeoClaw results with the laboratory values at the two wave gauges and two runup gauges requested for case 1. The gauge data for gauge 1 is initially very "noisy" but the overall behavior seems to be captured well. We suspect that since gauge 1 was in the wedge's path of travel and since the wedge was specified as part of our bathymetry, this created strong oscillations in our wave formations and an overshoot relative to the lab results.

Figure 3.8.3 shows a comparison of the GeoClaw results with the laboratory values at the two wave gauges and two runup gauges requested for case 2. As was the case for case 1, the gauge data for gauge 1 is initially very "noisy" but the overall behavior seems to be roughly consistent with the lab results.

3.8.4 Lessons learned

- It is not clear that the shallow water equations are a good model for this problem. The flow should be fully three-dimensional around this sliding wedge and it is not clear that any depth-averaged model will do well.
- At some distance away from the shore, the depth will be greater than wave length and the shallow water equations will no longer be valid.
- The vertical face causes numerical difficulties.
- Overall, GeoClaw seems to model the surface elevations with respect to still water level well for both cases. However, gauge 1 seems to have issues from shortly after the start of the simulation to about 2 seconds. As mentioned earlier, it seems that this phenomena is more of a result of how the bathymetry is specified than GeoClaw's ability to model this landslide. To smooth the data, one could try interpolating the data so that the moving bathymetry is smooth instead of piecewise. This should greatly reduce the heavy oscillations. Another approach would be to add a slope to the leading face of the wedge. This

would ensure a more gradual drop in bathymetry as the wedge propagates across the linear beach.

- This benchmark problem does not appear to be a good test for tsunami models. The dimensions do not seem to be reasonable relative to true submarine landslides problems. The vertical face does not seem realistic and causes numerical difficulties.

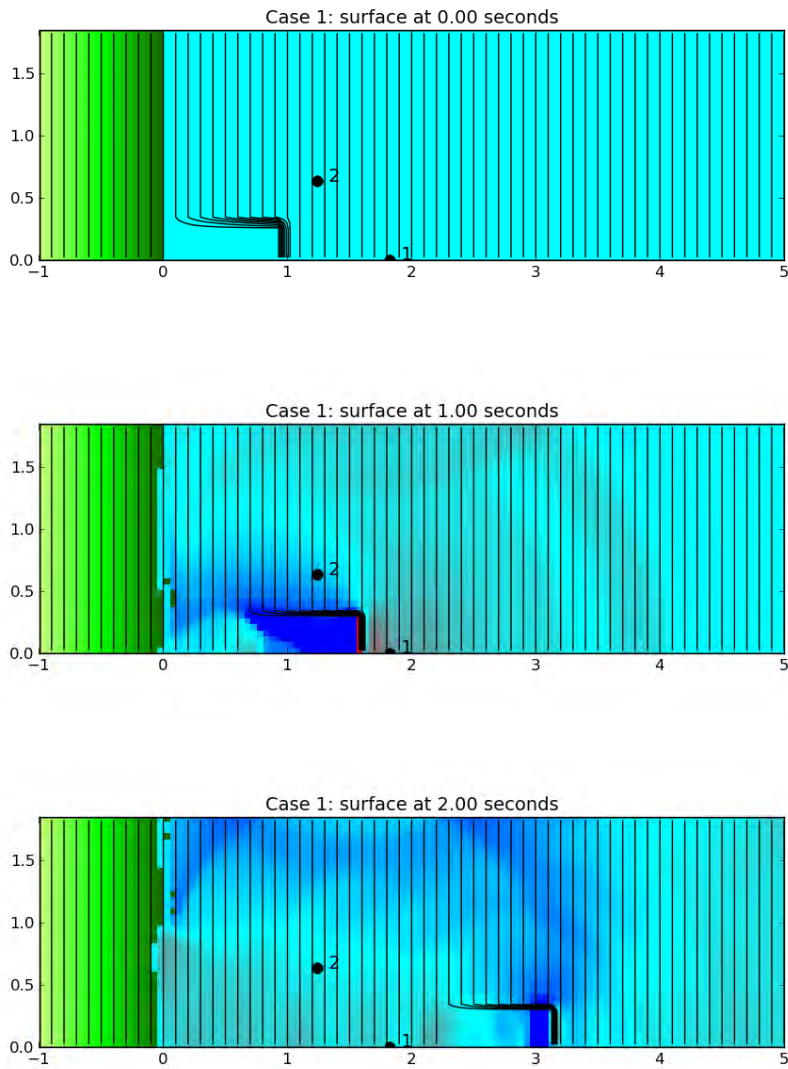


Figure 3.8.1: Single grid 140×40 GeoClaw simulation of Case 1 to illustrate moving bathymetry and gauge locations.

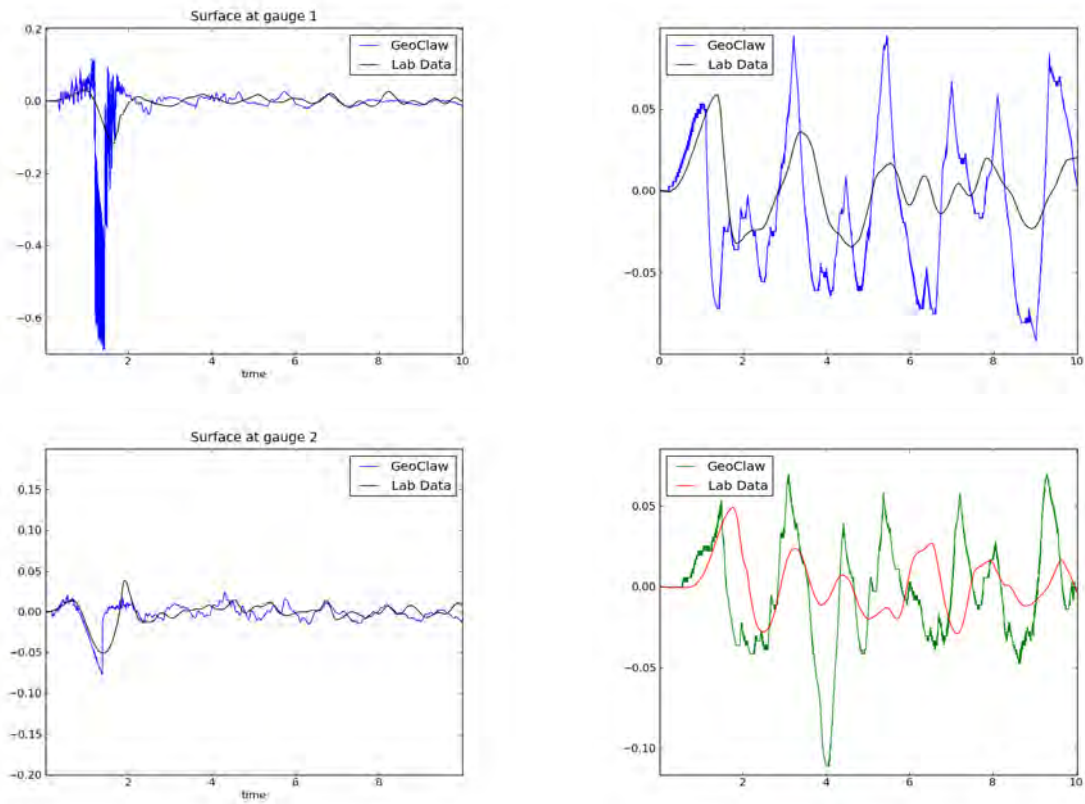


Figure 3.8.2: Left column: Time histories of the surface elevation with respect to still water level for case 1. Right column: Time histories of the runup measurements with respect to still water level for case 1, at Runup gages 2 and 3. Note: runup values are negated in this figure for both GeoClaw and lab data due to a programming glitch.

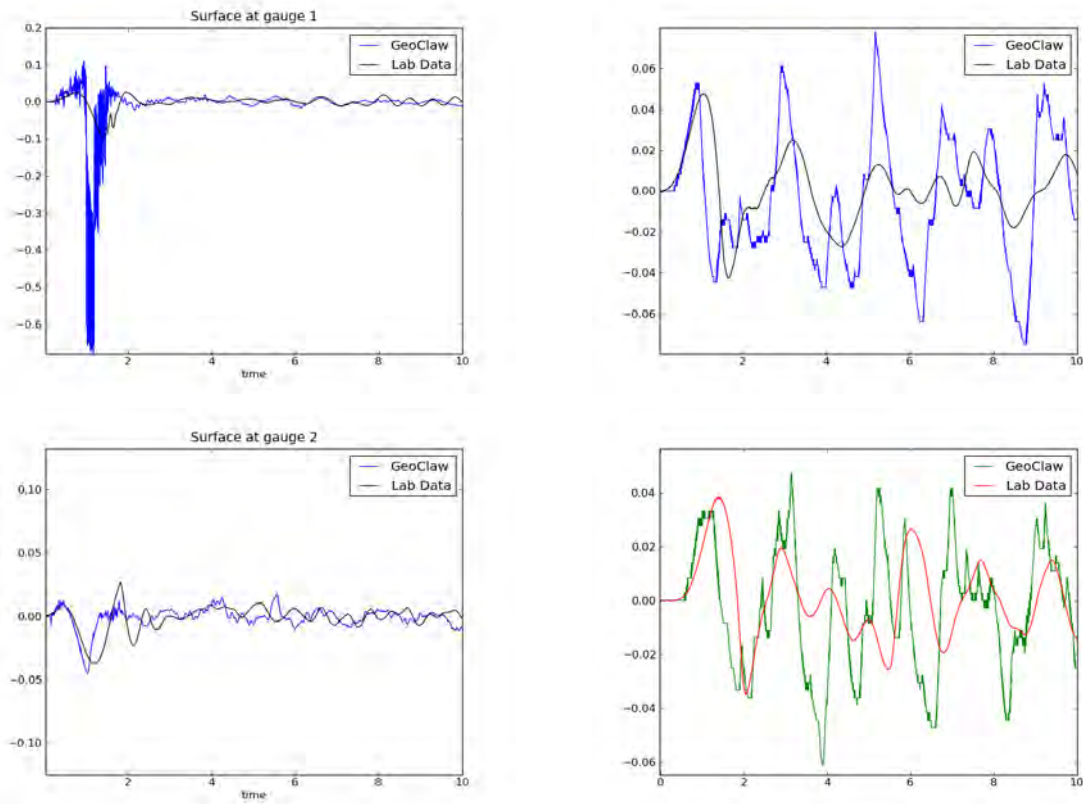


Figure 3.8.3: Left column: Time histories of the surface elevation with respect to still water level for case 2. Right column: Time histories of the runup measurements with respect to still water level for case 2, at Runup gages 2 and 3. Note: runup values are negated in this figure for both GeoClaw and lab data due to a programming glitch.

3.9 BP 9: Okushiri Island (Field)

Documentation:

- PMEL-135, pp 8 & 48-53 [40].
- A problem description is provided by Frank González at [3]:
BP09-FrankG-Okushiri_island/Description.pdf
- Numerous other publications also describe this event, in varying detail: [13, 24, 25, 41, 44]

3.9.1 Description

The goal of this Benchmark Problem (BP) is to compare computed model results with field observations of the 1993 Okushiri Island tsunami.

3.9.2 Problems encountered

Two basic problems were encountered:

1. Poor quality of the computational bathymetric/topographic grids
2. Inaccurate spatial registration of field observational data with the model grids.

3.9.3 What we did

- Used $g = 9.81$ and Manning coefficient 0.025 for the friction term. We also ran many of the tests with no friction for comparison.
- Used bathy/topo grids and source grid for the Disaster Control Research Center solution DCRC17a. Dmitry Nicolsky provided improved versions of the originals developed by Kansai University, in which severe misalignments in the original data were reduced (but not eliminated).

3.9.4 Problem Requirements

Requirements of this benchmark test were to compute:

1. Runup around Aonae
2. Arrival of the first wave to Aonae
3. Two waves at Aonae approximately 10 min apart; the first wave from the west, the second from the east
4. Water level at Iwanai and Esashi tide gauges
5. Maximum modeled runup distribution around Okushiri Island

6. Modeled runup height at Hamatsumae
7. Modeled runup height at a valley north of Monai

3.9.5 Results

Figures 3.9.1 through 3.9.4 show results of one computation where AMR is used to concentrate grid points near the southern Aonae Peninsula and (Requirements 1, 2, 3). The rectangular boxes show regions of refinement. The coarsest grid is a 60×60 grid on a 1-degree square as shown in Figure 3.9.1. Five levels of refinement are used going down by factors 2, 4, 4, and 6 from each level to the next. In this computation, Level 4 is only allowed on the southern half of Okushiri Island and Level 5 only around the Aonae Peninsula.

Figure 3.9.2 shows a zoom on the island and Figure 3.9.3 a further zoom on the peninsula. Arrival of the first wave at Aonae (Requirement 2) is seen from the west at about $t = 5$ minutes. The second major wave arrives from the east at about 10 minutes.

Figure 3.9.4 shows the inundation level on the peninsula. The color scale indicates the maximum depth of water recorded at each point on a fixed grid that is placed around this region. This can be compared to the photographs shown in Figure 3.9.5.

A slight modification of this run was done to focus on the Hamatsumae region just east of the peninsula. Figure 3.9.6 shows the maximum inundation in this region.

The bottom panel of Figure 3.9.7 shows the runup at various other points around the island as measured by the team of Y. Tsuji (top panel), along with values computed using GeoClaw. Figure 3.9.8 shows a scatter plot of the correlation between the observations and the computed values. The GeoClaw values were obtained by placing a small fixed grid around each observation point and recording the maximum water depth at each point on this grid at each timestep of the computation, using the built-in feature of GeoClaw. The maximum depth over time can also be accumulated at these points and updated each time step. Plots of the maxima over these grids gives a visualization of the maximum extent of inundation. Such plots are shown in Figures 3.9.4 and 3.9.9, with 4-meter contours. For most other observation points contours of topography at 2-meter increments were plotted in order to better estimate the maximum runup in a small region centered about each observation point.

Figure 3.9.9 shows the inundation map for the Valley north of Monai, with 4-meter contour lines (Requirement 7). Inundation to roughly 32 m is observed, in accordance with observations. For this run a finer grid was used in the region around the value (refining by a factor 24 rather than 6 in the level 5 grid), and the finer scale bathymetry provided in this region was used.

Requirement 4 is the comparison of observed and computed water level at the Iwanai and Esashi tide gage stations; the analog records are shown in Figure 3.9.10, taken from [41]. The digitized tide gage data are compared with the GeoClaw time series in Figures 3.9.11 and 3.9.12. At Iwanai, the digitized tide gage record is clearly undersampled (compare Figures 3.9.10 and 3.9.11), but does capture the peaks and troughs of the analog record. We see that the first wave arrival time and the overall wave amplitudes are comparable, but that the GeoClaw tsunami waves are about half the period of the waves recorded by the Iwanai tide gage. Considering the regularity of the long train of waves in the tide gage record, it is probable that longer period resonance

modes at Iwanai were excited by the incident tsunami; if so, then higher resolution bathy/topo grids would be required to capture these resonant oscillations in a numerical simulation. At Esashi, it appears that the digitized tide record reflects the main features of the analog record (compare Figures 3.9.10 and 3.9.12). However, the strange shape of the analog wave form makes it likely that there are problems with the tide gage record; the record suffers from either mechanical/electronic, or damage by debris, or simply a damped and/or mismatched response function in the tsunami frequency band. In spite of this, the first arrival and timing of the first two tsunami waves are in good correspondence, though the amplitude and individual wave forms are not.

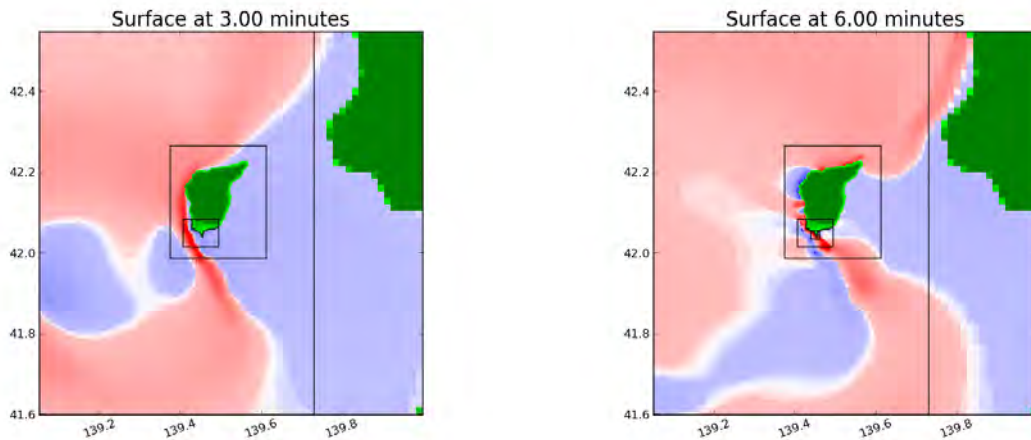


Figure 3.9.1: Full computational domain for one simulation, in which AMR grids are focused near the Aonae Peninsula at the south of Okushiri Island.

3.9.6 Lessons learned

This BenchMark problem requires much more work to qualify as a credible test of tsunami inundation models. We have little confidence in:

1. The quality of the bathy/topo computational grids. A number of mismatches and discontinuities still exist in the system of grids.
2. The accuracy of the geospatial registration of observational data with model latitude and longitude positions. Figure 3.9.7 presents the observation locations of each of three field survey teams – Professor Yoshinobu Tsuji, Tokyo University (Tsuji), the United States-Japan Cooperative Program on Natural Resources (UJNR) and the Tohoku University (Tohoku) teams. The bathy/topo computational grids were adjusted to match the positions of the Tsuji observations, but it is clear that this created a systematic error in the registration of the grids with the Tohoku field observations and, in all likelihood, the UJNR field observations. As another example, there appear to be discrepancies in the several field team reports of the latitude and longitude of the highest runup observed, i.e., the value of over 30 m in a “... small valley north of Monai ...”. Such positioning errors can be critical with respect to accurate comparisons of observed and computed runup.

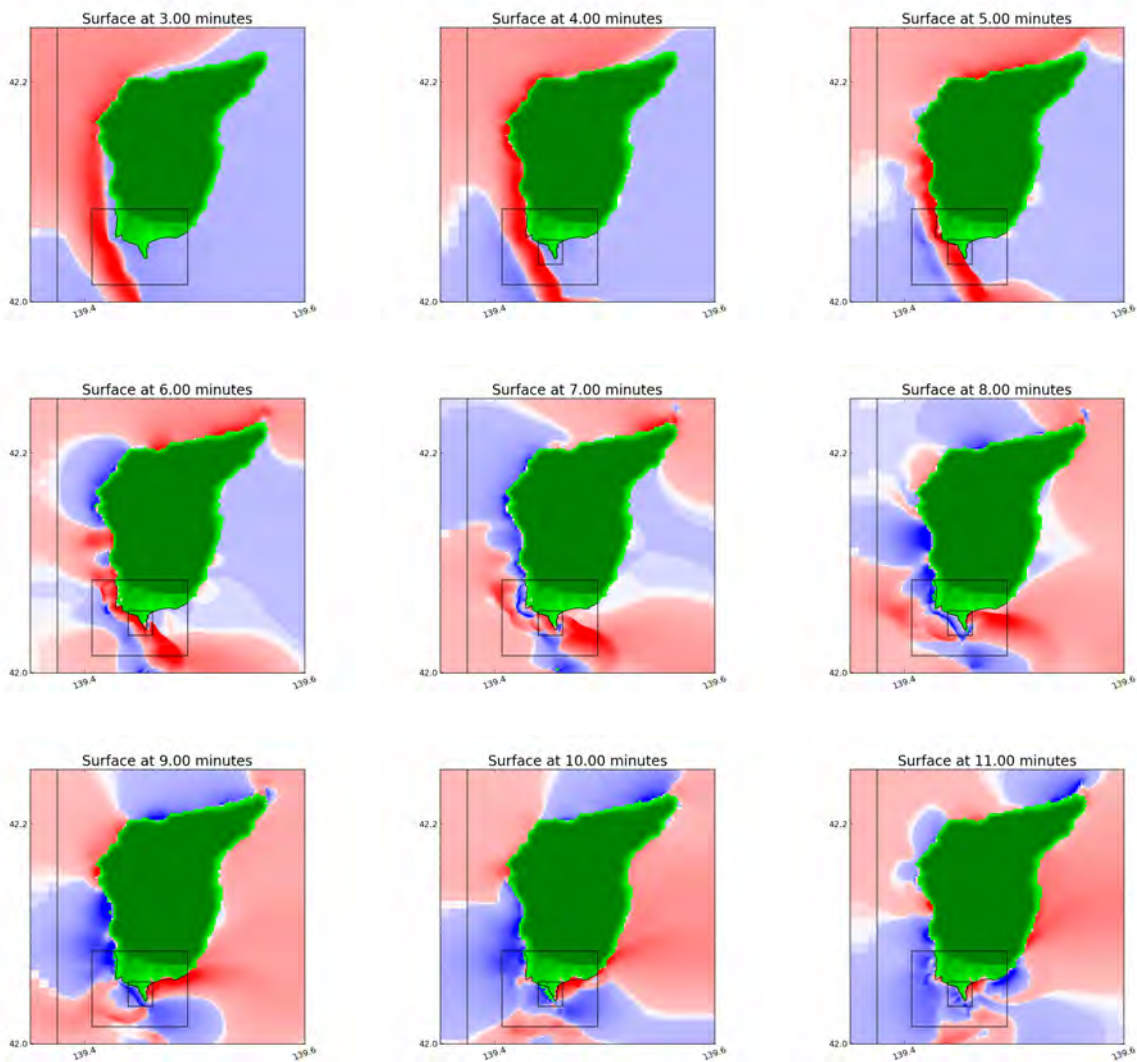


Figure 3.9.2: Zoom on Okushiri Island.

3.9.7 Recommendations

The Okushiri event tsunami runup and eyewitness reports remains one of the most valuable datasets for model comparisons in existence, but the quality of this dataset must be improved to qualify as a credible benchmark problem. We recommend that an effort be supported to

1. Develop a high quality bathy/topo grid system,
2. Resolve ambiguities and discrepancies currently found in the various team data reports, and improve the geospatial registration of observed and modeled values, and
3. Provide adequate documentation of the resulting benchmark problem dataset.

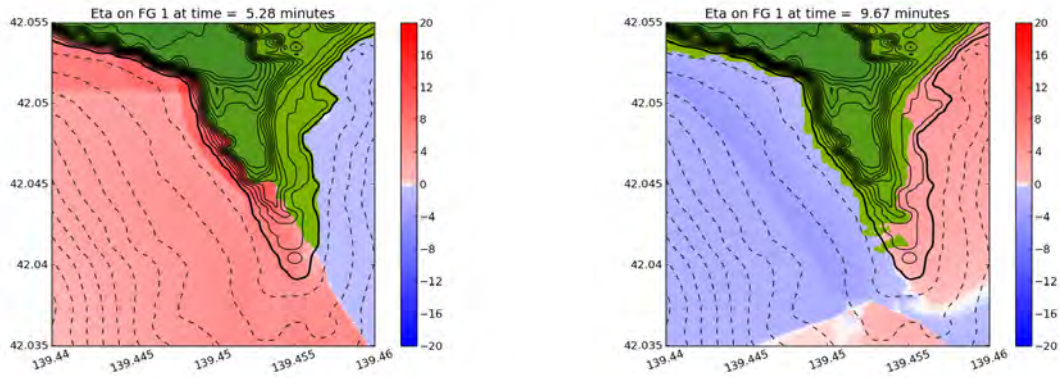


Figure 3.9.3: Zoom on Aonae Peninsula showing the first wave arriving from the east and the second from the west. Color map shows elevation of sea surface. 4-meter contours of bathymetry and topography are shown.

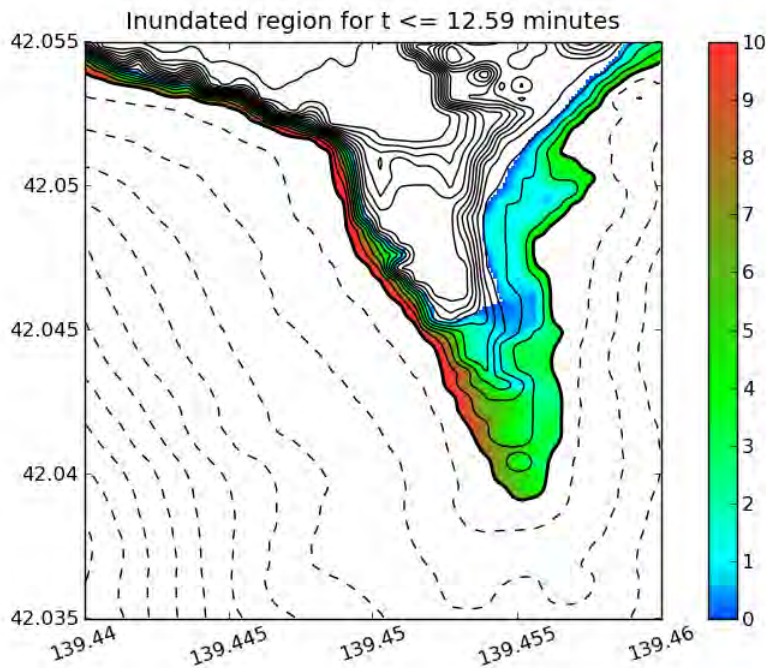


Figure 3.9.4: Inundation map of the Aonae Peninsula. Color map shows maximum fluid depth over entire computation at each point. 4-meter contours of bathymetry and topography are shown.



Figure 3.9.5: Photographs of the Aonae Peninsula taken shortly after the event. Left: From <http://www.usc.edu/dept/tsunamis/hokkaido/aonae.html>. Right: From http://nctr.pmel.noaa.gov/okushiri_devastation.html, credited to Y. Tsuji.

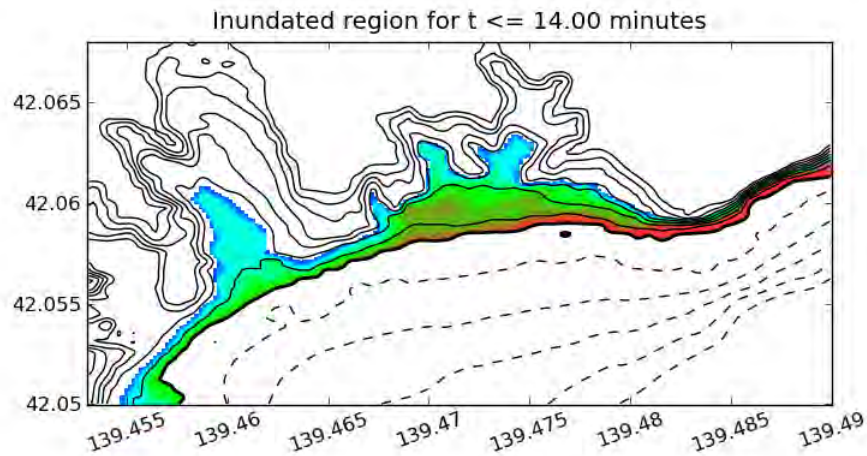


Figure 3.9.6: Inundation map of the Hamatsumae neighborhood just east of the Aonae Peninsula. Color map shows maximum fluid depth over entire computation at each point, with the same color scale as Figure 3.9.4. 4-meter contours of bathymetry and topography are shown.

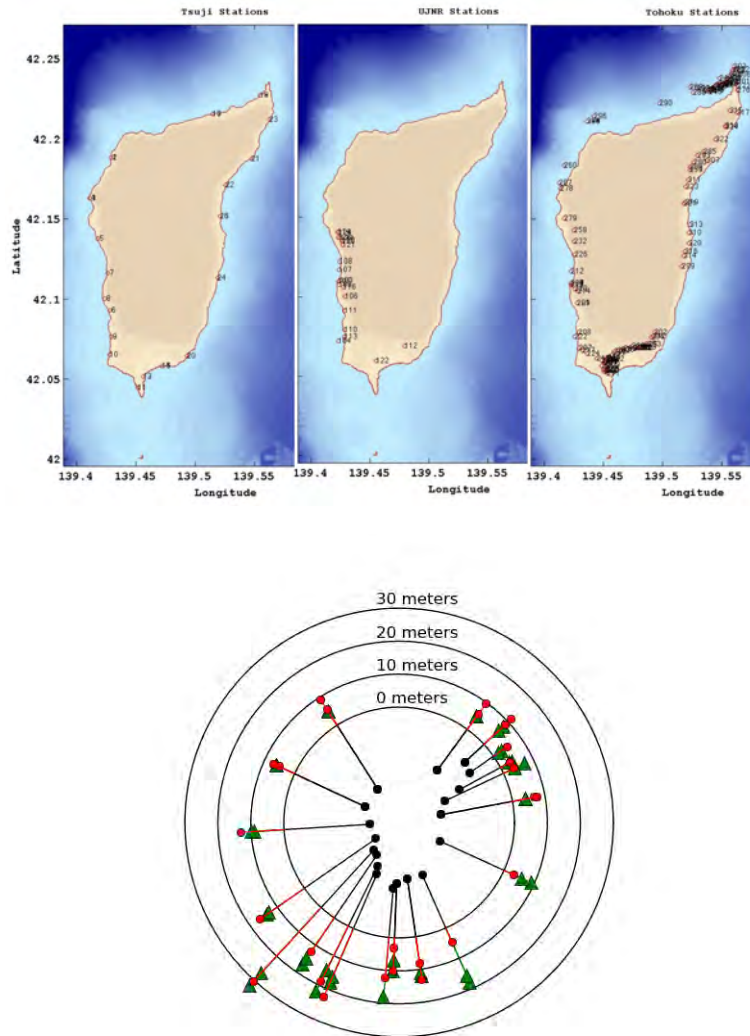


Figure 3.9.7: Top: Locations of field observations by three independent field survey teams, relative to the computational bathy/topo grid system. Only the observations of Tsuji (left figure) were used in this study due to misregistration of the other two data sets. Bottom: Measured and computed runup at 21 points around Okushiri Island where measured by the Tsuji team. Red circles are measurements, green diamonds are estimated from the computation. Two red circles at the same point represent estimates of minimum and maximum inundation observed near the point. Two green diamonds at the same point represent values estimated when the model was run with and without bottom friction (Manning coefficient 0.025). The runup computed with bottom friction is the smaller value.

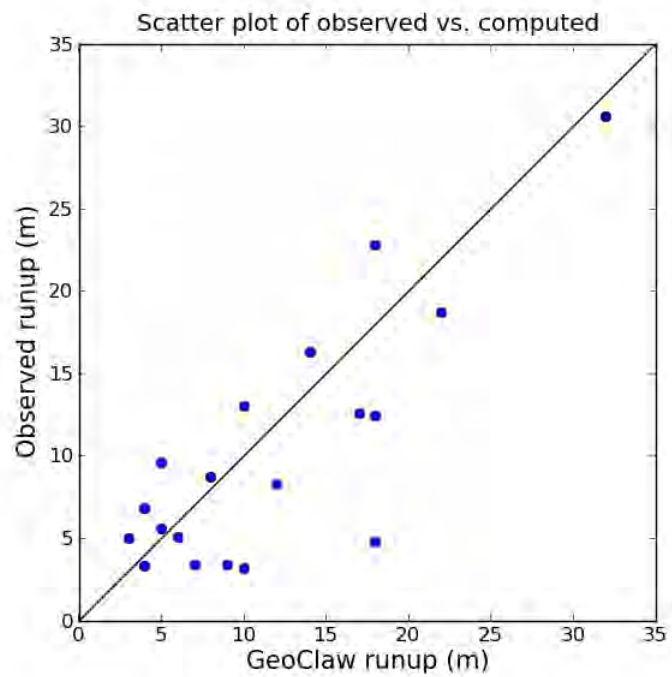


Figure 3.9.8: Scatter plot illustrating the correlation between measured and computed values for the values shown in Figure 3.9.7.

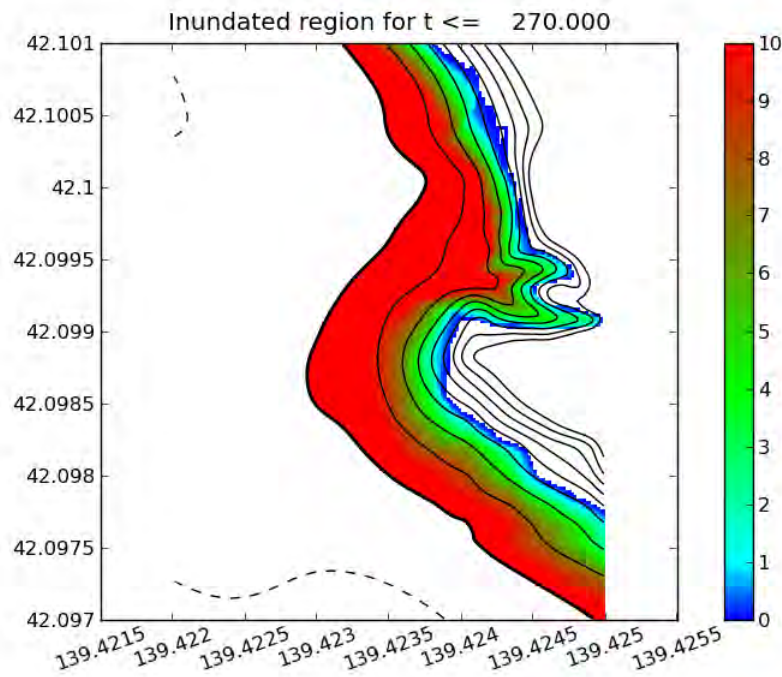


Figure 3.9.9: Inundation map of the valley north of Monai. Color map shows maximum fluid depth over entire computation at each point. 4-meter contours of bathymetry and topography are shown. Compare to Figure 3.7.4 showing the related wave tank simulation.

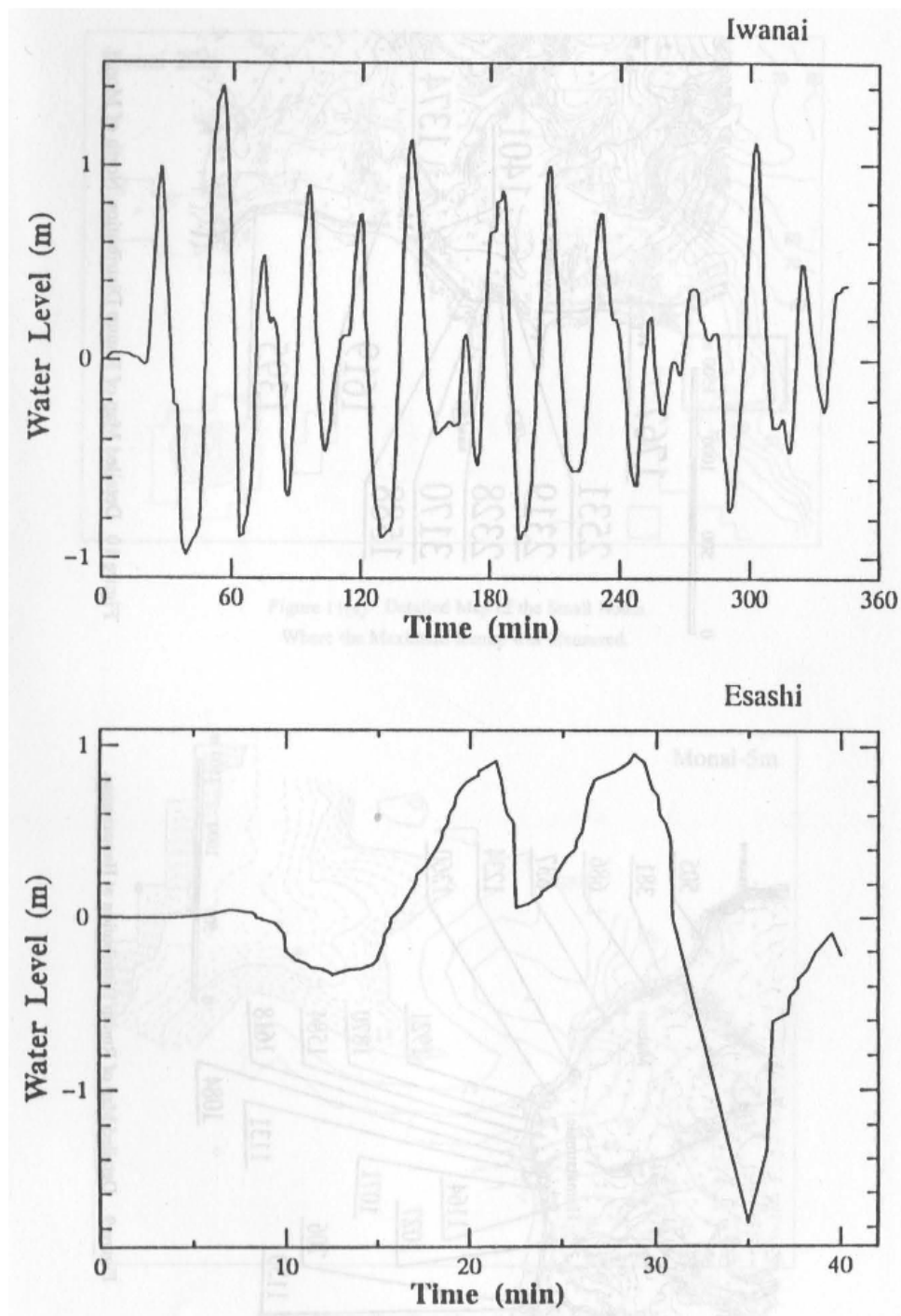


Figure 3.9.10: Analog tide gage records at Iwanai and Esashi. (Faint background figures are a scanning artifact; the article is printed on paper that is not totally opaque.)

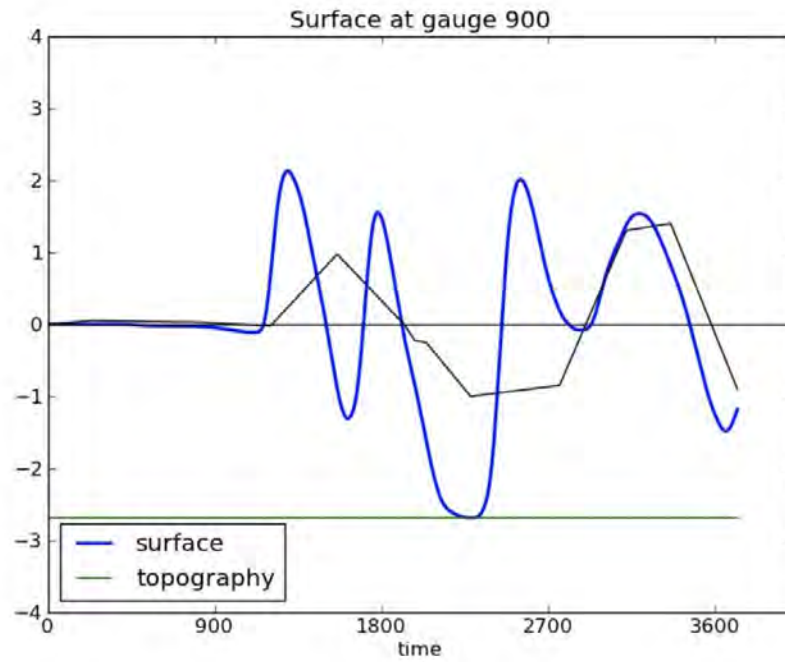


Figure 3.9.11: Iwanai digitized tide gage record (black line) and GeoClaw (blue line) time series.

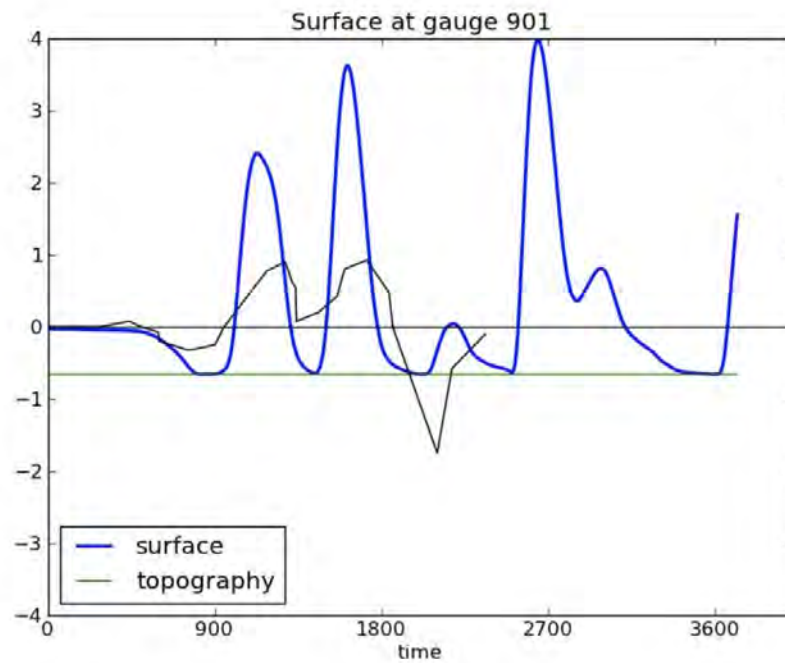


Figure 3.9.12: Esashi digitized tide gage record (black line) and GeoClaw (blue line) time series.

4 Further remarks and suggestions

4.1 Comments on the current benchmark problems

The current set of benchmark problems do a good job of testing some aspects of a tsunami simulation code. However, there are some shortcomings that have become apparent to us in the course of working through these problems and that could be addressed in the future.

- Several of the problems are not well specified in terms of the data provided. These difficulties have been noted in our discussion of the individual problems.
- In some problems there is not a clear description of how the simulation is supposed to be set up, or how the accuracy of the solution should be quantified. Allowing flexibility is perhaps necessary to allow for differences in capabilities of existing simulation codes, but we feel this could be better constrained. In particular, there is no indication in the problem descriptions of what grid resolution should be used. There are requirements to “demonstrate convergence”, but for practical applications it is important to know that adequately accurate results can be obtained on grids with a reasonable resolution in terms of computing time constraints.
- Friction parameter values significantly affect model runup computations at both laboratory and field experiment scales (see Figures 3.6.11 and 3.9.7). Different models may use different formulations of the friction terms and some consideration should be given to testing and reporting on the effect of different values of the friction parameter when conducting Benchmark Problem simulations.
- Runup computational algorithms frequently employ a parameter that sets a threshold level, below which a cell is declared dry, i.e., the Dry Cell Depth. As in the case of friction, the value of this parameter can also affect the resulting runup computation (see Figure 3.6.11), and some consideration should be given to testing and reporting on how variations in such model parameters can affect runup computation results for Benchmark Problems.
- Currently there is no requirement to report CPU time required to solve each problem. This would be interesting information to have when comparing different approaches, and would be a necessary component if the benchmark did require a particular grid resolution, since grid resolution alone is not necessarily a good indication of computational effort needed.
- Some of the benchmark problems concern comparison to exact solutions of the linear or nonlinear shallow water equations. For these problems any code that solves the equations in question should converge to the correct solution, but it may also be of interest to know how rapidly the error goes to zero, and how good the solution is on under-resolved grids that may be more representative of what would be used in actual tsunami simulations.
- Other benchmark problems require comparison with wave tank experiments. In some cases (e.g. with breaking waves) it can not be expected that the code converges to the experimental results since the equations used in tsunami modeling are only approximations. Different

codes may use different approximations and so this comparison may be valuable, but since many codes use the same shallow water approximations, for these problems it would be valuable to have some agreement as to what a “converged solution” of the shallow water equations looks like.

- Benchmark problem #8a studied in Section 3.8 does not seem to scale well as a model of a real landslide, and has difficulties associated with the vertical face that are not likely to be seen in real landslides, where momentum transfer is probably secondary to the vertical displacement of the water column in creating a tsunami. The short wavelength waves generated by the discontinuity in this problem also accentuate the need to use dispersive corrections in order to obtain reasonable approximations. While dispersive terms may be very important for some submarine landslide generated tsunamis, there may be other cases where they are less important and the ability to model such events with shallow water equations is important since these equations can be solved with explicit methods that are often orders of magnitude faster than implicit dispersive solvers. (This may be particularly important in doing probabilistic hazard assessment requiring a large number of scenarios.) We believe it would be valuable to develop landslide benchmarks that model events such as a large mass failure on the continental slope, which the current benchmarks do not address.
- The Okushiri Island benchmark problem #9 requires comparison to field observations. Beyond the technical difficulties with datasets for this problem, there are also questions regarding (a) the accuracy of the earthquake source being used, (b) the accuracy of some of the field observations and tide gauges. This makes it difficult to assess the accuracy of a simulation code. This will always be a problem in comparing with actual events, but our feeling is that to form a meaningful benchmark there should be some agreement in the community regarding how large the deviation between the computed solutions and the observations are expected to be, rather than an expectation that results converge to observations as the grid is refined.

4.2 Suggestions for future benchmark problems

We believe there are other possible benchmark problems that should be considered by community in order to better test tsunami simulation codes.

1. The one-dimensional test problems currently involve exact solutions that are themselves difficult to calculate numerically, e.g. requiring numerical quadrature of Bessel functions. It is very useful that tabulated values of these solutions have been provided. However, rather than using limited tests for which such “exact” solutions are known, it might be preferable to carefully test a 1d numerical model and show that it converges, and then use this with very fine grids to generate reference solutions. Fully converged solutions could be provided in tabulated form and could be as accurate as needed. It would then be possible to generate a much wider variety of test problems. In particular, more realistic bathymetry could be used, for example on the scale of the ocean, a continental shelf and beach, rather than modeling only a beach.

2. High-accuracy one-dimensional reference solutions can also be used to test a full two dimensional code, by creating bathymetry that varies in only one direction at some angle to the two-dimensional grid. A plane wave approaching such a planar beach would ideally remain one-dimensional, but at an angle to the grid this would test the two-dimensional inundation algorithms.
3. This idea can be extended to consider radially symmetric problems, such as a radially symmetric ocean with a Gaussian initial perturbation at the center. The waves generated should reach the shore at the same time in all directions, but the shore will be at different angles to the grid in different locations and it is valuable to compare the accuracy in different locations. The two-dimensional equations can be reformulated as a one-dimensional equation in the radial direction (with geometric source terms) and a very fine grid solution to this problem can be used as a reference solution.

Features could also be added at one point along the shore and this location rotated to test the ability of the code to give orientation-independent results. Some GeoClaw results of this nature are presented in [6, 34].

4. A very simple exact solution is known for water in a parabolic bowl, in which the water surface is linear at all times but the water sloshes around in a circular motion. This is a good test of wetting and drying as well as conservation. See for example [17, 42] and the test problem in GeoClaw:
<http://www.clawpack.org/clawpack-4.x/apps/tsunami/bowl-slosh/README.html>
5. Extensive observations are available for recent events such as Chile 2010 or Tohoku 2011, including DART buoys, tide gauges, and field observations of inundation and runup. It would be valuable to develop new benchmark problems based on specific data sets, including specified bathymetry and earthquake source (or seafloor displacement).

References

- [1] D. S. Bale, R. J. LeVeque, S. Mitran, and J. A. Rossmannith. A wave propagation method for conservation laws and balance laws with spatially varying flux functions. *SIAM J. Sci. Comput.*, 24:955–978, 2002.
- [2] J. Behrens and R. J. LeVeque. Modeling and simulating tsunamis with an eye to hazard mitigation. *SIAM News*, 44(4), May 2011.
- [3] Benchmark problem descriptions.
<https://github.com/rjleveque/nthmp-benchmark-problems>, 2011.
- [4] M. J. Berger, D. A. Calhoun, C. Helzel, and R. J. LeVeque. Logically rectangular finite volume methods with adaptive refinement on the sphere. *Phil. Trans. R. Soc. A*, 367:4483–4496, 2009.
- [5] M. J. Berger and P. Colella. Local adaptive mesh refinement for shock hydrodynamics. *J. Comput. Phys.*, 82:64–84, 1989.
- [6] M. J. Berger, D. L. George, R. J. LeVeque, and K. T. Mandli. The GeoClaw software for depth-averaged flows with adaptive refinement. *Adv. Water Res.*, 2011.
- [7] M. J. Berger and R. J. LeVeque. Adaptive mesh refinement using wave-propagation algorithms for hyperbolic systems. *SIAM J. Numer. Anal.*, 35:2298–2316, 1998.
- [8] M. J. Berger and J. Olinger. Adaptive mesh refinement for hyperbolic partial differential equations. *J. Comput. Phys.*, 53:484–512, 1984.
- [9] M. Briggs. Runup of solitary waves on a vertical wall. Coastal Hydraulics Laboratory <http://chl.ercd.usace.army.mil/chl.aspx?p=s&a=Projects;36>.
- [10] M.J. Briggs, C.E. Synolakis, and G.S. Harkins. Tsunami runup on a conical island. In *Proc. of Waves – Physical and Numerical Modelling, 21-24 August 1994, Vancouver, Canada*, pages 446–455, August 1994.
- [11] M.J. Briggs, C.E. Synolakis, G.S. Harkins, and D. Green. Laboratory experiments of tsunami runup on a circular island. *Pure Appl. Geophys.*, 144:569–593, 1995.
- [12] M.J. Briggs, C.E. Synolakis, G.S. Harkins, and D. R. Green. Runup of solitary waves on a circular island. In *Proceedings of the Second International Long-Wave Runup Models, Friday Harbor, Washington, 12-16 September 1995*, pages 363–374, 1996.
- [13] DCRC (Disaster Control Research Center). *Tsunami Engineering Technical Report No. 11*. Tohoku University, Tohoku, Japan, 1994.
- [14] F. Enet and S. T. Grilli. Experimental study of tsunami generation by three-dimensional rigid underwater landslides. *Journal of Waterway, Port, Coastal, and Ocean Engineering*, 133:442–454, 2003.

- [15] D. R. Fuhrman and P. A. Madsen. Tsunami generation, propagation, and run-up with a high-order boussinesq model. *Coastal Eng.*, 56:747–758, 2009.
- [16] K. Fujima, M.J. Briggs, and D. Yuliadi. Runup of tsunamis with transient wave profiles incident on a conical island. *Coastal Engineering Journal*, 42:175–195, 2000.
- [17] J. M. Gallardo, C. Parés, and M. Castro. On a well-balanced high-order finite volume scheme for shallow water equations with topography and dry areas. *J. Comput. Phys.*, 227:574–601, 2007.
- [18] GeoClaw documentation, 2011. <http://www.clawpack.org/geoclaw>.
- [19] D George. Adaptive finite volume methods with well-balanced Riemann solvers for modeling floods in rugged terrain: Application to the Malpasset dam-break flood (France, 1959). *Int. J. Numer. Meth. Fluids*, 2010.
- [20] D. L. George. *Finite Volume Methods and Adaptive Refinement for Tsunami Propagation and Inundation*. PhD thesis, University of Washington, 2006.
- [21] D. L. George. Augmented Riemann solvers for the shallow water equations over variable topography with steady states and inundation. *J. Comput. Phys.*, 227(6):3089–3113, March 2008.
- [22] D. L. George and R. M. Iverson. A two-phase debris-flow model that includes coupled evolution of volume fractions, granular dilatency, and pore-fluid pressure. *submitted to Italian Journal of Engineering, Geology and Environment*, 2010.
- [23] D. L. George and R. J. LeVeque. Finite volume methods and adaptive refinement for global tsunami propagation and local inundation. *Science of Tsunami Hazards*, 24:319–328, 2006.
- [24] HTSG (Hokkaido Tsunami Survey Group). Tsunami devastates japanese coastal region. *Eos Trans. Am. Geophys. Union*, 74:417, 432, 1993.
- [25] K. Kato and Y. Tsuji. Estimation of fault parameters of the 1993 hokkaido-nansei-oki earthquake and tsunami characteristics. *Bull. Earthq. Res. Inst., Univ. Tokyo*, 69:39–66, 1994.
- [26] J. O. Langseth and R. J. LeVeque. A wave-propagation method for three-dimensional hyperbolic conservation laws. *J. Comput. Phys.*, 165:126–166, 2000.
- [27] R. J. LeVeque. High-resolution conservative algorithms for advection in incompressible flow. *SIAM J. Numer. Anal.*, 33:627–665, 1996.
- [28] R. J. LeVeque. Wave propagation algorithms for multi-dimensional hyperbolic systems. *Journal of Computational Physics*, 131:327–335, 1997.
- [29] R. J. LeVeque. *Finite Volume Methods for Hyperbolic Problems*. Cambridge University Press, 2002.

- [30] R. J. LeVeque. *Finite Difference Methods for Ordinary and Partial Differential Equations, Steady State and Time Dependent Problems*. SIAM, Philadelphia, 2007.
- [31] R. J. LeVeque. A well-balanced path-integral f-wave method for hyperbolic problems with source terms. *J. Sci. Comput.*, 2010. To appear, www.clawpack.org/links/wbwave10.
- [32] R. J. LeVeque, M. J. Berger, et al. Clawpack software. <http://www.clawpack.org>.
- [33] R. J. LeVeque and D. L. George. High-resolution finite volume methods for the shallow water equations with bathymetry and dry states. In P. L-F. Liu, H. Yeh, and C. Synolakis, editors, *Proceedings of Long-Wave Workshop, Catalina*, volume 10, pages 43–73. World Scientific, 2004. <http://www.amath.washington.edu/~rjl/pubs/catalina04/>.
- [34] R. J. LeVeque, D. L. George, and M. J. Berger. Tsunami modeling with adaptively refined finite volume methods. *Acta Numerica*, pages 211–289, 2011.
- [35] P.L.-F. Liu, Y.-S. Cho, M.J. Briggs, U. K acnogl u, and C.E. Synolakis. Runup of solitary waves on a circular island. *J. Fluid Mech.*, 302:259–285, 1995.
- [36] P.L.-F. Liu, Y.-S. Cho, and K. Fujima. Numerical solutions of three-dimensional run-up on a circular island. In *Proceedings of the International Symposium: Waves – Physical and Numerical Modeling, 21-24 August 1994, Vancouver, Canada*, volume 2, pages 1031–1040, 1994.
- [37] K. T. Mandli. *Finite Volume Methods for the Multilayer Shallow Water Equations with Applications to Storm Surges*. PhD thesis, University of Washington, 2011.
- [38] M. Matsuyama and H. Tanaka. An experimental study of the highest run-up height in the 1993 Hokkaido Nansei-oki earthquake tsunami. *ITS Proceedings*, pages 879–889, 2001.
- [39] P. L. Roe. Approximate Riemann solvers, parameter vectors, and difference schemes. *J. Comput. Phys.*, 43:357–372, 1981.
- [40] C. E. Synolakis, E. N. Bernard, V. V. Titov, U. Kanoglu, and F. Gonz ales. Standards, criteria, and procedures for NOAA evaluation of tsunami numerical models. NOAA Tech. Memo. OAR PMEL-135, http://nctr.pmel.noaa.gov/benchmark/SP_3053.pdf, 2007.
- [41] Tomo. Takahashi, Take. Takahashi, N. Shuto, F. Imamura, and M. Ortiz. Source models for the 1993 hokkaido nansei-oki earthquake tsunami. *Pure and Applied Geophysics*, 144:74–767, 1995.
- [42] W. C. Thacker. Some exact solutions to the nonlinear shallow water wave equations. *J. Fluid Mech.*, 107:499–508, 1981.

- [43] H. Yeh, P. Liu, M. Briggs, and C. Synolakis. Propagation and amplification of tsunamis at coastal boundaries:.. *Nature*, 372:353–355, 1994.
- [44] H. Yeh, P. Liu, and C. Synolakis, editors. *Benchmark Problem 4. The 1993 Okushiri tsunami*—Data, Conditions and Phenomena. Singapore: World Scientific Publishing Co. Pte. Ltd., 1996.
- [45] S. Zhang, D. A. Yuen, A. Zhu, and S. Song. Use of many-core architectures for high-resolution simulation of Tohoku 2011 Tsunami waves. Submitted to Supercomputing 2011 conference, 2011.